Electret Properties of Polypropylene with Surface Chemical Modification and Crystalline Reconstruction

Wang, Jingwen

Institute of Physics and Astronomy

University of Potsdam

Dissertation submitted for the degree of

Dr. rer. nat.

in Applied Soft Matter Physics

Date of defence: 28th April 2020

Supervisors:
1st Supervisor: Prof. Dr. Reimund Gerhard
Institute of Physics and Astronomy, University of Potsdam
2nd Supervisor: Prof. Dr. Dieter Neher
Institute of Physics and Astronomy, University of Potsdam

Reviewers:
1st Reviewer: Prof. Dr. Reimund Gerhard
Institute of Physics and Astronomy, University of Potsdam
2nd Reviewer: Prof. Dr. Dmitry Rychkov
Sustainable Polymer Engineering, Deggendorf Institute of Technology
3rd Reviewer: Prof. Dr. Gerhard Sessler
Institute for Telecommunications Technology, Technical University of Darmstadt

Published online in the
Institutional Repository of the University of Potsdam:
https://doi.org/10.25932/publishup-47027
https://nbn-resolving.org/urn:nbn:de:kobv:517-opus4-470271

Declaration

I, Jingwen Wang, formally submit my thesis
"Electret Properties of Polypropylene with Surface Chemical Modification and Crystalline Reconstruction"
in fulfilment of the requirements set by the regulation for doctoral degree studies in the Faculty of Science at the University of Potsdam.

I hereby declare that the content presented in this thesis is not substantially the same as any that I have submitted or is being currently submitted to any other institutions of higher education.

I hereby certify that the work presented in this thesis is based on the research that I performed in the University of Potsdam by using only the means and source materials as noted therein.

Signed,

Acknowledgements

All work in the thesis was performed in the Department of Physics of the University of Potsdam, Germany. The completion of the PhD program would not have been possible without the help and support of many people.

First and foremost, I am indebted to my advisor Prof. Reimund Gerhard for giving me the opportunity to work with a group of excellent people and for showing me the importance of doing scientific research with integrity and responsibility.

I would like to express my sincere appreciation to my supervisor Prof. Dmitry Rychkov, who always helped me with more leading instead of pushing and guided me to overcome many obstacles in research projects.

Besides, I would like thank the reviewers, Prof. Reimund Gerhard, Prof. Dmitry Rychkov and Prof. Gerhard Sessler for their time and interest in my thesis. Many thanks go to the doctoral committee members, Prof. Dieter Neher and Prof. Helmut Schlaad for their support, and Prof. Svetlana Santer for chairing the examination process.

I am grateful for the kind help from our group members: the technical support from Dilp.-Ing. Werner Wirges and Manuel Schulz, the stimulating discussions with fellow PhD students Quyet Doan Nguyen, Thulasinath Raman Venkatesan, and many former colleagues.

A very special gratitude goes to my father, mother and brother, who always believe in me and support me in all my pursuits.

Last but not least, I would like to thank all my dear friends for their companionship and support.

Abstract

As one of the most-produced commodity polymers, polypropylene draws considerable scientific and commercial interest as an electret material. In the present thesis, the influence of the surface chemical modification and crystalline reconstruction on the electret properties of the polypropylene thin films will be discussed. The chemical treatment with orthophosphoric acid can significantly improve the surface charge stability of the polypropylene electrets by introducing phosphorus- and oxygen-containing structures onto the modified surface. The thermally stimulated discharge measurement and charge profiling by means of piezoelectrically generated pressure steps are used to investigate the electret behaviour. It is concluded that deep traps of *limited* number density are created during the treatment with inorganic chemicals. Hence, the improvement dramatically decreases when the surface-charge density is substantially higher than $\pm 1.2 \times 10^{-3}$ C·m^{-2}. The newly formed traps also show a higher trapping energy for negative charges. The energetic distributions of the traps in the non-treated and chemically treated samples offer an insight regarding the surface and foreign-chemical dominance on the charge storage and transport in the polypropylene electrets.

Additionally, different electret properties are observed on the polypropylene films with the spherulitic and transcrystalline structures. It indicates the dependence of the charge storage and transport on the crystallite and molecular orientations in the crystalline phase. In general, a more diverse crystalline growth in the spherulitic samples can result in a more complex energetic trap distribution, in comparison to that in a transcrystalline polypropylene. The double-layer transcrystalline polypropylene film with a crystalline interface in the middle can be obtained by crystallising the film in contact with rough moulding surfaces on both sides. A layer of heterocharges appears on each side of the interface in the double-layer transcrystalline polypropylene electrets after the thermal poling. However, there is no charge captured within the transcrystalline layers. The phenomenon reveals the importance of the crystalline interface in terms of creating traps with the higher activation energy in polypropylene. The present studies highlight the fact that even slight variations in the polypropylene film may lead to dramatic differences in its electret properties.

Kurzfassung

Als eines der meistproduzierten Polymere stößt Polypropylen (PP) auch als Elektretmaterial auf großes wissenschaftliches und kommerzielles Interesse. In der vorliegenden Arbeit wird der Einfluss chemischer Oberflächen-Modifikationen und kristalliner Rekonstruktionen auf die Elektreteigenschaften von dünnen Polypropylen-Schichten untersucht und diskutiert. Die nasschemische Behandlung mit Orthophosphorsäure kann die Oberflächenladungsstabilität der PP-Elektrete deutlich verbessern, indem phosphor- und sauerstoffhaltige Strukturen auf der modifizierten Oberfläche erzeugt und verankert werden. Aus thermisch stimulierten Entladungsexperimenten und Ladungsmessungen mit piezoelektrisch erzeugten Druckstufen ergibt sich, dass die Oberflächenbehandlung eine begrenzte Anzahl tiefer Haftstellen vor allem für negative Ladungen erzeugt. Daher nimmt die Verbesserung drastisch ab, wenn die Oberflächenladungsdichte einen wesentlich höheren Wert als $\pm 1.2 \times 10^{-3}$ C·m^{-2} hat. Die energetischen Verteilungen der Ladungsfallen in unbehandelten und in chemisch behandelten Proben ermöglichen Rückschlüsse auf die Oberfläche und auf die wesentliche Rolle der aufgebrachten chemischen Spezies für Ladungsspeicherung und -transport in PP-Elektreten.

Darüber hinaus werden an dünnen Polypropylenfolien mit entweder sphärolithischen oder transkristallinen Strukturen deutlich unterschiedliche Elektreteigenschaften beobachtet, was den starken Einfluss von Kristallstruktur und Molekülorientierung auf Ladungsspeicherung und -transport in der kristallinen Phase anzeigt. Generell führt das vielfältigere kristalline Wachstum in sphärolithischen Proben oft zu komplexeren energetischen Verteilungen der Ladungsfallen als in transkristallinen PP-Schichten. Zweischichtige transkristalline PP-Folien mit einer kristallinen Grenzfläche in der Mitte können durch beidseitige Kristallisation auf rauen Formgussoberflächen erzeugt werden. Auf jeder Seite der Grenzfläche in der Mitte der zweischichtigen transkristallinen PP-Elektrete findet sich nach thermischer Polung eine Schicht von Heteroladungen, während innerhalb der transkristallinen Schichten keine Ladungen beobachtet werden. Daraus wird die Bedeutung der kristallinen Grenzfläche für das Auftreten von Ladungsfallen mit hohen Aktivierungsenergien in Polypropylen deutlich. Die vorliegenden Studien zeigen, dass bereits geringe Variationen in der Nanostruktur der Polypropylenfolien zu dramatisch unterschiedlichen Elektreteigenschaften führen können.

Contents

1

Introduction of polypropylene electrets

1.1 Polypropylene—a polymer material

1.1.1 Brief history of polymer synthesis

As one of the most common materials in the modern world, polypropylene (PP) exhibits a wide range of applications. The usage of this remarkable polymer material scatters from the packaging of numerous items in the local supermarkets to the battery cases and interior instruments of state-of-the-art automobiles. In 2010, approximately 48 million tons of PP were produced world wide. The production reached *ca.* 60 million tons in the next two years [1, 2]. However, comparing to other common materials in everyday consumer goods, such as metals, ceramics, woods, paper, *etc.*, PP merely has a short history of less than 70 years.

In fact, the entire industry of synthetic polymer materials has only started in the recent one and half centuries. Although the human utilisation of the natural polymers can be traced back to antiquity, the first man-made polymer material was not introduced till the mid-19th century. The natural polymers existing in organisms, such as cellulose and various proteins, are made under the precise guidelines of DNA with the presence of many enzymes. To recreate the process *in vitro* can be a challenging task. Therefore, the conquest of the polymer synthesis started with modifying the existing natural polymers.

1. INTRODUCTION OF POLYPROPYLENE ELECTRETS

In the 1860s, Parkes discovered the solid residue of what remained from the nitric-acid-treated cellulose after the solvent evaporation, and he patented and showcased the material as Parkesine^{TM}. Later the Hyatt brothers continued to experiment with the cellulose nitrate for the billiard ball productions and coined the name "celluloid" in 1872. The celluloids had quickly become a commercial success, especially in the movie and photography film industries. But the material was discovered to be highly flammable and later replaced by the cellulose acetate safety films [3]. In 1897, another semi-synthetic plastic material—"galalith"—was produced in Germany *via* adding formaldehyde into casein (a milk protein), and this progress stimulated the research of other resinous substances. After ten years, the first fully synthetic polymer, known as Bakelite^{TM}, was obtained from the polycondensation of phenol with formaldehyde by Baekeland in 1907 and soon commercialised in 1909-1910. The industrial development of this phenol-formaldehyde opened the gate to the era of truly synthetic plastics [4].

The first decades of the early 20th century witnessed the explosive development of the polymer industry. Many of today's major plastics were developed during this period, including the commercial manufacture of polystyrene (PS) in 1931, the successful plasticisation of polyvinyl chloride (PVC) in the 1920s, the synthesis of the polyamides (PA, nylon)—nylon 66 in 1935 by Carothers at DuPont and nylon 6 in 1938 by Schlack at IG Farben, the discoveries of polytetrafluoroethylene (PTFE) in 1938 and of poly(methyl methacrylate) (PMMA) in 1933 [3, 4]. Most importantly, the high-pressure polymerisation of ethylene was accidentally discovered in 1933 by Gibson and Fawcett, which led to the active exploration of the polyolefins [5]. The method was later developed into a reproducible high-pressure synthesis process by their colleague Perrin. The first commercial production for low-density polyethylene (LDPE) was established in 1939 [4]. The material showed excellent potential for electrical insulation. Thus, it was investigated as a submarine cable insulator.

In the first decade after World War II, mass productions of PS and LDPE at low cost extended their usage from expensive special purposes to cheap daily commodity goods [3]. In the meantime, polymers were never discarded from the applications in the high-end technology, especially in the biomedical field. Because of their excellent adaptability and chemical stability, polymers have been widely studied and explored for

their applications in polymer-based nanoscale drug-delivery systems, polymeric hydrogel actuators for artificial muscles or tissue engineering, and biopolymer sensors [6, 7].

1.1.2 Development of polypropylene

The industrial manufacture of polyethylene (PE) met its historical landmark in the 1950s when a series of transition-metal catalysts were invented. The catalysts, famously known as "Ziegler-Natta catalysts", were a group of organometallic compounds that were capable of polymerising olefin monomers with more designed and diverse structural forms. The catalysts were first developed by Ziegler for PE, whereas PP benefited the most from this invention. Using this method, PP made its debut in the 1950s and prospered as one of the most produced commodity plastic materials in the world. The process led to semi-crystalline PP. Oligomeric and polymeric forms of propylene had been made before, but the low-molecular-weight amorphous products were of marginal practical value.

Because of the great contribution on the polymerisation of stereo-regular PP, Ziegler and Natta were awarded the 1963 Nobel Prize in Chemistry. However, the US patent for the preparation of the first crystalline PP evoked a long litigious debate between Natta from Europe and the Phillips Petroleum company from the US. In March 1954, Natta synthesised the crystalline PP using the type of catalysts derived from the work of Ziegler on PE. Whereas Hogan and Banks had produced PP in its crystalline form with a chromia-nickel oxide catalyst in an experiment conducted on June 5th, 1951—three years earlier—at Phillips Petroleum. By the end, a definitive patent was issued to Hogan and Banks on March 15, 1983—some 30 years after their original application.

The vast majority of global industrial output of PP (virtually 100%) was produced with the Ziegler-Natta catalysts since the first commercial operation in 1957. Due to the stereospecific manner of polymerisation under the control of the Ziegler-Natta catalysts, it is possible to manipulate the configuration of the methyl groups on the PP molecular chain, producing PP with different tacticities [1, 8]. When the methyl side groups predominantly point in the same direction, the PP product is designated as "isotactic", which is the most common and first marketed industrial PP. In addition, "syndiotactic" PP products are also commercially available, where the orientation of the methyl groups uniformly alternates from one side to the other along the polymer chain.

The two stereoisomeric forms of PP mentioned above contain substantial crystalline contents. A third type of the tacticity is called "atactic". Because of the randomly oriented side groups in this particular PP, it often appears as a rubbery amorphous material that is less desired. The schematic structures of the three most common PP stereoisomers are illustrated in Figure 1.1 [1, 3]. The isotacticity of commercial-grade PP is measured in terms of isotactic index that most varies from 85% to 95%. The degree of crystallinity is associated with the percentage of the isotactic content in a PP product, hence its properties, including the softening point, tensile strength and modulus, increase with the isotactic index [9].

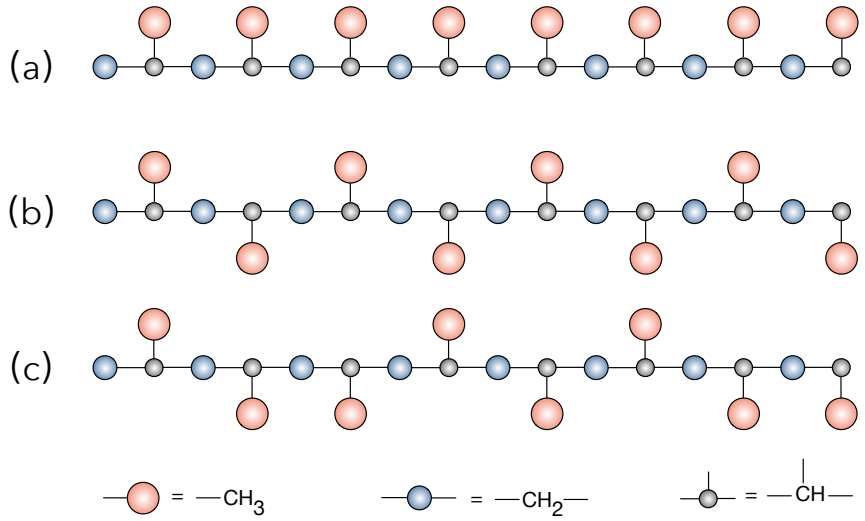

Figure 1.1: Schematic diagrams of the PP molecules in different tacticities. - (a) The isotactic structure: the methyl groups all point to one side; (b) The syndiotactic structure: the methyl groups orientate alternatively from one side to the other; (c) The atactic structure: the methyl groups orientate randomly along the chain.

Isotactic PP is often compared with the high-density polyethylene (HDPE) due to the similarities. Their mechanical and thermal properties are highly influenced by the molecular weight, purity and polymerising techniques. Both materials can frequently be found in many household goods, packaging and fibres. Many advantages make PP more preferable in this competition. The higher softening point of PP permits a higher operating temperature, and it can thus be used for the iron and hairdryer cases. Because of its ability to withstand boiling water and heat sterilisation, it is also the

perfect candidate for food packaging and dishwasher appliances [9]. Moreover PP is more transparent because of the smaller difference in density between its amorphous (0.85 g/cm^3) and crystalline (0.94 g/cm^3) regions, so that it can be made into syringes and laboratory supplies. On the other hand, PP suffers from its higher brittle point and susceptibility to oxidation. Such shortcomings may be fixed with suitable additives. Featured with many desired properties, PP was rapidly exploited as a commodity plastic since its commercialisation. In 1957, it was first marketed with the trademark Moplen^{TM} and used in the forms of fibres, films and injection mouldings. The explosive consumption rate sparked a production surge in the 1970s, resulting in a dramatic price drop. In return, the abnormally low cost of the material stimulated more growth in the usage. In just 30 years after the invention, PP moved into the third place in the league of the plastic production [3].

However, the conventional mass and disposable applications of PP and plastics in general have raised environmental concerns in recent years. The global plastic resin production exceeded 288 million tons in 2012. Majority of the plastic resins were consumed in the forms of packaging and non-durable goods. The lack of adequate disposal methods and regulations led to severe worldwide pollutions. Among the 275 million tons of plastic waste generated in 192 coastal countries in 2010, 4.8-12.7 million tons entered the ocean, causing harms to the marine system, wild lives and eventually human beings [10]. In addition, the plastic industry heavily relies on the non-renewable fossil resources, particularly the petroleum and natural gas. The anticipated depletion of the fossil resource forces the industry to seek the alternative bio-based feedstock. But it is also well acknowledged that the available biomass from plants is not an unlimited resource either. A controlled and optimised harvest of the biomass must be managed in order to achieve the ecological sustainability [11]. In the meantime, technologies for recycling and reusing plastic materials are in high demands. New concepts of clothing made from recycled plastics have been nicely received and supported in the market in recent years.

Due to the better recyclability, PP is currently a promising candidate to substitute the cross-linked polyethylene (XLPE) as the new high-voltage direct current (HVDC) cable insulating material [12, 13, 14]. Besides, with a melting temperature above 160 °C, the PP insulator shows the possibility for much higher cable current ratings. Failures in dielectric materials are often associated with the impurities. The better purity

allows PP to be used in high-performance electrical systems [15]. Certain prototype networks of PP-based high-voltage cables have already been produced and installed [16]. Another important electrical engineering application of PP is the electret, which is the core of this thesis. Products of non-woven fabrics and cellular ferroeletrets designed with PP were introduced and improved by numerous researchers. Compared with other popular polymeric electret materials, PP has the advantage of low cost and a less hazardous manufacture process due to the fluorine-free formula [17, 18]. More details regarding the fundamentals and development of electrets will be introduced in the following section.

1.2 Electrets

1.2.1 General background

An electret is defined as a piece of dielectric material exhibiting a quasi-permanent electric charge [19]. The electric charge can be "real" charges in the bulk or on the surface of the electrets. The electret charges may also originate from the "true" polarisation. In the case of polar materials, the elements on each side of the chemical bond can differ significantly in terms of their electronegativity. As the electrons "redistribute" between the atoms under their electron donating or withdrawing effects, the atoms appear to carry equal amount of opposite charges, forming an electrical dipole [20]. When the dipoles are aligned in the same direction, a "true" polarisation will be observed in the electrets.

The electric field generated by these quasi-permanent charges gives the electret a characteristic self-biased feature. It offers the possibility to omit the DC bias supply in some devices, which was exploited in the revolutionary invention of the self-biased condenser microphone by Sessler and West in 1962. A piece of thin-foil electret was one-side metallised, and next to the non-metallised surface a second electrode is placed with a thin air gap in between. The electret, the air and the two electrodes form a parallel-plate capacitor. The vibration of the electret foil alters the thickness of the air gap. The distribution of the compensating charges on the electrodes changes with the capacitance, which is detected as electrical signal in the external circuit. The design is essentially a transducer that couples the acoustical and the electrical energy. Therefore,

the concept can be applied in a microphone (from acoustical to electrical signal) or a loudspeaker (from electrical to acoustical signal). The excellent transduction quality and low cost of the electret acoustic transducer brought the great commercial success and mass production globally, which promoted the extensive research and industrial exploration of the polymeric electrets [19, 21].

The electret phenomenon in general was discovered more than 2500 years ago when the electrostatic attraction and repulsion were observed in certain amber *briefly* after charging [22]. In 1732, as documented in a letter, the electret properties of some wax and rosins were described as "perpetual attractive power" by Gray [23]. The subject started to draw more attention in the 19th century when Faraday theorised the concept in 1839 [24] and Heaviside coined the term "electret" in analogy to "magnet" in 1885 [25]. The term was promoted 35 years later by Eguchi who initiated the systematic research on electrets.

Since 1919, Eguchi published a series of studies conducted on electrets, including the thermal charging methods, the charge decay and recovery, and the influence of X-ray, heating or chemical reagents on the charge storage in electrets. He recorded the "permanency" or charge stability of the electrets at room temperature and experimented with different wax and rosin materials as well as their mixtures [26, 27, 28]. The electret materials suffer from the unsatisfactory charge stability at that time, especially at elevated temperatures. Thus, they can only be utilised in certain applications where the long-term charge storage was not involved. One typical example is the electrophotographic technique, commonly known as the xerography. In the 1920-1930s, methods for charging powders of insulating materials by means of the electron or ion injection were explored and developed by Selenyi [29, 30]. The technology subsequently led to the invention of the xerography in 1940, which used the charged electret powder as the toner and photosensitive material as the negative to copy images on papers. It only requires the charges on the powdered electret to be stable during the short period of the copying process [31, 32]. Applications that call for long-term charge stability, such as the self-biased condenser microphone and other transducers, were eventually realised with the polymeric electrets.

The polymers have the advantages of low ohmic conduction and low affinity to water, particularly the non-polar polymers, giving very stable electrets. The mechanical flexibility and easy processability allow most polymers to be available as thin foils [33].

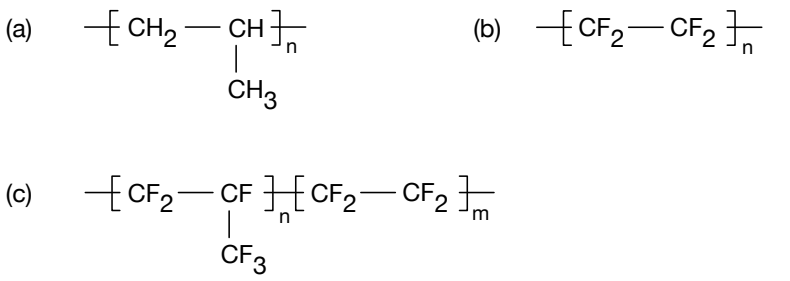

Figure 1.2: Chemical structures of polypropylene and the Teflon™ - (a) polypropylene (PP); (b) polytetrafluoroethylene (PTFE); (c) fluorinated ethylene and propylene copolymer (FEP).

The original design of the electret microphone in 1962 was demonstrated with the polyethylene terephthalate (PET) electret, and the performance was later improved by changing the material to Teflon™. Teflon™ is a trademark registered by DuPont, referring to the PTFE and fluorinated ethylene and propylene copolymer (FEP). The chemical structures of PP, PTFE and FEP are illustrated together in Figure 1.2 for comparison. PTFE was first discovered by Plunkett in 1938 at DuPont and later a pilot production was set up in 1943. Because of the exceptionally high melt viscosity of PTFE, it has to be fabricated by a cold-moulding method instead of the usual melting process. To overcome this problem, the hexafluoropropylene was added to the monomer feed of the polymerisation. The resulting product is FEP—a fluoropolymer that can be processed in an extruder [3, 4].

The remarkably strong carbon-fluorine bonds in the Teflon™ are able to tighten the structure of the molecules, giving the material its outstanding chemical inertness, water resistance, insulation characteristics, and extremely high melting temperatures for polymers: 327 °C for PTFE and 290 °C for FEP [3]. These properties allow the Teflon™ to work as the most stable space-charge polymeric electret. Besides the non-polar Teflon™ materials, the polar fluoropolymers are also of great importance to the electret community, *e.g.* the classic poly(vinylidene fluoride) (PVDF). The small atomic volume of fluorine in PVDF grants more freedom in terms of the molecular movements during the poling process. When the dipoles are aligned to one direction and "frozen-in", the large dipole moments of the individual VDF monomers will constitute the overall spontaneous polarisation. It brings about the ferroelectricity in the PVDF electret. The thin-foil PVDF electrets have been used in many commercial products,

after the piezoelectricity and pyroelectricity were discovered in 1969 and 1971, respectively [34]. In the PVDF infrared sensors, the rather small heat capacity of the thin film makes it possible to respond quickly to even weak infrared signal. Regarding the acoustic emission transduction, it was reported that some PVDF devices show comparable performance as the lead zirconate titanate (PZT) ceramic transducers in the 1980s, while holding the advantages of the versatile processability and flexibility [35]. The PVDF electret also allows the film to be locally active by the local poling process [36].

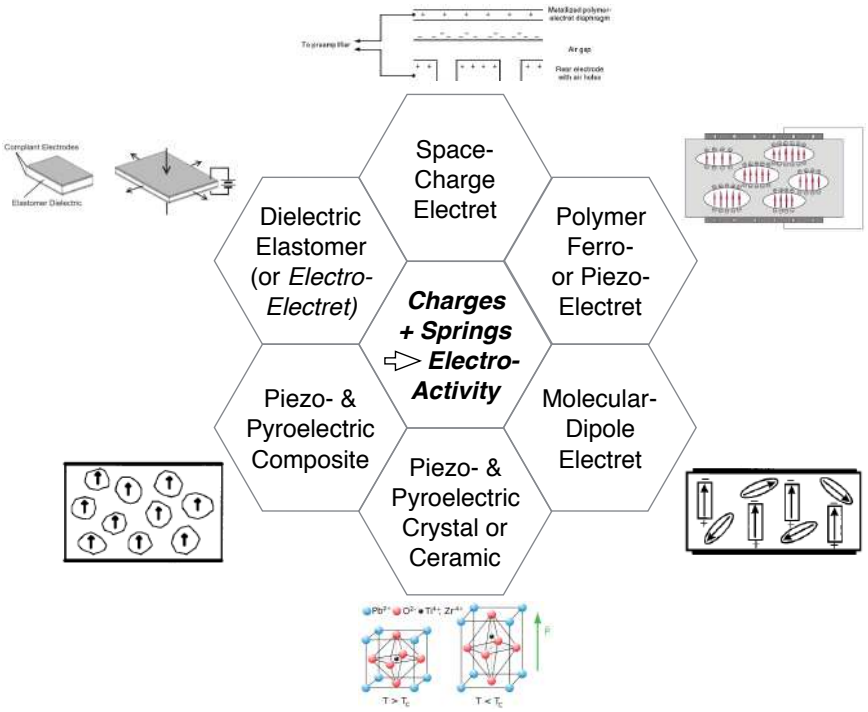

Figure 1.3: Six different types of electro-mechanical materials - The electric charges in these electrets are from many different origins and arranged differently in the material, but they all can provide the quasi-permanent electric bias [37].

This work mainly focuses on the polymer electrets, so the term "electret" used here and after refers to the space-charge electrets (*e.g.* PTFE) and molecular-dipole electrets (*e.g.* PVDF). However, one must keep in mind that there are different types of electrets under a broader definition, as the electro-mechanical materials shown in Figure 1.3 [37]. In the electro-electrets (dielectric elastomers), the electric charges are

in fact the opposite charges in the compliant electrodes on the surfaces of the material, which form the "dipoles" across the elastomer film. The dipoles in the electret materials can also be provided by the highly polar fillers in the electret composites or by certain asymmetrical crystal lattice sites in the piezo- and pyro-eletric crystals and ceramics. More and more new electret materials have been discovered and developed: for instance, the metal halide perovskite with the characteristic metastable polarisations from its spontaneous lattice strain and the calcium hydroxyapatite (HA) ceramics as bio-compatible electrets for the osteoblastic adhesion [38, 39]. In the meantime, some commonly existing materials were capable of offering surprising potentials with a simple "twist" in their structures [18, 40]. The resulting type of electret materials will be discussed in the next section.

1.2.2 Polypropylene as electret

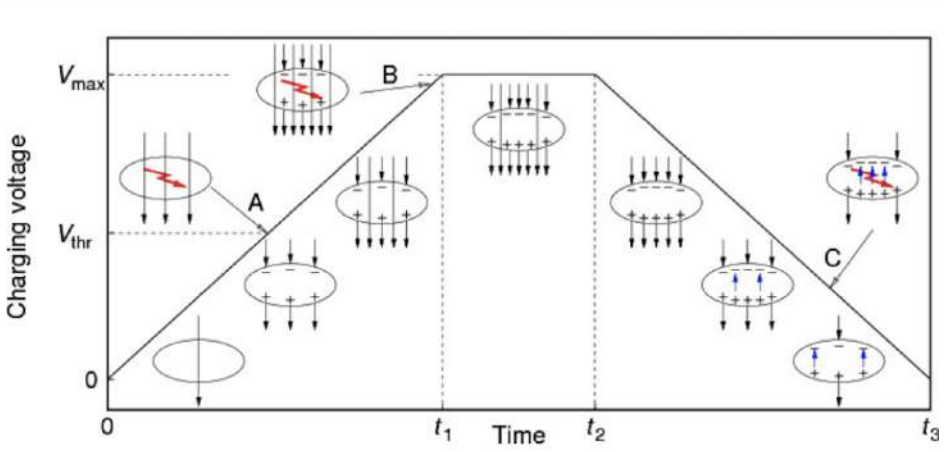

Figure 1.4: A schematic diagram of the charging process in a single void - (A) When the charging voltage reaches the threshold value (V_{thr}), Paschen breakdown is ignited. (B) At higher voltage, a second discharge may occur. (C) The reverse electric field from captured charge may result in a back discharge as the applied voltage decreasing.[41]

An "electrothermalmechanical" film made from the cellular biaxially-oriented PP was introduced by Savolainen and Kirjavainen in 1989 [40]. The "electrothermalmechanical" effect of the particular cellular PP film was essentially the ferroelectricity. The ferroelectric property, as mentioned above, is caused by the aligned dipoles in

the material. Hence, the idea of ferroelectricity in a non-polar material without any molecular dipoles is rather counterintuitive. The secret lies in the cellular structure of the PP films. As illustrated in Figure 1.4 [41], the Paschen breakdown occurs in the voids when the cellular film is subjected to a sufficiently high electric field, turning the voids into small plasma chambers. Positive and negative charges travel under the electric field to the opposite directions and are captured by the inner surfaces of the voids. The charges of different polarities are separated by the height of the void, forming a macroscopic dipole. This type of non-polar films with the spontaneous polarisation of void-dipoles are termed "ferroelectret" in order to be distinguished from the ferroelectrics with intrinsic molecular dipoles [18].

The dipole moment (μ) in any ferroelectric material regardless of molecular or macroscopic dipoles is the product of the separated charges (q) and the length of the dipole (l):

$$\mu = q \cdot l. \tag{1.1}$$

The overall spontaneous polarisation (P) responsible for the ferroelectricity is reflected in the sum of the dipole moments:

$$P = n \cdot \mu \cdot \langle cos\vartheta \rangle, \tag{1.2}$$

where n is the density of dipoles, and ϑ is the angle between P and μ. In the case of polymer ferroelectrics, the dipoles consist of the covalent bonds between the carbon atoms and they are stronger than the interaction among dipoles. The external compressing or expanding forces can only change the distance between dipoles, hence the dipole density n. On the other hand, the contraction or expansion on the cellular ferroeletrets primarily causes the deformation in the voids, leading to changes in the length of the dipoles (l). Here the polarisation is decreased or increased with the dipole moment (μ). Conversely, applying voltage across either the ferroelectric or the ferroelectret films can induce changes in their thickness or in the pressure that they exert onto the adjacent space [18].

The effects of the ferroelectrics and ferroelectrets are united by Gerhard, Bauer, and Qiu into one "charge-spring model". The concepts of the dipole and its surroundings are set aside in the model, and the entire piece of the ferroelectric or ferroelectret material is viewed as charges connected with springs of different spring constants instead (illustrated with a schematic diagram in Figure 1.5). The model can predict the

piezoelectric response of the polymer ferroelectrics (PVDF), ferroelectrets (PP foam) and even ferroelectric perovskite (PZT) with the corrected spring constant [42, 43].

In comparison to the PVDF and PZT ceramic ferroeletrics, the PP cellular ferroelectrets have much lower density and better coupling efficiency to gases on account of the air content in the voids. The small pyroelectric coefficient gives the PP cellular ferroelectrets high piezoelectric sensitivity. The ferroelectret-based electronic skin and large-area touchpad were reported. And the material is also suitable for the air-borne ultrasound detection and nondestructive testing applications [44, 45]. The development of the ferroelectret concept has extended to different materials and structures, the cellular foam-like and tubular-channel ferroelectrets with FEP were successfully built and investigated [46, 47, 48]. Although the charge retention ability of the PP foam is not as excellent as that of FEP, it is still favoured for its low material cost and simpler foaming process.

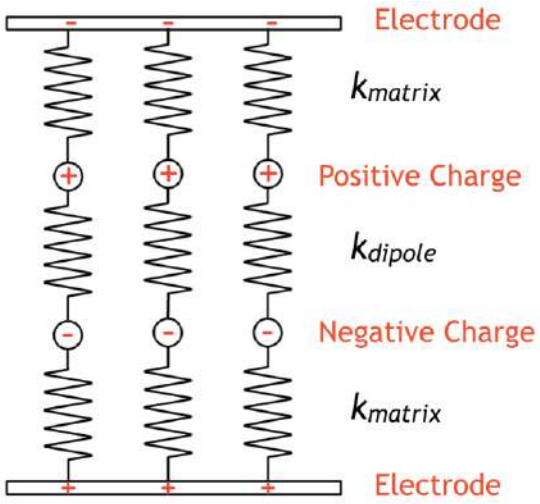

Figure 1.5: A schematic illustration of the charge-spring model for elastically heterogeneous dielectric materials. - The piece of dielectrics consists of a matrix phase, a dipole phase, and interface charges of opposite polarities between them [42].

Without the contribution of the cellular structure, PP can also be employed as a space-charge electret material. Prior to the ferroeletret foam application, PP electret was first used in the electret filters, which are gas filters consisting of fibres carrying electric charges. It is the essential component in the particulate-filtering facepiece respirators (*e.g.* the N95 type). As shown in Figure 1.6, the fibres are bipolar-charged

and pressed into randomly oriented fabric webs. The electrostatic field generated by the filter in its vicinity can attract the incoming particles with a long-range interaction of a strong electrical force. It works in a similar way that a magnet attracts the iron particles: the charged particles are drawn towards the electret filter by the Coulomb force and the uncharged particles by the inductive force. This mechanism allows the PP electret fabric webs to be made less dense than the conventional mechanical fibrous-filters, so that the resistance to the gas stream can be reduced while the filtration efficiency for sub-micron particles remains the same or even increases [33, 49, 50]. However, in both the cellular ferroelectret and electret filter applications, PP shows its limitation in terms of the surface charge stability. This issue will be addressed in chapter 4 - 6 of the thesis.

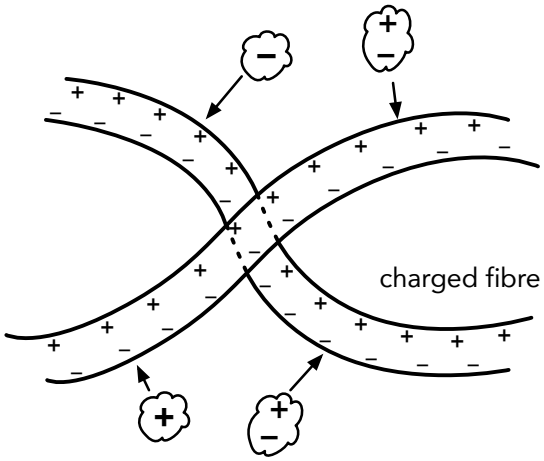

Figure 1.6: A schematic illustration of the fibrous electret filter. - The bipolar charged PP fibres can attract particles with a long-range interaction to achieve a higher filtration efficiency with much lower air resistance [33].

2

Charges in electrets

2.1 Theories of charge storage

2.1.1 Development of theoretical background

Since the beginning of the systematic research on electrets in 1919, the theoretical understandings of the charge storage in electrets have been developed along with the applications. Shortly after Eguchi's phenomenological investigations on the electret behaviour in various waxes and rosins, Gemant confirmed Eguchi's observation of the polarity reversals in 1935 and introduced the term "homocharge" and "heterocharge" to describe the charges of the *same* and *opposite* polarity to that of the adjacent electrode, respectively [19]. Following their footsteps, Gross conducted a series of quantitative experiments on carnauba wax in the 1940s. The coexistence of homo- and heterocharges in the electret and the compensating mirror charges on the electrodes induced by the sum of homo- and heterocharges were discussed. He also attempted to explain the mechanism of the charge storage and found the existing theories of the ionic charge carriers and dipole theories unsatisfactory [51, 52]. Later, Gerson and Rohrbaugh used a collection of carnauba waxes with the different thicknesses and forming field strengths to test the ionic space charge and dipole theories in 1955. They concluded that these theories were not sufficient for explaining the existence of the homocharges in the electret and proposed the "trap" theory. The theory suggested that the homocharge carriers moved into certain "traps" simultaneously with the formation of heterocharges and were released later upon heating. It was also pointed out that the trapping rate

must show the temperature dependence [53]. The theory was first presented as a tentative hypothesis and was later supported by Gross and Perlman [54, 55].

The electron trapping model was examined with X-ray radiated amorphous and semi-crystalline *polymers* by Fowler [56]. In the same period, the theoretical fundamentals of the impurity conduction in doped inorganic semiconductors were established: an impurity conduction band was formed for the continuous charge transport, when the concentration of the impurities was high enough to cause a strong overlap of their states and overcame their localised characteristics. However, when the impurity concentration was below such threshold, a stochastic transport model of charge carrier "hopping" from an occupied localised state to an unoccupied one was suggested by Mott and Conwell independently in 1956 [57, 58, 59, 60, 61]. A trap-modified energy band model for the charge storage and transport in polymer electrets was proposed by Bauser in 1972, which combines the "trapping" and "hopping" theories [19, 62, 63]. The model is still well received today and will be introduced in section 2.1.2.

2.1.2 Trap-modified energy band model

As discussed in section 1.2, the typical origins of the electric charges in a polymeric electret are the "true" polarisation and the "real" charge. The former is commonly achieved by orienting the intrinsic dipoles under a sufficiently high electric field at elevated temperatures and subsequently cooling them to freeze-in the alignment (the so-called poling process). The total polarisation is the sum of the effective dipole moments as shown in (1.2). Therefore, the apparent electric charges of the electret are stored in the ordered arrangement of the dipoles, owing to the energy input during the poling process. The aligned dipoles will thus have the tendency to relax into a lower-energy state with a random orientation. The polarisation of the electret (P_d), under isothermal conditions (T is constant), often decays in a classical thermodynamic manner as a function of time (t):

$$P_d = P_{d(t=0)} exp(-\alpha(T)t), \tag{2.1}$$

in which $\alpha(T)$ is the dipole relaxation frequency with a temperature dependence of

$$\alpha(T) = \alpha_0 exp(\frac{A_i}{kT}). \tag{2.2}$$

The α_0 and A_i are the frequency constant and dipolar activation energy, respectively [19, 64].

It is rather straight forward to comprehend where and how the electric charges are stored in the dipolar materials. However, when it comes to the "real" charges in the non-polar polymeric electrets without the intrinsic charge carriers, the understanding of charge storage and dissipation can be tricky. The excess charges deposited in the electrets are known as the space charges (referring to both surface and bulk charges), which can be found in the dipolar electrets as well. Hence, it is of great importance to understand the mechanism behind the phenomenon.

In the description of the cellular PP ferroelectrets formation in section 1.2.2 and in Figure 1.4, the term "capture" was used to refer the transfer of the positive and negative charges from the plasma to the inner surfaces of the voids. In the trap-modified energy band model proposed by Bauser, the space charges are captured by the "traps" in the PP electrets [63]. The concept was derived from the energy band theory of semiconductors. In semiconductors, when a molecular orbital is unoccupied, it is a potential host for a negative charge; whereas if a molecular orbital is occupied by an electron, it is a potential host for a positive charge, since a positive charge is defined as the removal of one electron (named "hole"). The neighbouring lowest unoccupied molecular orbitals (LUMO) will overlap to form the conduction band (E_c) for electrons and the highest occupied molecular orbitals (HOMO) will form the valence band (E_v) for holes. The negative (electrons) and positive (holes) charges can move to the opposite electrodes along the conduction and valence bands, respectively, under the electric field in an ideal semiconductor with a perfect periodic-lattice structure. But in real semiconductors, impurities or structural defects can cause disruption of the energy bands and perform as traps for the negative and positive charges. The trapping and immobilisation of the charges may impair the charge transport of the semiconductor in the photovoltaic or light-emitting diode, thus reducing the efficiency [65].

The concept of energy bands cannot be applied to the common polymeric electrets directly, because the majority of the polymers are semicrystalline: the long chains of polymer molecules are partially packed in a roughly ordered lamella structure in the crystalline region and the rest are coiled randomly in the amorphous domains. Each of the atoms or groups of atoms presents an individual state, due to the influence of their surrounding environment. Their orbitals are not able to overlap and to act

as a continuous conduction or valence band. Instead, there exists a distribution of localised states near the mobility edges (E_v and E_c) and they behave in a very similar way as the traps in the semiconductors. The energy diagrams for a polymeric electret and the localised states are shown in Figure 2.1 [19, 62, 63]. To a certain extent, the polymeric electret can be understood as a piece of semiconductor with a large amount of "impurities" or "defects", so that the entire continuous energy-band structure is overthrown by the localised traps. When the electrets are poled by means of charge injection or deposition, the excess space charges will be captured by these localised states. The negative charges will be trapped near the E_c and the positive charges near the E_v. The energetic difference between the trap and the nearest mobility edge (E_v or E_c) is called the trap depth (E_{trap}).

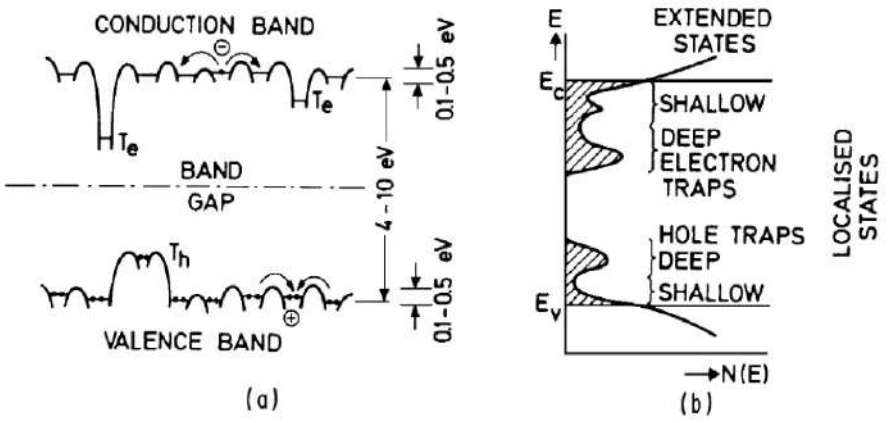

Figure 2.1: The trap-modified energy band model - (a) The energy diagram for a polymer electret; T_e represents the electron traps and T_h, the hole traps [63]. (b) The density of states $N(E)$ for a polymer electret. The localised states (traps) are shaded. E_c and E_v are the mobility edges [19].

The space charges of the polymeric electrets are stored in the traps of "impurities" in analogy to the semiconductors, ergo it is only sensible to use the "hopping" model of the impurity conduction in semiconductors to describe the charge transport in the real-charge electrets [58, 60, 63]. In Mott's and Conwell's models, the charges move between the discrete traps by a hopping motion. The hopping transport of the space charges involves the random diffusion due to the concentration gradient, the drifting

process under the electric field, and the ohmic conduction. Only the drifting and ohmic conduction are reflected by the current density (i_c) through the electret:

$$i_c = (g + \mu_{s+}\varrho_{s+} + \mu_{s-}\varrho_{s-}) \cdot E, \tag{2.3}$$

where the $\mu_{s\pm}$ is the space-charge mobility and the $\varrho_{s\pm}$ is the space-charge density, and g is the ohmic conductivity. The process is driven by the internal electric field—E. The term of the ohmic conductivity (g) in (2.3) is governed by the density of the intrinsic charge carriers ($n_\pm$) and their trap-modulated mobility ($\mu_\pm$) with

$$g = e \cdot (n_+\mu_+ + n_-\mu_-). \tag{2.4}$$

Both quantities are negligibly small in the electret-forming polymers, which are essentially insulators. The excess space charges move under the electric field by the hopping motion along the shallow traps near the mobility edges and are frequently captured by the deep traps. The time (τ) of a charge spent in a particular trap before being released is expressed as

$$\tau = \nu_{esc}^{-1} exp(\frac{E_{trap}}{kT}). \tag{2.5}$$

The trapping time is influenced by the attempt-to-escape frequency (ν_{esc}), which is a temperature-dependent factor, while it increases exponentially with the activation energy that is the trap depth (E_{trap}). Therefore, the life time of the charges is dominated by the activation energy of the deep traps. Even if the charge first falls into a shallow trap upon poling, it will soon escape from the shallow trap and likely be captured by a neighbouring deep trap. As a result, the deep traps are mostly responsible for the experimentally observed activation energy distribution in an electret [19, 66].

Commonly, the traps in the amorphous and semicrystalline polymeric electrets consist of the structural and compositional disorders, which create energy barriers or disruptions with their own energy level that differs from that of their surroundings. The traps in a piece of electret can be classified position-wise as the surface traps and bulk (or volume) traps, and they are often associated with the impurities, morphology, and chemical composition of the polymer molecules, *etc.* [66]. Furthermore, the fluctuation of the polymer structure and conformation upon its temperature change can vigorously impact the positional distribution and energy state of the traps. Thus, the thermal properties of a polymer material also influence its electret behaviour [62]. The nature of the traps in the polymers and their effect on the electret properties will be discussed in section 3.3.

2.2 Charging methods

Different charging methods are often required to obtain the dipolar and space-charge electrets. Even with the same electret film, the result may vary significantly with different charging conditions. The space charges in an electret can be either transferred from the external sources or generated internally by certain stimuli. In the case of external transfers, the low energy sources usually deposit the charges on the electret *surfaces*, for instance, the triboelectrification [50], corona discharge [67], and dielectric breakdown discharge of the cellular ferroelectrets shown in Figure 1.4 [41]. When the high-energy electron or ion beams are employed, the charges can be injected or bombarded into the *bulk* of the electrets [29, 30]. The mono-energy particle sources are often chosen for a precise control over the penetration depth, *i.e.* the location of the implanted charges.

For some electret materials, pairs of positive and negative charge carriers, *i.e.* the excitons, can be generated under the harsh radiation of X-ray, β ray or γ ray. The charge pairs are immediately separated by the electric field across the electret to avoid the charge recombination [68]. A softer radiation source of ultraviolet or visible lights can also generate the charge pairs in certain electrets named "photoelectrets". The internal charges might also originate from the impurities or triboelectrification during the manufacturing procedures, which are screened by each other and only contribute to the electret effect after being separated. Regardless of the origin of the charge pairs, the separation process is otherwise the same as that of the X-ray radiated electrets [19]. The charge separation may be performed at elevated temperatures to accelerate the process, which involves thermal charging. The principle and operation of the thermal and corona charging will be introduced in section 2.2.1 and 2.2.2 below, respectively.

2.2.1 Thermal charging

The thermal charging is one of the oldest electret charging techniques, where an electric field is applied to a piece of electret at a properly selected poling temperature, followed by cooling with the field continuously present. The temperature and electric field profiles during the thermal charging are presented in Figure 2.2. The method is widely used for poling the dipolar electrets as discussed in section 2.1.2. For most of the semicrystalline polymers, the poling temperature (T_p) is typically set above the glass

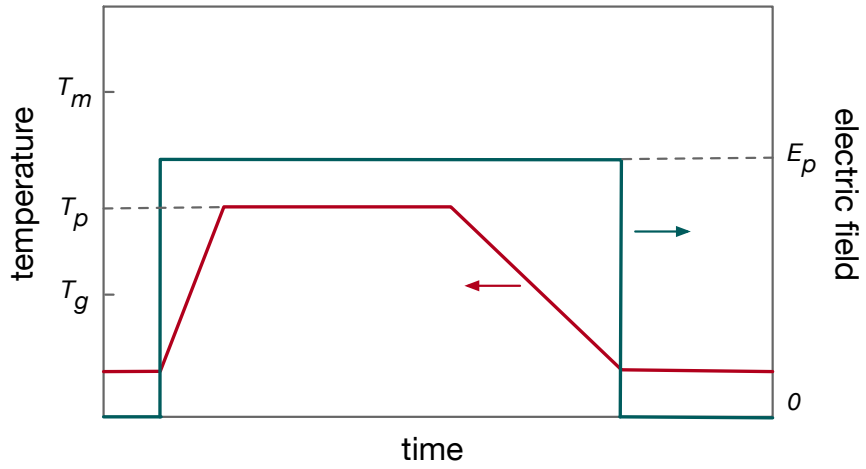

Figure 2.2: A graph of temperature and electric field profiles over time in a typical thermal charging process - T_g is the glass transition temperature, and T_m is the melting temperature of the electret. T_p and E_p are the poling temperature and electric field, respectively.

transition temperature (T_g) while below the melting temperature (T_m). In this way, the molecular chains have sufficient mobility at the poling temperature, but stay immobile at the freeze-in temperature by the end of the charging process. It is because the dipoles in the polymeric electrets are the polar segments of the repeating units on the polymer chains. The sufficient freedom of the movement must be ensured for a more effective dipole orientation [19, 26, 69].

Depending on the electret material and electrode arrangement, different phenomena other than dipole orientation can take place in the thermal charging. When there exist pairs of charge carriers in the electret, a charge separation can be realised by thermal charging. The poling temperature in this case needs to be selected in regard to the mobility of the charges and that of the trap-associated molecules, due to the strong temperature-dependence of the space-charge transport in the polymer electret, as expressed with (2.5). The polarisation of the electret film is composed of the heterocharges after the charge separation. Therefore, it is important to adjust the applied field (E_p), charging time and the electrode arrangement in order to prevent the neutralisation of the space charges at the electrodes [19, 65, 68]. A barrier can be created between the electrodes and electret surfaces by adding an air gap or blocking layer. One must, however, be aware that the homocharge deposition on the electret might

occur due to the spark discharge in the air gap or blocking layer. This can be avoided by choosing an appropriate poling field and/or a blocking layer with a higher dielectric strength than that of the electret sample.

2.2.2 Corona charging

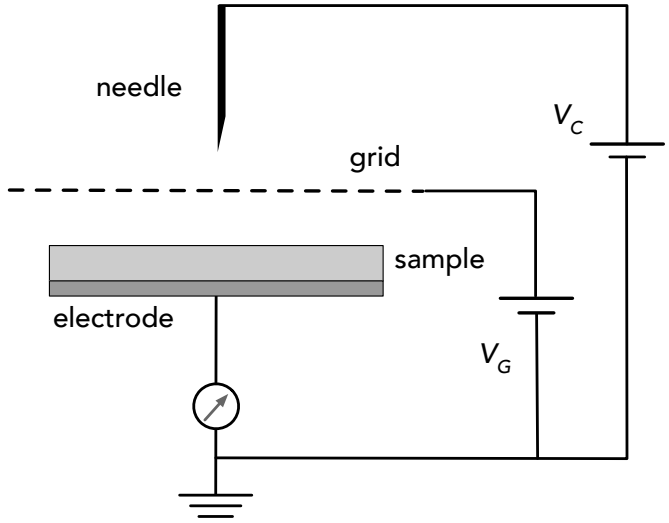

Figure 2.3: A schematic diagram of the classic corona charging apparatus - V_C is the corona voltage and V_G is the control-grid voltage [67].

The corona discharge is one of the sources for externally depositing charges onto a piece of polymer to form an electret directly. Besides, the corona deposited charges can provide the electric field for the dipole poling or charge-carrier separation for electrets with different characteristics. The most important part of the corona-charging apparatus is the "sharp" electrode with a high curvature that is responsible for the discharge. The shape of the electrode can be a needle, a wire or a blade. The opposite electrode is often a grounded plate or a cylinder that also provides support to the electret films. The point-to-plane corona setup, as shown in Figure 2.3 [67], is frequently used in the laboratory, while the wire and blade shapes are common for the industrial roll-to-roll production of the charged films on a cylindrical counter electrode. A high voltage of few kV is applied onto the point electrode (V_C) to create a sufficiently high electric field that can initiate the ionisation of the gaseous molecules. Once some charged particles are generated, they collide with more neutral molecules in their surroundings, which results in a large amount of ions between the point electrode and the sample surface.

The polarity of the charged particles solely depends on the polarity of the corona voltage (V_C), and the species of the ions are determined by the gas medium. When the corona discharge is carried out in air, the prevailing negative ions are $CO_3{}^-$. The positive corona can generate $(H_2O)_nH^+$ in humid air (n increases with the humidity), while $(H_2O)_nNO^+$ and $(H_2O)_n(NO_2)^+$ begin to show dominance when the relative humidity decreases to low values [70]. Unlike the ion beam charging method where particles with the energy of keV magnitude strike and penetrate the electret surface, the ions in the corona discharge only drift along the electric field extending from the corona point to the sample surface, with energy comparable to that of the ambient environment and a mobility of several $cm^2V^{-1}s^{-1}$ [67]. Hence, the ions gently land on the electret surface and their charges are captured by the traps on the surface, leaving the neutralised molecules re-entering the environment. A well-controlled homogeneous surface potential can be achieved with the aid of a wire-mesh, commonly known as the control grid. It is positioned slightly above the electret surface with the same potential (V_G) as the desired value for the electret surface. The mesh allows the ions to pass through, until a zero electric field condition is created between the grid and the sample surface to prevent further charge deposition when the surface potential of the electret is built up to the potential of the grid [19].

The ions are not able to penetrate through the surface of the electret *via* a corona charging, whereas the possibility of the deposited charges migrating into the bulk of the electret depends on the properties of the material and the charging conditions [19]. For instance, it was reported that the charge penetration into the bulk of PP electrets did not occur when it was corona charged at room temperature [71]. The same observation has been made on FEP as well. However, if the corona charging of FEP is implemented at an elevated temperature for a longer duration, the deposited charges can drift into the electret film under the internal electric field. This can result in a uniform charge spreading through the bulk of the FEP electret [72]. Furthermore, the dipolar electrets like PVDF can be effectively poled with a corona setup as well [69, 73]. These methods marry the corona charging with the thermal charging for various outcomes. The corona charging technique can also be incorporated with the charge and potential measurement setups in order to monitor the charging process and charge transport in electrets [67, 74, 75].

3

Characterisation of electrets

3.1 Charge stability—Thermally stimulated discharge

After the charges are introduced in an electret with a proper charging method, the first question at this point would be how stable the charges will be. The level of charge stability is vital for an electret with space charges or molecular dipoles, because it directly influences the possible life time and service conditions of the electret devices. In the trap-modified energy-band model, the life time of each individual charge is determined by the temperature and the activation energy (E_{trap}) of the trap (2.5). When a charge acquires sufficient energy to overcome the barrier of E_{trap}, it can escape the trap and drift in the local electric field. The process will lead to a current or a potential decay in the electret as an external response of the charge dissipation. The charge stability of an electret is a macroscopic concept, which is often described with an energetic distribution of the traps. Generally, when the electret charges are subjected to a scan of the input energy, a spectrum of the external current or potential decay in respect of de-trapping energy can be obtained. The energy input is typically a photo- or thermal-stimulation.

The photo-stimulated discharge (PSD) spectrum was used by Brodribb *et al.* in 1973 for the examination of the trapped charges in the single-crystal anthracene and other insulators [76]. In the early 2000s, Mellinger employed the technique in the ultra-violet (UV) range to measure the trapping parameters of a series of polymer electrets [77, 78, 79, 80, 81]. The PSD method has the advantage of a wider-range energy scan and a more precise control over the input energy resolution with the monochromatic

light sources. However, it also presents several difficulties. The experiment needs to be performed in ambient environment for the space-charge electrets, especially for the surface-charge electrets, where the UV light is often scattered by the air. Although the polymeric electret films are quite thin, it may still have some issue of the non-uniform light absorption with different penetration depths [82]. In addition, it has been reported that the photocurrent in UV range due to the photoelectric effect of the electrode can interfere with the real current of de-trapping charges in the electret [83]. The PSD measurement was initially introduced to complement the thermally stimulated discharge (TSD) method, which had been applied extensively in electret studies [54, 55, 84].

The temperature of the electret film is increased linearly in a TSD measurement. During the heating, the space charges become mobile and will be neutralised either at the electrodes or within the sample. Since the 1970s, the TSD measurement was widely used on both the dipolar and space-charge polymeric electrets. Different techniques and better theoretical understandings were developed [33, 64, 66, 85, 86]. In a short-circuit TSD, where the electret film is sandwiched between two connected electrodes, a current can be detected in the external circuit as the consequence of the charge de-trapping. If the electric charges are located on the electret surface, an open-circuit TSD can be used to protect the surface charges. In the open-circuit TSD current measurement, one of the electrodes is not in direct contact with the sample surface, but slightly lifted with a very thin air gap in between. In this way the discharge can still be monitored with the change of the compensating charges on the electrodes. The same current-temperature plots, in principle, can be extracted with the open-circuit TSD measurement. However, the air gap might introduce some variables and unknown factors, from which the accuracy of the results may suffer. In the case of surface-charge electrets, the non-contact TSD potential-decay measurement is a more reliable choice.

The TSD potential-decay setup consists of a heating system that increases the temperature of the electret film at a constant rate and a Kelvin vibrating capacitive sensor (Kelvin probe) as the detector of the potential decay in the sample [87]. The Kelvin probe is essentially an electrode of small area placed near the open surface of a single-side metallised thin-film electret, which is either mechanically excited with a dynamic vibration or periodically shielded with a rotating shutter. The metal electrode of the electret and the probe electrode with the electret and thin air gap in between form a parallel-plate capacitor. Compensating charges are induced on the electrodes

due to the electric field of the electret charges. The vibrating or shielding motion alters the electric field acting upon the probe and thus changes the induced charges on the probe, which is detected as an AC voltage. The Kelvin probe was used to measure the electrical polarisation of thin dielectric materials by Tyler *et al.* in 1955 [84]. In their experiment, the alternating voltage was directly measured by a vacuum-tube voltmeter, which is often referred as the dynamic-capacitor method. However, this method requires an accurate control over the distance between the probe and the electret surface. To overcome the limitation, instead of measuring the AC voltage directly, a DC voltage can be applied to the probe to compensate the induced voltage and to nullify the electric field in the air gap. By monitoring the compensating DC voltage, one can easily obtain the value of the induced voltage on the Kelvin probe [19].

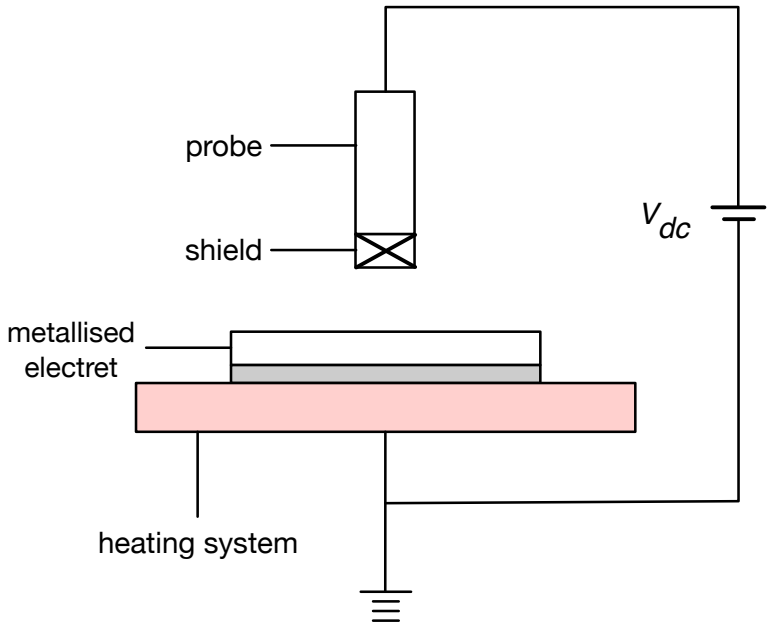

Figure 3.1: A schematic illustration of the open-circuit thermally stimulated discharge (TSD) potential measurement apparatus - V_{dc} is the compensation DC voltage, which is equal to surface potential (V) of the electret.

A general schematic diagram of the setup for the compensation TSD method is illustrated in Figure 3.1. In this method, the voltage applied on the probe (V_{dc}) changes with the potential on the tested surface (V) and the potential decay of the electret can be obtained as a function of temperature [88, 89]. The effective surface-charge density

(σ) of the space-charge electret follows

$$\sigma = \varepsilon_0 \varepsilon V/s, \tag{3.1}$$

where ε is the relative permittivity of the measured electret material and s is the thickness of the electret film. The discharging current (I) in the electret sample can be calculated from the rate of the potential decay as

$$I = C_{air}\frac{dV}{dt} = C_{air}\beta\frac{dV}{dT}, \tag{3.2}$$

in which C_{air} is the capacitance of the air gap between the Kelvin probe and electret surface, and β is the linear heating rate of the thermal stimulation. The non-contact procedure of the TSD potential-decay measurement can minimise the disturbance on the electret surface [19].

Many parameters regarding the electret properties of the measured material can be extracted from the TSD results. For the molecular-dipole electrets, the theoretical evaluation and models of the TSD method were extensively studied and introduced by van Turnhout in [64]. In the case of space-charge electrets, such as PP, the most commonly evaluated quantities are the activation energy (E_{trap}), the attempt-to-escape frequency (ν_{esc}), and the energetic trap distribution ($N(E_{trap})$). Thermodynamic models are often used to describe the progressive charge de-trapping in polymer electrets. Almost all such models operate on the basis of a fundamental condition: the thickness of the electret sample (s) is much smaller than its other dimensions, so that the parameters (electric field, charge density, *etc.*) are functions of the distance to the surface only. In Kelvin probe TSD, the boundary conditions are electrical grounding at the lower surface and zero electric field at the upper surface [88].

As introduced in section 2.1, the trap-modified energy band model considers that the charge transport is restricted to hopping between shallow traps at the transport states [63]. It implies that the charge transit time is much smaller than the mean characteristic de-trapping time, so that the geometric factors can be eliminated. The potential decay is mainly determined by the de-trapping kinetics. Another reasonable assumption is made for the discharge models of disordered media, like polymeric electrets: the dispersive transport regards the trapping levels as a continuous energy distribution [61]. In addition, the E_{trap} is considered a demarcation energy, and any contribution from traps with energy lower than E_{trap} can be neglected at the corresponding temperature.

It means that the E_{trap} is a line between occupied deep traps and shallow traps at transport states [90].

Numerous models were developed based on above approximations. A de-trapping controlled space-charge decay model, introduced by Simmons and Tam in 1973 [91] and further evaluated by Watson in 1995 [92], connected the thermally stimulated de-trapping current ($I(T)$) to the energetic trap distribution ($N(E_{trap})$) of polymeric electrets with:

$$I(T) = C_{air}\beta\frac{dV}{dT} \propto N(E_{trap}). \tag{3.3}$$

One can obtain the trap distribution by plotting the thermally stimulated current (or first-order derivative of the potential decay with respect to temperature (dV/dT)) *versus* the energy (E_{trap}) that is converted from the temperature by:

$$E_{trap} = T(a \cdot lg\frac{\nu_{esc}}{\beta} + b) - c. \tag{3.4}$$

Because a (1.92×10^{-4}), b (3.2×10^{-4}) and c (0.0155) are constants, the E_{trap} is proportional to T [91]. It is a simple and straightforward model to quickly evaluate the trap-depth distribution in some polymeric electrets, including PP. However, it was pointed out by Watson that the model, in comparison to a detailed numerical computation, underestimated the density of *shallow* traps, since the re-trapping influence during the charge drifting was not considered [90, 92].

The characteristic trap depth of PP electrets has been calculated based on different models and experimental measurements. The value is often influenced by the methods, manufacturer and/or sample preparations. It typically falls between 1.02 and 1.11 eV [90, 93, 94]. The characteristic trap energy of the as-received PP electret used in this thesis was evaluated with (3.3) and (3.4) in [95], and it was 1.05 eV. The present work mainly focuses on the influence of different treatments on the electret behaviour of the PP films, thus the *change* of the trap distribution is more relevant than the absolute value of the trap depth.

The TSD results of the polymeric electrets present the charge-decay process with respect to temperature, which makes it possible to correlate the charge de-trapping with different movements of the molecular chains. For example, a decay in the polymeric electret might be from local motion of a polar side group or a start of whole-chain motion due to glass transition. These miscellaneous processes often take place at different

temperatures, resulting in current peaks or potential decays at various locations on the TSD curves. It is important for identifying the structural or molecular association of the traps with each particular energy level, especially for the polymeric electret materials with both dipolar polarisations and space charges, *e.g.* PET [64]. The TSD result can be influence by the heating rate, since the polymer chains need time to respond to the temperature increase. Therefore, it is necessary to keep the heating rate consistent for comparing different measurement results. Furthermore, the concept of Kelvin probe has been incorporated with atomic force microscope (AFM), leading to a Kelvin probe force microscope (KPFM). The technique is used for mapping the charge storage and monitoring the charge transport in a nanoscale on the surface of the electrets, semiconductors, inorganic ferroelectric crystals, *etc.* [96, 97]. In the thin-film polymeric electrets, the charge distribution and transport in the thickness direction are of a broader interest. The methods for charge profiling over the thickness-axis of the electret films will be discussed in the following section.

3.2 Charge distribution—Piezoelectrically generated pressure step

The excess charges can be deposited on the surface or injected in the bulk of the polymeric electret films by different charging methods. The charges are later captured in the surface or bulk traps. For many polymers, the surface and bulk portions of the films exhibit different properties, due to the film manufacturing procedures [98]. Therefore, identifying the location of the trapped charges is important for studying the structural and compositional origins of the traps. In addition, many charging techniques, such as the electron-beam charging and high-temperature corona charging, require the close monitoring of the charging depth. Methods for measuring charge distribution in the electret have been developed to meet the demands of microscopic investigations on the electret properties.

Gross and de Moraes used a sectioning method to study the internal charge distribution of the carnauba wax: the charged wax electret samples were cut into sections of different thickness and measured with TSD method individually to obtain a charge distribution in respect of the depth under the samples surface [54]. It is, of course, a coarse method that involves some problems: first of all, the sectioning may destroy

some charges that are in contact with the blade. Besides, the method is only possible for measuring thick samples, but not suitable for the thin-film polymeric electrets with a typical thickness ranging from tens to hundreds of micrometers. Thus, many other techniques have been developed for profiling the charge distribution in the thickness direction of the thin-film electrets.

Most of the charge-profiling methods rely on the concept that the electret can be *virtually* dissected by activating the sample "slice-by-slice": the inhomogeneous excitations of the charges are established across the sample thickness by means of a sharp pulse or sudden step of a stimulus propagating or diffusing in time through the electret film. The application of the heat pulse was proposed by Collins [99, 100] and Lang [101, 102]. Sessler and coworkers suggested to use a virtual electrode of an electron beam to sweep the charges distributed in the sample [103]. A method that involves decomposing the electret film with a pressure wave was proposed by Laurenceau *et al.* in 1976 [104]. A laser-induced pressure pulse (LIPP) method was introduced in 1982. When a short (< 1 ns) laser pulse is applied to a graphite coated surface of the electret sample, a recoil due to the ablation of the graphite layer can launch a pressure pulse into the sample [105]. Other than the thermal expansion method, pressure pulses generated by acoustic methods using a shock tube [104] or a spark gap [106] and pressure steps with a short rise time produced by a piezoelectric quartz crystal were used to probe the charge distribution in the polymeric electrets [107]. The last method is known as the piezoelectrically generated pressure step (PPS) measurement.

A schematic diagram of the PPS set-up is illustrated in Figure 3.2 [69, 108]. The cable-discharge generator on the left side can produce a square voltage step with a duration of 100 ns that drives the piezoelectric quartz to exert a pressure wave in a step function to the sample surface. If there are surface charges on the electret sample, a spacer is placed between the charged sample surface and the rubber electrode to protect the surface charges. An uncharged film that is identical to the tested polymeric electret sample is usually used as the spacer for a better acoustic coupling. Furthermore, the quartz-oil-sample-spacer-rubber sandwich structure is slightly pressed together to optimise the acoustic contact between different layers. In this way, the pressure step can travel through the sample and spacer with the velocity of sound and compress the sample volume behind the front of the step wave. The inhomogeneous compression of the electret film causes a motion of the electric charges trapped at the location

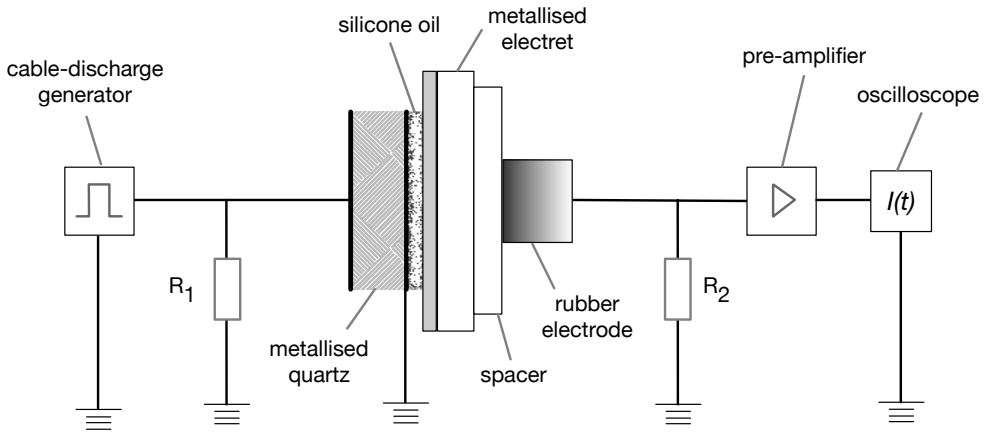

Figure 3.2: A schematic set-up of a piezoelectrically generated pressure step (PPS) method. - Pressure steps generated by the quartz travels through the sample and compresses the sample volume with the bounded electric charges, causing a current signal in the circuit.

where the front of the step wave passes. The movement of the charges in the sample brings about a temporary rearrangement of the induced charges on the electrodes, which can be detected as a current between the rubber electrode and the grounded quartz metallisation facing the sample. Therefore, the current signal can be plotted as a function of time (t) since the pressure step has entered the sample. The spatial charge distribution *versus* thickness (distance to the rear electrode) of the electret film can be obtained by scaling the time domain with the propagating sound velocity (c) of the pressure step in that particular sample material.

The mathematical relations between the current response and the desired charge or electric-field distribution can be derived from the first principles, which was explained in detail by Gerhard in [109]. The resulting equations are applicable for analysing the current signal collected from the pressure steps, pressure pulses and even arbitrary pressure profile experiments. If a step function is used, as in the PPS technique, the electric-field distribution of the sample can be determined directly from the observed current signal [110]. An approximate relation of the short-circuit current, $I(t)$, and the electric field $E(x = ct)$ at location x in a non-polar dielectric sample was shown as

$$I(t) = \frac{\varepsilon_0 \varepsilon A}{s^*}\left(\frac{4}{3} + \frac{\varepsilon}{3} - \frac{2}{3\varepsilon}\right)\frac{p}{\rho_0 c} \cdot E(ct), \tag{3.5}$$

where p is the amplitude of the pressure step and ρ_0 is the density of the tested electret

material. The geometric factor A is the active area of the quartz-oil-sample-spacer-rubber structure, which is typically controlled by the the area of the rubber electrode with a diameter of 4.5-5 mm. The other geometric parameter s^* is the distance between the quartz-electrode contacting the silicone oil and the rubber electrode, that is the thickness of the sample and spacer in sum [108, 109]. The distribution of the electric field and the electric charges can be expressed in simpler forms:

$$E(ct) = C_1 \cdot I(t), \tag{3.6}$$

and

$$\rho(ct) = C_2 \cdot \frac{dI(t)}{dt}, \tag{3.7}$$

respectively. C_1 and C_2 are the experimental constants related to the electret material properties (ε, ρ_0, c), the pressure function (p), and the geometry of the set-up (A, s^*) [110, 111]. The values of C_1 and C_2 can be obtained by calibrating the measurement system with identical samples whose charge distributions are known. However, for tracking the changes of charge distribution on one single sample or on multiple samples in the same material and geometry, the exact values of C_1 and C_2 are not necessary, as long as the measurement conditions are consistent for all tests.

The resolution of the PPS method relies on the rise time of the pressure step, which is approximately 1 ns for the set-up used in the present work, and it is also limited by the sound velocity of the sample material. For a typical PPS measurement, the resolution is around 2 μm. Thus, the method is not suitable for the ultra-thin electret films [69, 108, 110]. Because PPS is a non-destructive method, the charge distribution of the electret sample can be probed with many pressure steps sent in sequence. A better accuracy can be achieved by averaging the results collected from thousands of pressure steps.

3.3 Relevant electret properties

As discussed in previous chapters, the dipoles in the polar polymers originate from the electron withdrawing and donating effect between atoms with different electronegativities [20]. The traps for capturing electric charges in the inorganic semiconductors are mostly from the energetic interruptions of the impurities and structural defects on the conduction and valence bands. The nature of the traps in the polymeric electrets is

much more complex. Early theories in the 1970s [112, 113] suggested multiple trapping levels associated with different molecular structures in polymers. Recent developments on the computer simulation of charge storage and transport in polymer electrets agreed with some existing theories, but also offered additional deeper understandings on the subject.

3.3.1 Compositional and structural association of traps

On the atomic level of the polymer molecules, the trap depth and binding force to charges with different polarities are influenced by the electronegativity and size of the atoms. One typical example is the fluorine atoms in PTFE. Recent computations by Sato *et al.* [114] showed that the electron traps in PTFE have equal contributions from the carbon and fluorine atoms, whereas the hole traps are mainly localised to the carbon atoms in the backbone of the molecular chains. The high electronegativity of fluorine atoms in the fluoropolymers is believed to cause their severe asymmetrical stabilities for charges of different polarities: the negative charges are more stable than the positive charges in the fluoropolymer electrets.

The influence of the chemical composition of the polymer chains on trapping energy extends to groups of atoms. Simulations run on cyclic transparent optical polymers (CYTOP) with various end groups revealed the association between the depth of electron traps and the electron affinity of the end groups. The results were in qualitative agreement, however not quantitatively comparable with the experimental data, because the simulated molecules had only few repeat units standing alone without interaction with the adjacent molecules. As a result, the shorter polymer chains in the simulation experienced a stronger terminal effect from the end groups, due to the atomic ratio of the end group and the whole molecule. In real polymers, the macromolecular chains always entangle with each other and form structures with various degrees of order, which leads to heterogeneous local morphological populations, *e.g.* lamellar crystallites, amorphous regions and interfaces [115].

It has been reported that the electret properties of polymers show a significant dependence on the spatial conformation of the molecular chains and the packing density. Based on the trap-modified energy band model (section 2.1.2) and the quantum mechanical principles, it was shown in [114] and [116] that the holes (positive charges) in the PE electret hop between the localised states (traps) near E_v (mobility edge) created

by the polaronic effect on the molecular chain. In the amorphous PE, the characteristic length of the localised states for the hole transport roughly matches the Kuhn length of PE chains. Kuhn length is the length of the hypothetical free-joined segments that allows the polymer chain to be considered as a random-walk or self-avoiding walk model [117]. In the crystalline region of PE, the trap-modulated hole mobility increases with the length of the simulated molecular chains. It is worth noticing that, when the chain length reaches the thickness of the lamellar crystallite in PE, the mobility and activation energy for the hole transfer are in reasonable agreement with the experimental values. The computation results indicate the significance of the system morphology in the electret properties of polymers. Similar phenomena were observed in experiments on the polymer electrets with different crystalline structures [13, 118, 119]. Because the morphology of the polymer electrets is determined by the folding and packing of many molecular chains, the traps associated with the crystalline and amorphous structures are highly sensitive to the chain mobility of the polymers. Therefore, given the similar chemical composition and molecular structure, the polymers with higher thermal stability generally have a better charge stability.

Besides the atomic composition and chain conformation, which are intrinsic properties of the polymer molecules *per se*, the traps of a polymer electret are highly influenced by the impurities in the system. The impurities in a polymer can be the oxidation products, additives from the processing, by-products and catalysts from the polymerisation, and even random chemical contaminations mixed into the system during the manufacture. The traps from the chemical impurities in the polymeric electrets are usually deeper than the traps formed by the morphological disorders, according to the computation based on the density function theory (DFT) in [120]. The result shows great consistency with the calculation by Bauser, which concluded that the traps associated with structural defects are shallower than that with foreign chemicals [63]. Thus, in order to improve the charge stability by increasing the trap depth of the space-charge electrets, different types of "impurities" were intentionally and strategically introduced to the polymers by chemical reactions [121, 122, 123], doping, and mixing nanoparticles to form the nanocomposites, *etc.* [124, 125]. The impurities of foreign chemicals and disorders on the polymer chains, such as double-bonds, chain ends and bulky side groups, have the tendency to move to the surface during the film processing. There are pronounced differences between the surface and bulk traps in many polymer electrets,

for instance, PE, PET, FEP and PP [126, 127]. Therefore, the surface of the thin-film polymers often plays an important role in terms of the electret properties, especially for surface charges.

Owing to the aforementioned association between the traps and the compositional and structural properties, characterisation on the material properties of the polymers is often implemented in the electret research. The features on the surface of the polymer film, which might serve as the potential surface charge traps, can be detected with the scanning electron microscope (SEM). The contributions on deep traps from the impurities of foreign chemicals intentionally or accidentally introduced to the electret system are identified with the Fourier-transform infrared spectroscopy (FTIR). In addition, the differential scanning calorimetry (DSC) is commonly used to reveal the thermal properties and degree of crystallinity of a polymer material, and the polarised light microscope (PLM) is a simple and quick method for observing the crystalline morphology in polymers. The principle and purpose of the SEM, FTIR, DSC and PLM experiments will be briefly introduced in the section below.

3.3.2 Characterisation of composition and structure in polymers

3.3.2.1 Scanning electron microscopy

SEM is an important and versatile tool for the high-resolution analysis of surfaces and often used in electret studies. In electron microscopes, the role of the visible light in the optical microscopes is played by the electron beam emitted from a thermionic, Schottky or field-emission cathode source. The electrons are accelerated through a high voltage difference for a high particle energy, typically ranging from 0.1 keV to 50 keV. The higher the particle energy, the better the resolution the electron microscope can potentially achieve. For changing the trajectory of the electrons to focus the electron beam, electron-optical lenses with carefully shaped magnetic fields based on Lorentz force are used to replace the transparent glass lenses in the optical microscopes. In SEM, an additional set of scan coils and scan generator circuit is coupled to the instrument for changing the trajectory of the incident beam to scan the specimen line by line. An SEM is usually equipped with multiple detectors to monitor the particles emitted from the specimen upon interactions with the primary electrons from the accelerated electron beam.

The particles emitted from the specimen typically consist of the secondary electrons (SE), backscattered electrons (BSE) and Auger electrons. The SE are the electrons that escaped from the atomic orbitals of the sample molecules upon the inelastic collision with the primary electrons. The BSE are the decelerated electrons undergone multiple scattering through large angles and energy losses, due to their elastic interaction with the atomic nucleus. The energy of BSE ranges between 50 eV and the energy of the original primary electrons, which is higher than that of the SE. When the atomic electrons of a higher energy level are de-excited and fill the vacancies on a lower-energy orbital caused by the primary electron interaction, the excessive energy of the atomic electrons can be converted to X-ray radiation or transferred to other atomic electrons and leave the specimen as the Auger electrons.

Based on the principle of the interactions, different properties of the surface can be obtained by analysing the detected electrons. The SE are often collected on a tilt angle to the specimen surface, so that the emission from small particles, edges and shadow contrast are enhanced. Thus, the SE are very suitable for the investigation of the surface topography. The detection of BSE also requires a tilt angle from the surface, so it is possible to be used for the surface topographic studies. But most importantly, the backscattering coefficient of the BSE shows strong dependence on the mean atomic number of the local specimen, which manifests the contrast on the resulting image. This allows phases with different elements to be recognised. The X-ray and Auger electrons are mostly utilised for elemental analysis [128].

The resolution of SEM is directly related to the energy of the electron beam, but it is also influenced by the density and quality of the specimen and imaging mode. The SEM instrument used in laboratories usually can achieve resolutions of a few tens or hundreds nanometers. The ultra-high resolution model available from Hitachi is capable of achieving a resolution of 0.4 nm. The surface of the polymeric electrets plays a significant role in terms of the electret properties as discussed in the previous section. The high-resolution atomic analysis and surface topographic investigations on thin-film polymer electrets were implemented with SEM, and some traps with greater activation energies were attributed to the characteristics on the surface [70, 122, 129].

3.3.2.2 Fourier-transform infrared spectroscopy

The atomic composition of a surface can be analysed with SEM in a very high spatial resolution. However, it is a task for FTIR to examine how the atoms are connected and which functional groups the atoms form. FTIR is a technique based on the vibrations of the atoms in a molecule. The vibrations are caused by the atoms moving out of the present plane or by varying the distance between two atoms (bond length). The former movement is called "bending" and the latter "stretching". Each particular type of the atomic vibrations in a particular molecular environment requires a specific energy. Therefore, when an infrared radiation is passing through a sample, some fractions of the incident radiation will be absorbed at some particular energies, resulting in a FTIR spectrum of the sample. The peaks in an absorption FTIR spectrum correspond to the vibrations of the atomic groups in the sample.

The quality of the results depends on the sensitivity of the FTIR instrument and the concentration of the atomic groups of interest. If the chemical composition of the sample *surface* needs to be analysed, the attenuated-total-reflection infrared (ATR-IR) spectroscopy is a suitable tool. The ATR-IR spectroscopy utilises the total internal reflection phenomenon: by adjusting the angle of the incident infrared beam, one can manage to only allow the beam to penetrate a fraction of the wavelength beyond the sample surface before being reflected to the detector [130]. In this way, only the molecules on the sample surface participate in the measurement. The information of the chemical composition of the electret surface can be collected, while that of the bulk is excluded.

3.3.2.3 Differential scanning calorimetry

The thermal stability and characteristic thermal transitions of the polymer electrets are critical for their performance in terms of the charge stability. For the thermal analysis of polymer materials, DSC is one of the most widely used techniques. In DSC the sample substance and the reference are subjected to a controlled temperature program, while the heat flow into the sample and the reference pans are monitored. When a thermal transition or a phase change takes place in the sample, more heat or less heat will flow into the sample pan. The thermal properties of the sample can be extracted from the difference in the heat flow rates of the two pans as a function of temperature

[131]. The concept can be technically realised in two different ways, namely the power compensation DSC and the heat flux DSC. The power compensation method is highly sensitive and excellent for academic studies, but the calibration is not easy and it frequently suffers from the unstable baseline. The heat flux DSC is more robust. The simplest models of heat flux DSC are able to carry out tasks of qualitative controls and the most sophisticated models can match the sensitivity of the power compensation DSC [132].

The charge mobility and trap parameters of the polymer electrets are highly dependent on the chain mobility. Characteristic temperatures for the molecular chain mobility in polymers can be obtained with the DSC measurements: the glass-transition temperature (T_g), the melting temperature (T_m) and the crystallisation temperature (T_c). The crystallinity (X_c) of the sample, that is, the percentage of the crystalline phase in the polymer, can be calculated from the enthalpy of fusion (melting) (ΔH_f) during the DSC test, based on

$$X_c = \frac{\Delta H_f}{\Delta H_{f100}} \cdot 100\%. \tag{3.8}$$

The ΔH_{f100} is the enthalpy of fusion in a 100% crystallised sample of the same polymer material [133].

3.3.2.4 Polarised light microscopy

The structure of the crystalline and amorphous regions can be directly observed with PLM. A PLM is a transmission optical microscope equipped with a rotatable stage, a polariser in the illumination system, and an analyser between the objective lens and the eyepiece. The polariser and analyser are polars, which can selectively transmit light that is polarised in one specific plane. The transmitted polarisation planes of the two polars are usually placed to be perpendicular to each other, that is the so-called "cross-polars". With such arrangement, the view of an ideal isotropic specimen will be completely dark, because the analyser cannot transmit light that has come through the polariser. However, when a birefringent material (anisotropic) is subjected in the view of PLM, the light waves passing through the sample can be considered as divided into two polarisation planes that vibrate at a right angle to each other. Thus only a fraction of the light from the illumination source can be transmitted *via* the analyser to the observer [134].

The most typical crystalline structure in polymers is the spherulite, which appears as a bright "Maltese cross" with the arms lying parallel and perpendicular to the extinction direction of the polars under PLM, as shown in Figure 3.3 [135]. The cross figure remains stationary upon rotating the specimen in its own plane, implying the radiating units of the polycrystalline spherulite are crystallographically equivalent. The spherulites in polymers are composed of lamellar crystallites by fibrillation due to the interfacial concentration instability [136] or by splaying and branching into multiple generations of lamellae [137]. The polymer chains in the lamellae are usually packed with the orientation perpendicular to the lamellae face, *i.e.* along the thickness direction of the lamellae. Thus, the polymer spherulites are birefringent owing to the periodically ordered microstructures. The refractive index of the birefringent spherulites depends on the direction of the electric field in the light, which is the reason that the spherulites appear as the Maltese-cross figures under the cross-polar PLM [134, 138].

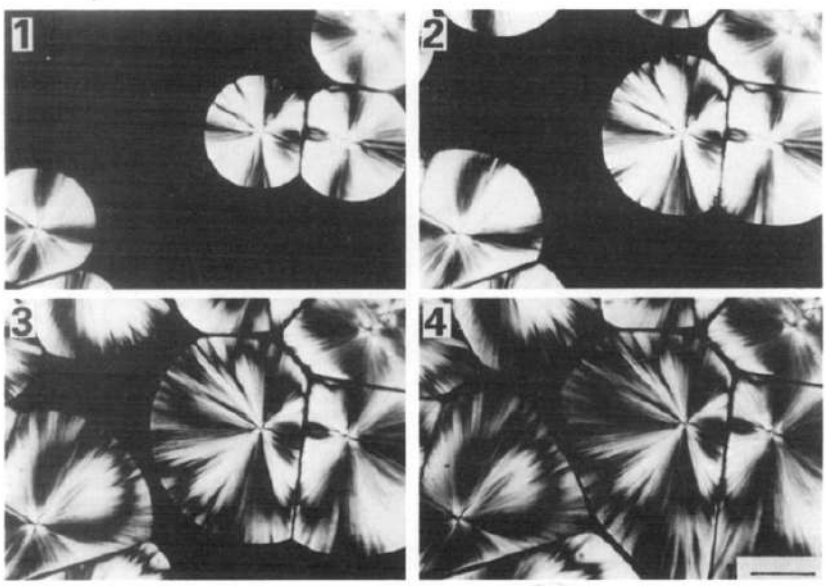

Figure 3.3: Views of the spherulites of polypropylene under polarised light microscope (PLM). - The spherulites grew *in situ* by isothermal crystallisation from melt, and the images were taken after (1) 21.2 h, (2) 31.8 h, (3) 46.0 h, (4) 70.0 h. The scale bar is 200 μm [135].

The resolution of the PLM is limited by the wavelength of the visible light, but it is sufficient for visualising even small spherulites with diameters of several micrometers.

PLM is a useful tool for analysing the morphology-related traps in polymers. If the neighbouring spherulites are nucleated simultaneously, there will be a planar outline between them. Otherwise, the boundary where they impinge is going to present a hyperboloid of revolution [138]. It is possible to perform *in situ* crystallisation experiments under PLM that has the incorporated heating system as illustrated in Figure 3.3. Many studies have been conducted with the aid of PLM, regarding the influence of the size and density of spherulites on the electret properties of polymers [118, 139, 140].

3.3.3 State of the art on polypropylene electrets

The performance of the PP ferroelectrets and electret filters relies on the charge stability. For enhancing the charge stability of PP, it is of great importance to understand its charge storage and transport mechanisms. PP has one of the simplest compositions among polymers but many versatile structures. Although it has one more methyl group on the repeating unit than PE, PP films are believed to be cleaner than those of PE. The structures of PP are very diverse in terms of the molecular tacticity, spatial conformations and crystalline structures. Therefore, studying the correlation of the compositional and structural properties to the parameters of the associated traps in PP can be a fundamental step. It can offer a general guidance to modify any other existing polymeric electret materials and to strategically design new materials or structures for electrets. In addition, the charge storage and transport in PP is also extremely relevant for its insulator applications [12].

The charge-mobility and electrical-conduction properties of PP were investigated under DC voltages to mimic the environment of the HVDC cable insulation applications [141, 142]. The pulse electro-acoustic (PEA) method was implemented to monitor the charge transport under various electric field and at different temperatures [14, 143]. The storage and transport of the space charges trapped on the surface or in the bulk of the PP films were modelled and experimented as well [144, 145]. The charge trapping behaviour and charge distribution were significantly influenced by the chemical composition of the PP molecular chains, *i.e.* PP as a homopolymer, block-copolymer or random-copolymer with ethylene monomers [13, 14, 141].

The strong association of deep traps with the foreign chemicals in the polymeric electret systems has been discussed in previous sections. The foreign chemicals usually

consist of the impurities mixed into the system during manufacturing and certain chemical structures that are intentionally introduced to the electret by chemical treatments. Experiments with wet treatments and molecular-layer depositions on the surfaces of fluoropolymers have shown promising results. The chemical treatments were able to close the gap of the charge stability between positive and negative charges on PTFE and FEP surfaces [121, 146, 147]. The studies of the influence of titanium tetrachloride ($TiCl_4$) and orthophosphoric-acid (H_3PO_4) treatments on the surface charge stability have been extended to LDPE electrets as well. The treatments can increase the thermal stability of both the positive and negative surface charges on LDPE films by at least 40 K. The significant improvements were attributed to the newly-formed deep traps from the "island" structure of foreign chemicals on the treated surfaces [122, 148].

Similar liquid and gas treatments were carried out on PP cellular ferroelectrets with the hydrofluoric acid (HF) solution and fluorine (F_2) gas mixture, respectively. Solutions and gas mixtures with series of concentrations, different treatment conditions and combinations of supplementary chemicals were experimented to optimise the modification on PP. Good results were obtained on the PP cellular ferroelectrets, whose thermal stability and piezoelectric activity were both enhanced. The improvement was due to the increase of deeper traps for surface charge storage and the decrease of Young's modulus of the foam structure [149, 150, 151, 152, 153]. However, the fluorination with HF and F_2 might be hazardous. The fluorine in the treated PP electrets may not be as stable as that in the fluoropolymers, which can be released to the environment more easily. Besides the foreign chemical agents, plasma can also be used to treat PP electrets. It was reported that the PP surface can be selectively functionalised with specific oxygen-containing functional groups after the underwater plasma treatment [154].

The etching technique was used for studying the charge storage properties of PP electrets, which utilised the different reactivities of the amorphous and crystalline phases upon contact with strong acids, such as permanganic acid, chromic acid and sulphuric acid. The method was primarily used to identify the traps associated with amorphous and crystalline phases and their difference in the activation energy level. It was reported that both the trap depth and trap density were influenced by etching on the PP surfaces [123, 155]. However, the changes in the surface-trap parameters after the etching treatment cannot be fully attributed to the removal of the amorphous phase on the surface. It is because the etching processes also leave some chemical residues on

the treated PP surface, which can serve as deeper traps to improve the surface charge stability thereof [156, 157].

The etching method for correlating the activation energy of traps and their locations in spherulites was invasive and complex with the intertwined chemical effects. Another technique was introduced in [118] using the Sudan-blue dye particles (with a size of 2.7 μm). The oppositely charged dye particles were attracted by the electret charges trapped in the spherulitic PP. The trap distribution on the spherulites can be visualised under the optical microscope in this way, and the trap depth was examined by means of thermal stimulation. It was concluded that the number of the shallow traps decreased with the spherulite size increasing. There have been many discussions regarding the contribution to charge trapping from the amorphous and crystalline regions. It was discovered in the morphology studies of polymers that the surface of the commercially produced polymer films were covered with a thin amorphous layer [98, 158]. The surface and bulk traps in PP electrets were investigated in [127] with the TSD current measurement incorporated with the corona charging and electron beam charging, respectively. The energy and distribution of the traps on the surface and bulk are influenced by their morphological differences.

The density and depth of the traps in the PP electrets are influenced by the size and number of the spherulites, but also by the degree of crystallinity. The experimental results show that the trap density usually decreases when the spherulites are bigger in diameter and fewer in number [118, 144, 159]. The difference in the size, number and crystallinity of the PP spherulites are commonly achieved by means of mechanical and thermal treatments. The treatments include stretching the films to different ratios, annealing at different temperatures [119, 160], isothermal crystallisation for longer or shorter times [161], cooling the sample from melt with various rates [119, 159], quenching [162], or adding nucleating agents [139]. The charge storage and transport properties of PP also vary with the type of spherulites (β or γ) that results from the copolymerisation of PP with PE [13].

Besides the spherulite, there exists a less-common crystalline structure in PP called "transcrystalline" [98, 156]. The transcrystalline structures of many polymers were studied by the morphology and polymer composite communities [164, 165], after the discovery of the transcrystalline structure of polyurethane in 1952 [166]. It is a surface/interface crystalline structure that stems from the surface and grows along the

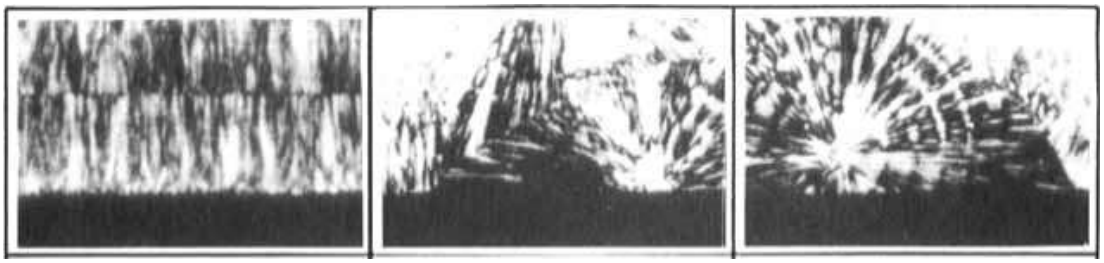

Figure 3.4: Polarised light microscope (PLM) images of the transcrystalline and spherulitic polypropylene. - Polypropylene crystallised against surfaces of PTFE (left), FEP (middle), and Glass (right) [163].

normal direction of the surface without the lateral growth. The transcrystalline structure is often observed at the interface of the fillers and matrix in polymer composites, due to the high concentration of heterogeneous surface nuclei. The hypothesis was first proposed by Schonhorn [167] and later carefully examined and proved by Hata *et al.* [163]. When a PP film is crystallised from melt against a moulding surface, different crystalline structures can be formed depending on the concentration of the nuclei on the moulding surface. If the surface-nucleus concentration is low, the crystallites of PP can expand from the nucleating centre to all directions into the polymer film, resulting in a regular hemispherical spherulitic structure (before the neighbouring spherulites impinging). In the case of densely packed surface nucleating points, the crystallisation can only propagate in the normal direction of the film surfaces, and any growth to the lateral directions is forbidden by the immediate neighbour-nuclei. Thus, to some extent, the transcrystalline structure in the PP films can be understood as a special one-dimensional spherulite that originates from the surface and propagates solely on the thickness direction of the film. Microscope images of transcrystalline and spherulites of PP are shown in Figure 3.4 [163].

The heterogeneous nuclei on the moulding surfaces are provided by the surface roughness: the surface nuclei concentration is high when the surface is rough and low when it is smooth. The transcrystallisation phenomenon of PP is very relevant to the electret research, because the most commonly used moulding surfaces for producing transcrystalline and spherulitic structures are PTFE and FEP, respectively [163, 168]. When the PTFE and FEP films are thermally fused onto a PP film for building electret devices or used as a non-sticky substrate under the melted PP, different crystalline

structures are formed in accordance to the moulding surfaces. Therefore, it is of great importance to investigate the electret properties of these two different crystalline structures in PP films.

3.4 Scope of the thesis

In the present thesis, the influences of the foreign chemicals and morphological structures on the charge storage and transport of the PP films are discussed. The experimental results and interpretations are based on the thin-film PP electrets, but also of significant concern to polymeric electrets in general, especially polyolefin electrets.

In chapter 4, the effects of the surface chemical modification on PP electret film with H_3PO_4 will be presented and analysed. The surface charge stability of the PP electrets with and without the chemical treatment will be compared. The influences of the treatment on the surface trap parameters, including the energy, density and distribution of traps, will be presented. In addition, the mechanism of the deeper trap formation associated with the chemical and physical modifications will be discussed, which is necessary for the design and optimisation of PP electrets in the future.

Regarding the morphology-related electret properties of PP, the spherulites have been extensively studied in the past decades. However, the effort devoted to the transcrystalline structure of PP electrets is insufficient in comparison. The charge storage and transport behaviour of the transcrystalline PP will be investigated in comparison with that of the well-known spherulites in chapter 5. The charge distribution under different conditions in the single- and double-layer transcrystalline PP electrets will be discussed in chapter 6. It can provide the important insights into the difference of the charge trapping behaviour in the intra- and inter-crystalline (spherulitic) regions. The research on the simple and highly-ordered transcrystalline structure can be a fundamental step for understanding the charge storage and transport in the semicrystalline polymeric electrets at large.

4

Surface chemical modification of PP electret

4.1 Chemical treatment on PP surface

4.1.1 Treatment procedure

The oriented PP films (OPP-TSS) with a nominal thickness of 50 μm are supplied by Pütz Folien. 10 nm chromium (Cr) and 100 nm aluminium (Al) were deposited on one side (outer side of the film roll) of the PP films in the Leybold Univex 350 vacuum system with the INFICON SQC-310 deposition controller for sufficient electrical contact during the corona charging and electrical measurements. Some of the metallised films were used as-received for reference, named "non-treated" samples, and the rest were treated with H_3PO_4 on the non-metallised surface—the so-called "chemically treated" samples.

The treatment was carried out with the arrangement in Figure 4.1: the open surface of the PP film was covered with 12 ml of 85% H_3PO_4 solution from Carl-Roth and the metallised surface was *not* in contact with the acid solution. Because of the excellent chemical resistance of PP at room temperature, the treatment needs to be performed at elevated temperature. The PP films and the H_3PO_4 solution were kept on the heating system (PRAZITHERM) at 120 °C for 24 hours with a covering lid for safety. Afterwards, the PP films were cooled slowly down to room temperature together with the H_3PO_4 solution, and then thoroughly rinsed with distilled water to remove the H_3PO_4. After the samples were dried overnight, they were annealed at 160 °C and

subsequently quenched to room temperature in order to eliminate any differences among samples in their thermal history during the acid treatments.

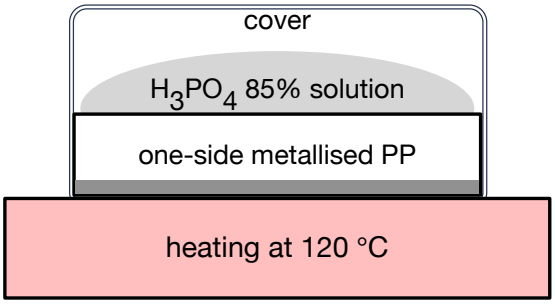

Figure 4.1: An illustration of the chemical treatment on polypropylene surfaces. - The non-metallised surface of the PP film was covered with H_3PO_4 solution and the films and chemicals are heated together at 120 °C for 24 hours.

4.1.2 Compositional and structural characteristics

The Bruker Alpha-P FTIR device was used in the ATR-IR mode to determine the chemical composition of the sample surfaces. The resulting spectra can reveal the compositional information of the open surface of the PP films, while the spectroscopical information of the sample bulk was excluded. The characteristic absorption bands at the higher wavenumber range that represent the chemical groups of the PP molecules remain at their positions after the chemical treatment. However, the baseline of the spectrum of the chemically treated PP is "lifted" up between 900 and 1250 cm^{-1}, which can be observed in Figure 4.2. This wavenumber range coincides with the extra absorption band on the spectrum of the H_3PO_4-modified LDPE surfaces in comparison with that of the non-treated ones. The band was attributed to the phosphorus-containing structures on the treated LDPE [122]. But, unlike LDPE, isotactic PP exhibits its own regularity bands in the range of 700-1400 cm^{-1} [169]. Therefore, in the case of the chemically treated PP, the regularity bands and the extra absorption bands from the chemical modification merge and appear as a lifting of the baseline.

For analysing the chemical compositions that contribute to this phenomenon, the extra bands (red solid line with symbols) are isolated from the PP regularity bands and shown in Figure 4.2. The absorption band between 900-1125 cm^{-1} represents the asymmetric P−O−C stretching, while the 1050-1165 cm^{-1} band is from the aliphatic P=O

stretching [130]. Such results indicate that the phosphorus- and oxygen-containing functional groups from H_3PO_4 are covalently bonded to the PP molecules *via* chemical reactions. The heating during the chemical treatment and the subsequent annealing have no contribution in the change of the ATR-IR spectrum of modified PP, which is explained in [95].

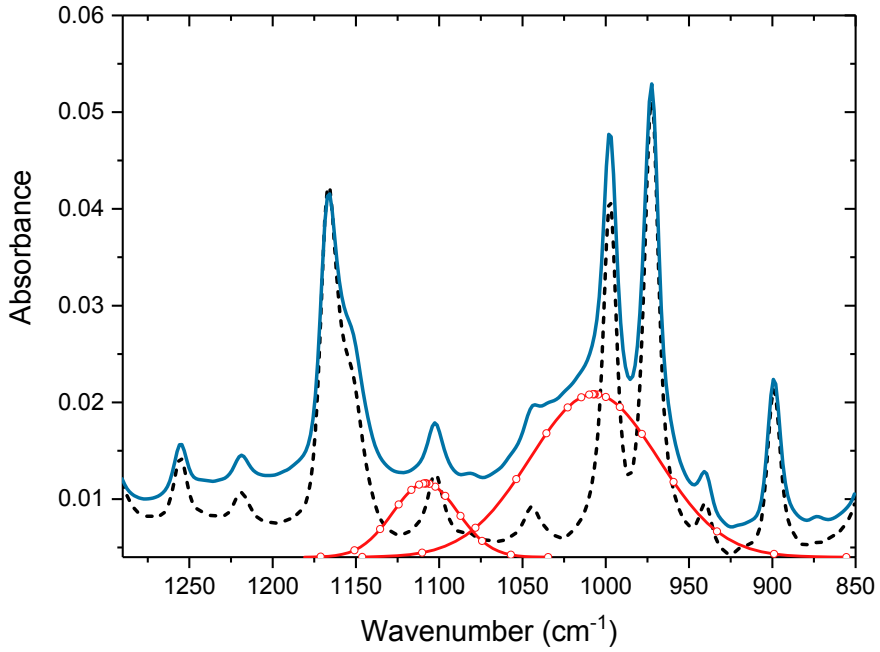

Figure 4.2: Attenuated-total-reflection infrared (ATR-IR) spectra of non-treated and chemically treated polypropylene films. - The spectrum of the chemically treated PP (blue solid line) is lifted from the spectrum of the non-treated PP (black dashed line), because of the extra absorption bands (red solid line with symbols) of the phosphorus- and oxygen-structures.

Besides the absorption bands between 900 and 1250 cm^{-1} on the ATR-IR spectrum of the H_3PO_4-treated surface, the phosphorus- and oxygen-containing groups also bring some topographic features onto the PP surface. The micrographs of the PP surfaces in Figure 4.3 were obtained using a Zeiss Ultra/plus 55 SEM, which exhibit the detailed topographic feature of the chemically modified surface (b) in comparison with the as-received surface (a) of the PP films. Because PP is an insulating material, the surface under observation was previously coated with 5 nm of gold for the surface conduction of the electron beam in SEM. As shown in Figure 4.3, the SEM image of the non-treated PP surface is smooth without any special features. The surface

modified with H_3PO_4 displays the island-like structures with diameters of 90-450 nm and number densities of 1.5-2.0 μm^{-2}. Similar island structures were observed on the H_3PO_4-treated LDPE surface as well [122]. The configurational and/or compositional disorders at the phosphorus- and oxygen-islands can create the energetic disruption on the band structure of the polymeric electrets and capture charges as deeper foreign-chemical traps [95].

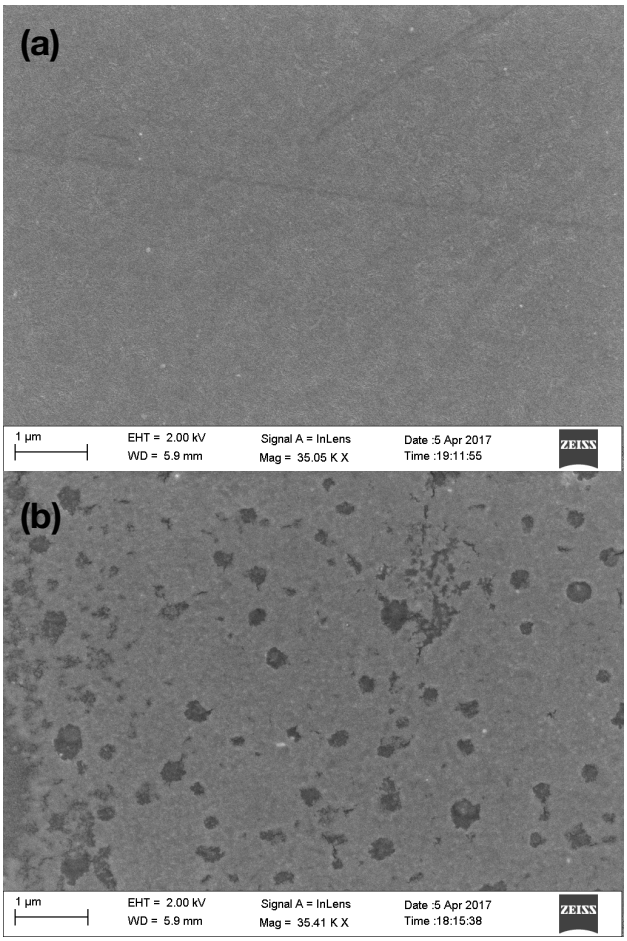

Figure 4.3: Scanning electron microscope (SEM) images of the non-treated and chemically treated polypropylene surfaces. - (a) The smooth non-treated PP surface without any special features; (b) The H_3PO_4-treated PP surface with island-like structures.

The characteristic thermal transitions and degree of crystallinity of the non-treated and chemically treated PP films were measured with a DSC set-up from NETZSCH

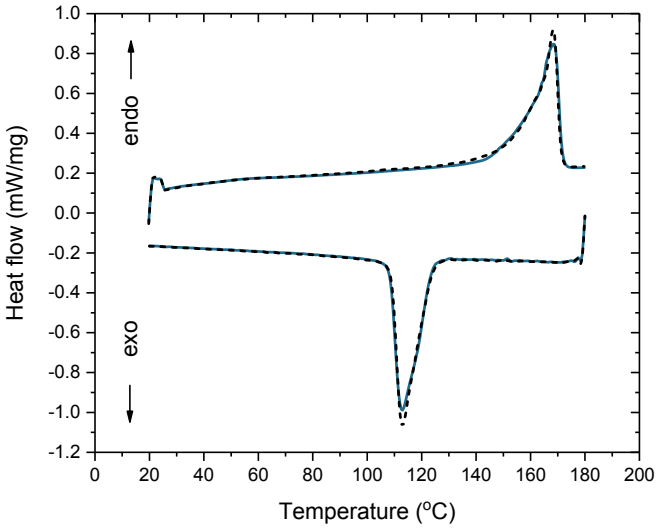

Figure 4.4: Differential scanning calorimetry (DSC) curves of the non-treated and chemically treated PP films - The two curves (non-treated sample in dashed line and chemically treated sample in solid line) are identical, which indicates that the treatment and the subsequent annealing process do not influence the thermal properties and crystallinity of the PP films.

(model 214 Polyma) under a heating and cooling rate of 5 °C/min. Approximately 5 mg of the sample was used in each DSC test. The DSC results of the non-treated and chemically treated PP samples in Figure 4.4 indicate that the thermal properties of the film are not influenced by the treatment. This is because only the surface of the PP film was modified by the H_3PO_4 treatment, whereas the bulk as the majority of the film volume remains at its original chemical composition. In addition, the thermal process during the subsequent annealing and quenching procedures is very similar to that during the manufacture (extrusion and film forming) of the PP films. Therefore, the thermal transitions on the curves—melting and crystallisation—during the first heating and cooling cycle of the non-treated and H_3PO_4-treated PP appear to overlap completely with each other. It is also verified that the subsequent annealing of the treated samples can eliminate any possible difference among the treated samples in the thermal history during the treatment. The melting and crystallisation temperatures (T_m and T_c) of the non-treated and chemically treated PP are extracted from the DSC results and their degree of crystallinity (X_c) is calculated with (3.8), which are all listed in Table 4.1. The differences between their X_c (1%) in the table is within the typical

Table 4.1: The melting and crystallisation temperatures (T_m and T_c) and degree of crystallinity (X_c) of non-treated and chemically treated PP samples

Samples	T_m **range**	T_m **peak**	T_c **range**	T_c **peak**	X_c
non-treated	161-171 °C	168 °C	124-109 °C	113 °C	44.8 %
chemically treated	160-172 °C	168 °C	124-108 °C	112 °C	45.8 %

error of the DSC measurements on identical PP samples. Therefore, the main influence of the chemical treatment on the PP samples lies in the chemical and topographic characteristics on their surfaces.

4.2 Influence of chemical treatment on PP electret

4.2.1 Charging and thermally stimulated discharging

The charging of the PP electrets was performed at room temperature in the ambient environment with a corona triode apparatus as illustrated in Figure 2.3 for 15 seconds. The corona needle was positioned 20 mm above the open surface of the PP film and the control grid was 7-8 mm above the sample that was fixed into a ring-shaped holder. The corona voltage (V_C) was set at ±12 kV for all the samples and the control-grid voltage (V_G) was set at ±500 V, ±1 kV, ±2 kV and ±3 kV to obtain different surface charge densities on the PP electrets: the expected values of the charge densities calculated with (3.1) are $\pm 1.9\times10^{-4}$, $\pm 3.9\times10^{-4}$, $\pm 7.8\times10^{-4}$, and $\pm 1.2\times10^{-3}$ C·m^{-2}, respectively.

The ATR-IR and SEM results confirmed that the modifications in the chemical composition and topographic features took place on the surface of the H_3PO_4-treated PP films. The surface-charge stability of the chemically treated and non-treated PP was studied and analysed with the TSD measurements. The deposited surface charges on the PP electret decayed with the temperature increasing at 3 °C/min in the TSD set-up, while the surface potential was recorded with the non-contact electrostatic voltmeter (model 314B provided by TREK) placed 4-5 mm above the sample surface as a function of the temperature in the range of room temperature to 160 °C (shown in Figure 3.1). The accuracy of the potential measurement is within 20 V. Due to the geometry of the ring-shaped sample holder, the initial surface potential (V_0) of the PP films was 3-4% lower than the grid voltage and it was normalised to the grid voltage for a more

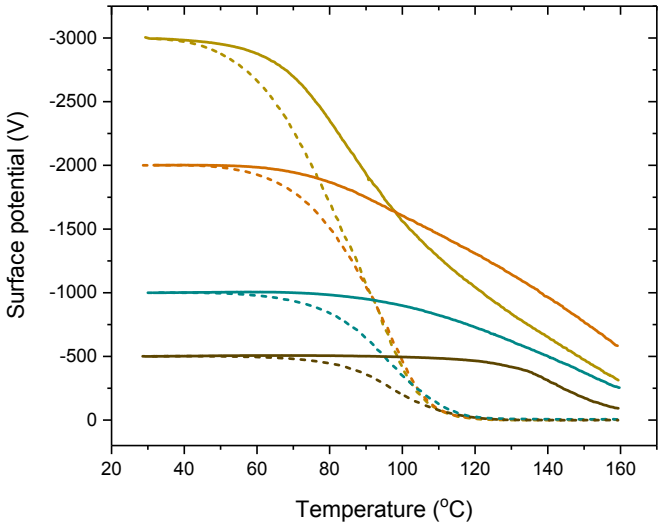

Figure 4.5: Thermally stimulated discharge (TSD) curves of the negatively charged non-treated and chemically treated PP electrets. - The plots of the surface potential decay as a function of temperature in the non-treated (dashed line) and chemically treated (solid line) PP films charged to −500 V, −1 kV, −2 kV and −3kV.

accurate data processing. Each TSD curve presented in the graphs was the average of the results from 3-5 individual samples.

Samples with different surface potentials were measured with the TSD set-up to investigate the influence of the surface-charge density on the H_3PO_4-treated and non-treated PP electrets. The results of the surface-potential decay as a function of temperature are plotted in Figure 4.5 for the negative surface charges and in Figure 4.6 for the positive surface charges on the chemically treated (solid line) and the non-treated (dashed line) PP electrets. It is obvious that the H_3PO_4 modification on the PP surface can significantly improve its surface charge stability. The TSD curves of all the chemically treated PP electrets are clearly shifted right to higher temperatures compared to those of the corresponding non-treated PP in Figures 4.5 and 4.6. In addition, the negative surface-charge stabilities are influenced more by the H_3PO_4 modification than the positive ones.

One characteristic parameter commonly used for describing the charge stability of an electret in the TSD measurements is the half-value temperature ($T_{1/2}$). It is the temperature where the surface potential decays to half of the initial value. The $T_{1/2}$s of all the chemically treated and non-treated PP electrets, as well as the improvement

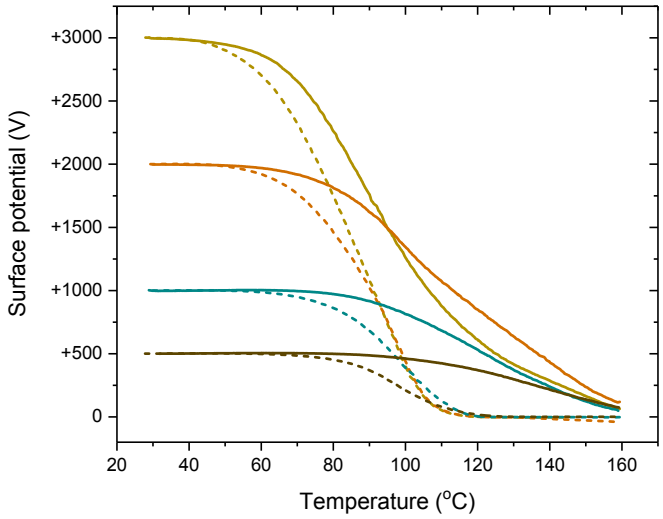

Figure 4.6: Thermally stimulated discharge (TSD) curves of the positively charged non-treated and chemically treated PP electrets. - The plots of the surface potential decay as a function of temperature in the non-treated (dashed line) and chemically treated (solid line) PP films charged to +500 V, +1 kV, +2 kV and +3kV.

of the $T_{1/2}$ due to the treatment ($\Delta T_{1/2}$) obtained from Figure 4.5 and 4.6 are listed in Table 4.2.

The $T_{1/2}$ of the non-treated PP electret decreases only slightly with the increase of the initial surface potential (V_0): it goes from 97 °C to 83 °C with V_0 from −500 V to −3 kV; and from 98 °C to 83 °C with V_0 from +500 V to +3 kV. Moreover, the TSD curves of the non-treated PP electrets from different V_0s remain symmetrical for both polarities. However, the chemically treated PP films respond differently to the negative and positive surface charges. For instance, the TSD result of the H_3PO_4-treated PP charged to V_0= −500 V has a $T_{1/2}$ of 144 °C, whereas that of the identical PP sample charged to V_0= +500 V only has a $T_{1/2}$ of 136 °C. This leads to different degrees of the enhancement brought by the chemical modification onto the PP electrets with negative and positive surface charges, which are 47 °C and 38 °C at most, respectively.

The chemically treated PP electrets additionally experience more influence from the increase of the initial surface potentials. From ±500 V to ±3 kV their $T_{1/2}$ decreases by 42 °C to 102 °C for the negative charges and by 41 °C to 95 °C for the positive charges. With the non-treated PP electrets barely reacting and the chemically treated PP electrets dramatically becoming less stable to the same initial-surface-potential

Table 4.2: Half-value temperatures ($T_{1/2}$) of non-treated and chemically treated PP electrets charged to different initial surface potentials (V_0) and their differences ($\Delta T_{1/2}$)

V_0	**Non-treated**	**Chemically treated**	$\Delta T_{1/2}$
−500 V	97 °C	144 °C	47 °C
−1 kV	95 °C	140 °C	45 °C
−2 kV	91 °C	138 °C	47 °C
−3 kV	83 °C	102 °C	19 °C
+500 V	98 °C	136 °C	38 °C
+1 kV	96 °C	121 °C	25 °C
+2 kV	90 °C	113 °C	23 °C
+3 kV	83 °C	95 °C	12 °C

growth, the improvement of the $T_{1/2}$ reduces to 19 °C and 12 °C for V_0= −3 kV and V_0= +3 kV, respectively.

More importantly, in Figures 4.5 and 4.6, the chemically treated PP samples charged to V_0= ±3 kV are so unstable that their surface potentials at higher temperature range drop below that of the identical PP samples charged to the lower V_0 of ±2 kV, causing their TSD curves to cross. This phenomenon is referred as the "cross-over", which is a typical behaviour of the LDPE electrets [170, 171, 172]. The discharge in the treated PP electrets starts earlier when the initial surface potential is higher. The temperature, where the potential decay of the chemically modified surface starts, decreases from 94 °C for V_0= −500 V to room temperature for V_0= −3 kV. However, one must notice that the surface potential of the H_3PO_4-modified samples with V_0= ±3 kV appears to decay in *two* stages. There are a faster decay at the lower temperature range before the cross-over point and a slower decay at the higher temperature range that prevent the curve from further crossing with TSD curves other than that of the V_0= ±2 kV samples. The two stages are better separated and easily observed when taking the first-order derivative of the surface potential with respect to temperature (dV/dT), as displayed in Figure 4.7 for the negatively charged and in Figure 4.8 for the positively charged PP electrets. The derivative curves are smoothed by means of the Savitzky-Golay method to eliminate the noise from the overly dense data points.

The graphs of dV/dT *versus* temperature in Figure 4.7 and 4.8 represent the internal drift-current plot based on (3.2) and the shape of the energetic distribution of the traps

in the PP electrets [91]. It is rather obvious that the derivative curves of both the non-treated (dashed line) and chemically treated (solid line) PP electrets expand to the lower temperature side as the initially deposited charge density increases. This indicates that the charges in the electrets tend to fill in the deeper traps first and move onto the shallower traps when there are no more deeper traps available [66], causing the down shift of the $T_{1/2}$ values with increasing V_0. There are some differences in the way that the trap distribution changes with the charge density for the non-treated and chemically treated PP samples. The peak position of the derivative curve of the non-treated PP remains at approximately 95 °C for V_0 from ±500 V to ±2 kV and broadens towards the lower temperature when V_0 reaches ±3 kV. For the H_3PO_4-modified PP electrets, there is only one peak at very high temperature when the samples are charged to a low value of V_0= ±500 V, and the peaks weigh more to the left when V_0 is increased to ±1 kV. With the V_0 of the chemically treated PP reaching ±2 kV, their dV/dT curves exhibit two peaks/shoulders at two temperature ranges: the left peak/shoulder is located at *ca.* 95 °C which coincides with the peak position on the curves of the non-treated PP; the right one appears at the same temperature range as the single peak observed on the treated sample charged to ±500 V.

As suggested by the correlations of the peak positions, the two peaks on the curves of the chemically treated PP charged to higher V_0 are the results of the charge-escape from two groups of traps: the deeper traps generated by the H_3PO_4 modification on the PP surface, and the shallow traps that are intrinsic to the commercial PP films. The chemical surface modification certainly formed a limited amount of deeper traps, while the original traps of the PP surface were not completely erased from the treatment. This agrees with the ATR-IR spectra and SEM images in the last section. The absorption bands from the PP molecules are still intense on the ATR-IR spectrum of the treated PP surface. Besides, only some discrete island-like structures, instead of a continuous new layer, are observed on the treated surface under SEM. There is another strong evidence of the contribution from the original shallow traps from the PP electrets. When the peaks on the derivative curves of the non-treated PP weigh towards lower temperatures as V_0 reaches ±3 kV, the left peaks on the curves of the chemically treated samples with the same V_0 also moves together to the same lower temperatures. Thus, it can be concluded that the intrinsic traps remaining on the H_3PO_4-treated PP surfaces are

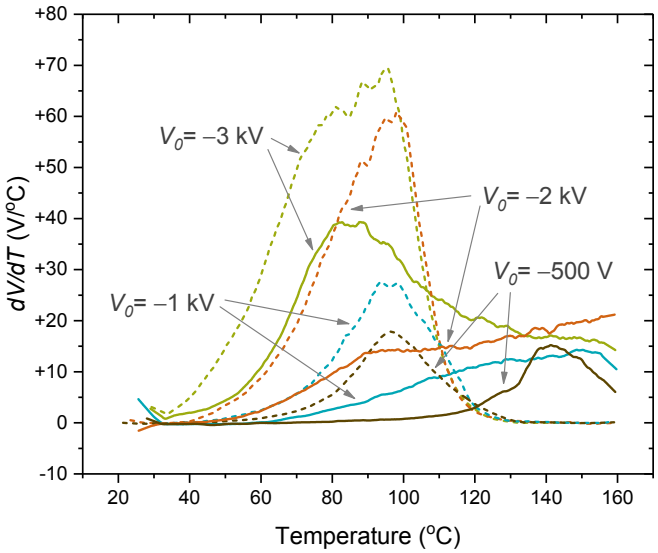

Figure 4.7: First-order derivative of surface potential with respect to temperature (dV/dT) of the negatively charged non-treated and chemically treated PP electrets. - The dV/dT curves are obtained from the TSD measurements of the non-treated (dashed line) and chemically treated (solid line) PP electrets charged to −500 V (brown), −1 kV (blue), −2 kV (red) and −3kV (green).

responsible for the fast charge decay at low temperature when the surfaces are charged to higher potentials.

The left-shift of the peak from the intrinsic shallow traps of the PP films happens only when the V_0 is as high as ±3 kV, which may explain the aforementioned cross-over between the TSD curves of the treated samples charged to ±2 kV and ±3 kV. Not only the deep traps introduced by the H_3PO_4 modification are not sufficient to host all the deposited charges with the density of $\pm 1.2\times10^{-3}$ C·m^{-2} (V_0= ±3 kV), but also the original traps on the PP film surface cannot capture all these charges. As a result, large fractions of the deposited charges in this case might be pushed into the bulk of the film under the high internal electric field. In the bulk the traps may be shallower and the charges may decay faster [172]. The charges on the non-treated PP samples with V_0 of ±2 kV are less stable and decay at lower temperatures. Thus, their TSD curves do not cross with that of the non-treated PP with V_0 of ±3 kV, and they overlap instead. However, when deeper traps are created by the H_3PO_4 treatment on the PP surface, more charges can survive till high temperatures on the treated PP charged to ±2 kV. Whereas many charges in the same PP with V_0= ±3 kV are pushed into the

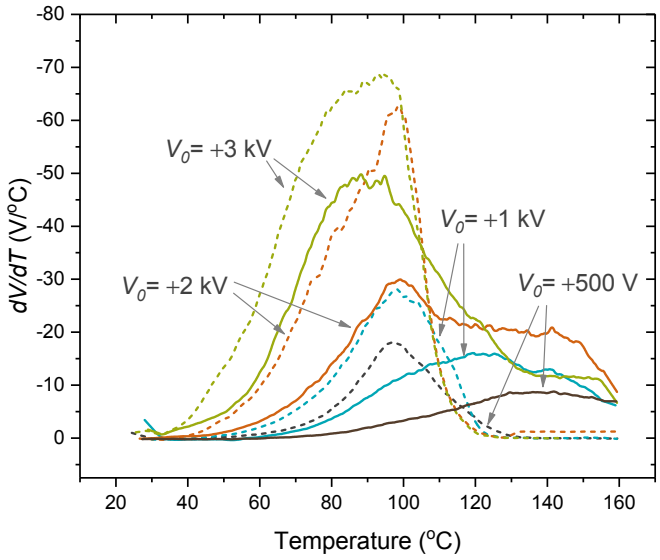

Figure 4.8: First-order derivative of surface potential with respect to temperature (dV/dT) of the positively charged non-treated and chemically treated PP electrets. - The dV/dT curves are obtained from the TSD measurements of the non-treated (dashed line) and chemically treated (solid line) PP electrets charged to +500 V (brown), +1 kV (red), +2 kV (blue) and +3kV (green).

bulk before being captured by the newly formed deep surface traps due to the high electric field. Hence, the cross-over phenomenon occurs only in the treated PP with high initial surface potentials.

The asymmetrical charge stability of the PP electrets regarding different polarities only occurs after the H_3PO_4 treatment. It might be caused by an interplay between the electronegativity of the foreign phosphorus and oxygen atoms on the treated PP surface and their interaction with the ions of the corona-discharge process. The highly electronegative fluorine atoms offer a much higher binding force with the negative charges, thus resulting in the asymmetry of the negative- and positive-charge stability in the fluoropolymers. Although the electronegativity of the phosphorus and oxygen is not as high as fluorine, it is still much higher than that of the hydrogen and carbon atoms in the PP molecules. The foreign chemical groups create greater energy disruptions to trap the charges of both polarities, and favour the negative charges due to their higher electronegativity. In addition, it was reported by Yovcheva and coworkers that the negative corona discharge performed on the PP-electret surface can increase the amount of the bonded oxygen, whereas the positive corona discharge can act oppositely

[70]. When the surface of the PP film is not treated, the oxygen content is too low to exhibit any pronounced asymmetry in the charge stability. However, on the H_3PO_4-treated PP surface, the oxygen content is much higher and more critical for the charge trapping at higher temperatures. So the asymmetrical charge stability for different polarities is magnified by the chemical modification in this case.

4.2.2 Charge distributions during thermal discharging

The macroscopic electret properties of the non-treated and H_3PO_4-treated PP, including the charge stability, influence of surface-charge density and polarity on the charge decay behaviour, *etc.*, were studied with the TSD measurements. Many important information related to the traps on the surface and in the bulk of the PP electrets with and without chemical modification can be extracted from the results. The microscopic pictures of the spatial trap distribution in the non-treated and H_3PO_4-treated PP films are investigated with the PPS method.

The samples used in the PPS measurements were charged with a grid voltage (V_G) of ± 2 kV for sufficiently high signal. To demonstrate the change of charge distribution during the discharge process, the charged PP films were partially discharged with the TSD set-up at the same heating rate of 3 °C/min to different critical temperatures: R. T. (no thermal discharging performed), 60 °C, 90 °C, 120 °C. They were immediately quenched to room temperature to abort the discharging and to freeze the charge distribution at that corresponding temperature. Samples discharged to different stages are examined to illustrate the locations of the newly-formed deep traps and the charge de-trapping and re-trapping during the TSD process. According to (2.5), the partial thermal discharge can purge the traps with the activation energy below certain levels, thus separating the shallow intrinsic traps and the deep traps from the chemical modification. The partial discharging was *not* performed on one sample in sequence, but a piece of freshly charged new PP film was used for each partial discharge and PPS measurement.

As shown in Figure 3.2, an uncharged clean PP film with a thickness of 25 μm was used as a spacer to protect the charged sample surface from the rubber electrode. The thickness of the sample films showed slight deviations from the nominal value, and thus it had to be normalised to 50 μm. The final charge distribution results were averaged from 4-7 individual samples. On the thickness axis, 0 was the metallised surface and

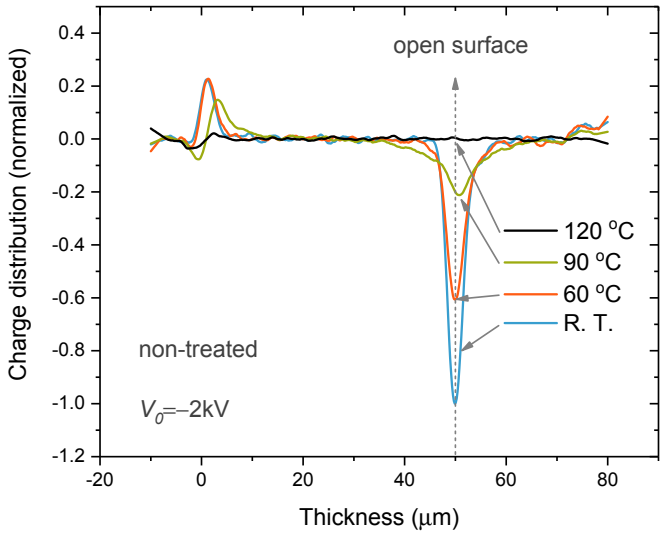

Figure 4.9: Charge distributions of partially discharged non-treated PP electrets with the negative corona charges. - The charge profiles in the thickness direction of the non-treated samples charged to −2 kV. The curves are obtained from the samples partially thermal-discharged to R. T. (non-discharged) (blue), 60 °C (red), 90 °C (green), and 120 °C (black).

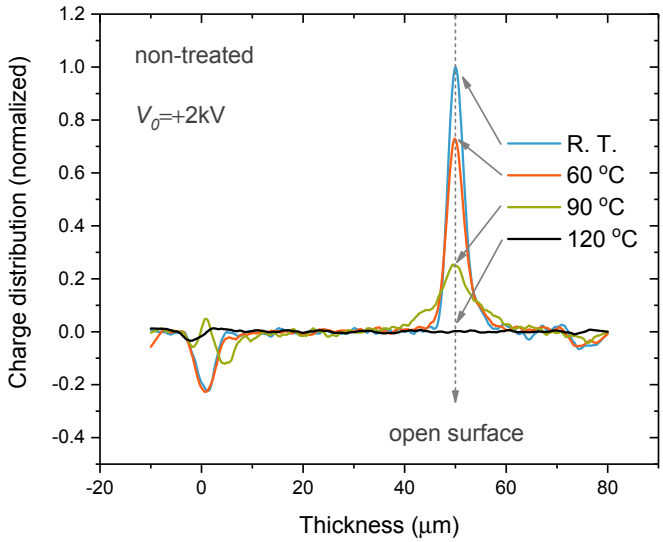

Figure 4.10: Charge distributions of partially discharged non-treated PP electrets with the positive corona charges. - The charge profiles in the thickness direction of the non-treated samples charged to +2 kV. The curves are obtained from the samples partially thermal-discharged to R. T. (non-discharged) (blue), 60 °C (red), 90 °C (green), and 120 °C (black).

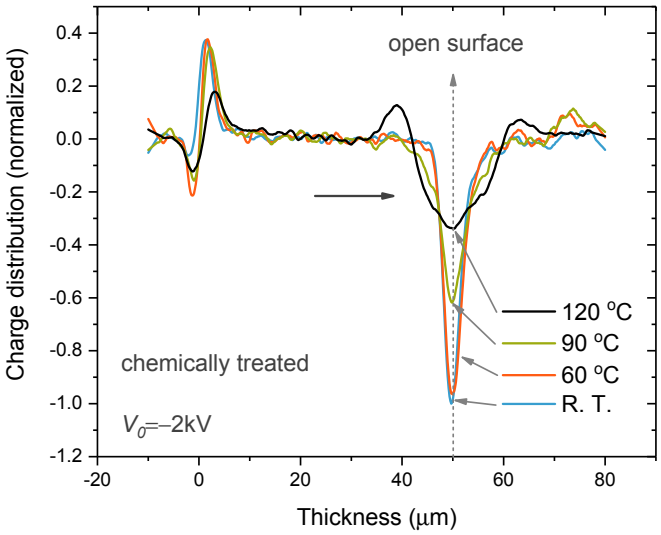

Figure 4.11: Charge distributions of partially discharged chemically treated PP electrets with the negative corona charges. - The charge profiles in the thickness direction of the chemically treated samples charged to −2 kV. The curves are obtained from the samples partially thermal-discharged to R. T. (non-discharged) (blue), 60 °C (red), 90 °C (green), and 120 °C (black).

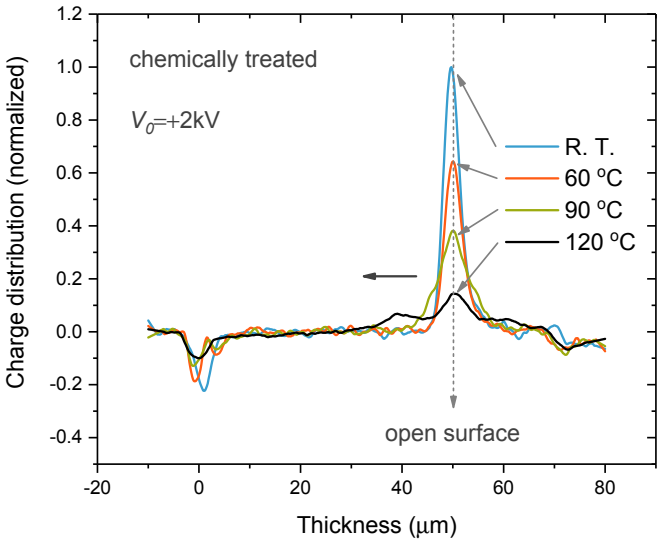

Figure 4.12: Charge distributions of partially discharged chemically treated PP electrets with the positive corona charges. - The charge profiles in the thickness direction of the chemically treated samples charged to +2 kV. The curves are obtained from the samples partially thermal-discharged to R. T. (non-discharged) (blue), 60 °C (red), 90 °C (green), and 120 °C (black).

50 μm was the charged open-surface of the PP sample. To better illustrate the charge decay process, the vertical scale of charge density was normalised by the absolute value of the surface charges without any partial discharge. It means that the amplitudes of the peaks at 50 μm on the R. T. curves were all ±1.0, with the sign indicating the polarity.

The charge distributions of the non-treated and chemically treated PP electrets are illustrated for the negative and positive charges in Figures 4.9, 4.10 and in Figures 4.11, 4.12, respectively. From all four R. T. curves of the charge distributions in the figures, it is clear that the corona discharge at room temperature only deposits charges on the surface of the PP electrets without any injection to the bulk. The deposited charges remain on the surface of the non-treated PP films till the end of the charge decay, as demonstrated in Figure 4.9 and 4.10. The results agree with that obtained by Ono and coworkers with the LIPP method in [71]. The peaks of the charge distribution remain at the open surface (50 μm) of the non-treated films, though some slight peak broadening is observed after the samples being partially thermally discharged to 90 °C. The broadening might be the influence of the reduced signal-to-noise ratio due to the lower surface charge density. Similar peak broadening effect after discharged to 90 °C appears on the charge distribution curves of the chemically treated PP in Figure 4.11 and 4.12 as well.

Unlike the non-treated PP electrets, where no charge is present at 120 °C, there are still significant amount of charges on the chemically treated PP films at the same temperature (seen in Figure 4.11 and 4.12). It was demonstrated in Figures 4.7 and 4.8 in the previous section that the charges remaining at 120 °C are captured in the deeper traps generated by the H_3PO_4 treatment. As shown in Figure 4.11, all the negative deposited charges are trapped on the treated surface, indicating that the chemical modification is restrained on the surface of the PP films without penetrating to the bulk. The negative charges on the surface are not only stable enough to withstand a temperature as high as 120 °C, but can also attract the opposite charges from the rear electrode to travel through the bulk of the film and to build a layer near the open surface, as illustrated with the arrow. The bulk portion of the PP film is not treated with H_3PO_4, unlike the surface. Hence, the positive mirror charges on the rear electrode can be easily transported to the open surface side in the same manner as that in the non-treated PP electrets at 120 °C. In this case, the electric field of the remaining

surface charges on the treated PP acts as a high driving force for the positive charges. However, the energy barrier created by the H_3PO_4-treated surface is strong enough to block the positive charges from immediately neutralising the deposited negative charges on the surface. Thus, a layer of the positive charges is still visible in the PPS results, coexisting, at least temporarily, with the nearby negative charges on the sample surface.

The situation is different in the positively charged PP films treated with H_3PO_4. First of all, the charge distribution curve at 120 °C in Figure 4.12 for the positive surface charges exhibits peaks with much smaller area at the open surface than that in Figure 4.11 for the negative charges. This result is consistent with the asymmetrical charge stability observed in their TSD measurements. In addition, it can be seen that the positive surface charges migrate further into the H_3PO_4-modified PP film at 120 °C, appearing as a second peak near the surface, as indicated by the arrow. It shows that the positive charges are able to acquire enough energy at this point to escape the newly formed traps on the chemically treated PP surface. And they drift towards the rear electrode under their own electric field, as opposed to the behaviour of the deposited negative charges in Figure 4.11. The negative charge stability of the PP electret is more influenced by the H_3PO_4 treatment than the positive charge stability, which explains the difference in the $\Delta T_{1/2}$ in Table 4.2. At 120 °C, the positive corona charges near the treated PP surface stay in two separate layers, appearing as two peaks instead of merging into one wide peak on the PPS result. It once again shows the barrier between the chemically modified surface and the non-treated bulk of the PP films. This distinction reflects that treatment on the *surface* can bring about dramatic improvement to the electret properties of the PP films, even though the majority of the volume remains the same.

The experiments on the microscopic scale with the PPS method reinforce the interpretation of the different binding force between the phosphorus- and oxygen-based structures and the deposited charges of different polarities. The deeper traps associated with these foreign chemical structures are negative-charge preferential, thus resulting in the asymmetrical charge stability of the modified PP electrets. The phenomenon does not take place in the non-treated PP samples where the foreign chemicals play only a minor role in terms of charge trapping. Thus, it can be concluded that the foreign chemicals in the *treated* PP electrets dominate the electret properties as the deeper traps, which agrees with the results from [120] and [63].

Another phenomenon worth noticing from the PPS measurements in Figure 4.9 to 4.12 is that, at any point of the thermal discharge, there is no charge present in the bulk of the non-treated or chemically treated PP film, except near the surface region. It indicates that the charge re-trapping in the bulk does not occur during the charge transport through the film volume. This means that the bulk traps are much shallower than the surface traps. So they do not contribute on the life time of charges and the spatial charge distribution as significantly as the surface traps when the samples are charged to ±2 kV. Combining with the observation and analysis of Figure 4.7 and 4.8, the intrinsic traps, responsible for the low-temperature peak at *ca.* 95 °C, in the H_3PO_4-treated PP with V_0= ±2 kV are located on the surface instead of in the bulk. On the other hand, when the modified PP films are charged to the higher V_0 of ±3 kV, the shallower bulk traps start to participate in the charge storage. In this case, the deep surface traps—both newly formed and intrinsic traps included—are not able to accommodate all the deposited charges. It explains the cross-over phenomenon observed in Figure 4.5 and 4.6, which is consistent with the interpretation in [172].

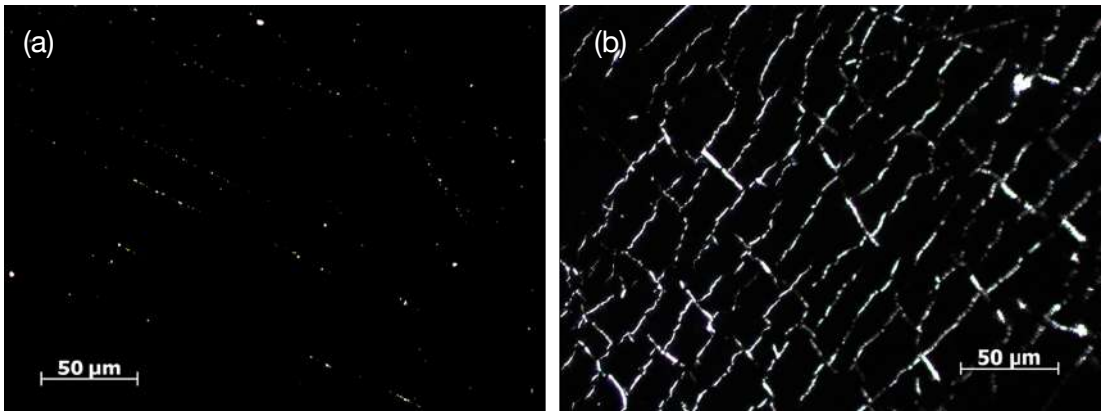

Figure 4.13: Optical microscope images of the evaporated electrode on the PP films with and without heating - Microscope images of the evaporated Cr/Al electrode on the PP electrets before (a) and after (b) being heated to 90 °C.

Only the peaks of the charge distribution on the open surface side (at 50 µm thickness) have been discussed and explained so far. However, the peaks of the compensating charges on the rear electrode side (0 thickness) of the non-treated and chemically treated PP films also exhibit some interesting variations at different discharging temperatures. The abnormal double peak feature appears at the rear electrode for all the chemically

treated samples and the non-treated samples discharged to 90 °C, but *not* on the R. T. and 60 °C curves of the non-treated PP. It is caused by the poor electrical conduction of the evaporated electrode after being heated above 90 °C. When the non-treated PP film is heated to 90 °C for the partial discharge or the chemically treated PP film is annealed at 160 °C during the sample preparation, the oriented PP molecular chains gain sufficient mobility to recoil from the stretched state. The evaporated electrode is essentially a layer of metal particles attached onto the PP film, and it moves with the molecules. This results in the patterned cracks on the electrode as shown in the optical microscope images (Figure 4.13) of the electrode before and after heating to 90 °C. The impaired electrical contact of the rear electrode causes the double peaks at 0 thickness on the charge distribution curves of the corresponding PP samples. The PPS measurements can be carried out on samples without electrode, hence the damage of the electrode on the PP films does not influence the reliability of the results for the deposited charges on the open surface.

5

Spherulitic and transcrystalline PP electrets

5.1 Spherulitic and transcrystalline PP

5.1.1 Crystallisation of spherulitic and transcrystalline PP

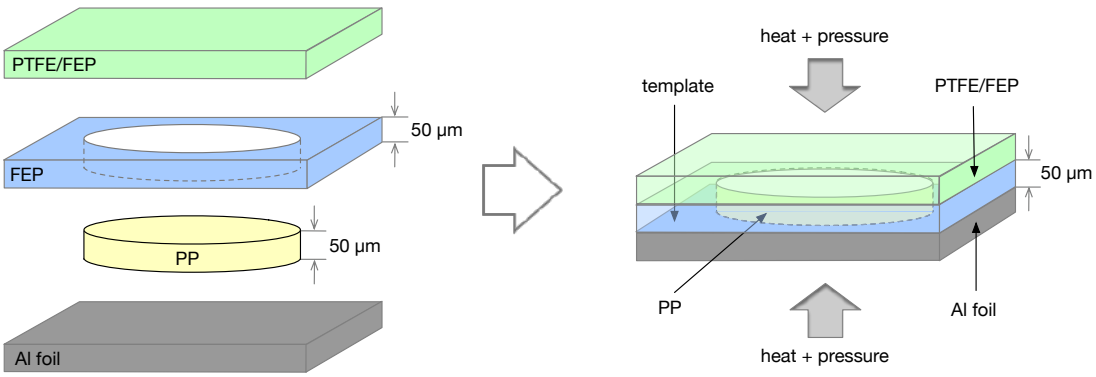

Figure 5.1: A schematic diagram for the crystallisation of the spherulitic and transcrystalline polypropylene - A piece of PP film placed between the moulding surface of FEP or PTFE and Al substrate is melted and slowly cooled to form the spherulite or transcrystalline structures with a template for thickness control.

The PP films supplied by Pütz Folien with a nominal thickness of 50 µm were cut into round pieces with a diameter of 60 mm. The moulding surfaces for the spherulitic and transcrystalline structures were FEP (thickness of 127 µm) and PTFE (thickness of

100 μm) films, respectively, which were both manufactured by DuPont (Teflon^{TM}). The 30 μm-thick aluminium (Al) foil from neoLab Migge GmbH was used as the substrate with the matt side of the foil in contact with the PP samples. The circular PP film was sandwiched between the 72×72 mm square-shaped corresponding moulding surface and Al foil. Another FEP film of 50 μm thickness with a circular opening in the size of 60 mm diameter was placed around the PP film as a template for the thickness control. The melted PP can be retained in the space with 60 mm in diameter and 50 μm in height untill solidified. The arrangement of the sandwich structure is illustrated in Figure 5.1. All the films were cleaned with isopropanol and dried with nitrogen prior to using.

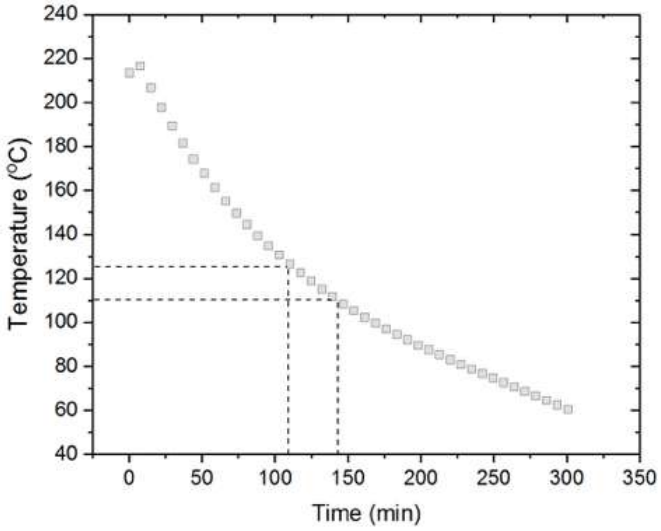

Figure 5.2: The temperature profile for the crystallisation of the spherulitic and transcrystalline polypropylene - The slow cooling allows the melted PP to crystallise into large spherulitic or transcrystalline PP for 30 min between 125 °C and 110 °C as indicated by the dashed lines.

The entire three-layer sandwich structure with the template shown in Figure 5.1 was placed between two heating plates with a pressure to ensure sufficient contact between the PP film and the moulding surface. The PP film was completely melted at 210 °C for 10 min. Even the isotactic PP films are supposed to already melt at 169 °C, according to the DSC result of the non-treated sample in Figure 4.4. The excess heating was for eliminating any possible crystalline embryo residue that might influence the crystallisation of the new spherulitic and transcrystalline structures. The

PP melt was subsequently cooled slowly with a rate of approximately 0.5 °C/min. The temperature profile of the cooling process is shown in Figure 5.2. The slow cooling can grant roughly 30 min between 125 °C and 110 °C for the PP film to form large crystalline structures through the entire film thickness to maximise their influence on the electret properties of the film.

After the PP film was solidified, the moulding surface was carefully removed, leaving the surface with the crystalline nuclei open. The Al foil was thermally fused onto the other side of the PP film during the crystallisation, which remains attached as an electrode for a good electrical contact during the charging and surface potential measurements later. For the polarised light microscope, thermal and conformational characterisation, the Al foil was carefully removed from the PP film.

5.1.2 Spherulitic and transcrystalline PP under the microscope

The spherulite and transcrystalline structures in the PP films were designed to start from the nucleus centres on one surface of the films and to grow through the films to the other surface. Therefore, in order to obtain a clear picture of the crystalline growth from the start to the end, one needs to observe the film from the side view with the incident light in parallel with the film surface, as illustrated in Figure 5.3. As introduced in section 3.3.2.4, the crystalline structures of polymers are typically observed with the cross-polar PLM, in which the polarised light transmits through the ordered crystals and selectively passes through the analyser. It requires the specimen to be thin enough to allow the light transmittance. So narrow stripes of specimens were sliced off the PP films for the PLM. With the aid of a template, the specimens of the spherulitic and transcrystalline PP with the width of 40-50 μm were obtained. The thin sample was placed between two glass slides, so that it can be fixed into the focal plane of the microscope. The crystalline structures of the PP specimens were examined with a Zeiss Axio ImagerA1m PLM.

The images of the spherulite and transcrystalline in the PP films are exhibited in Figure 5.4 (a) and (b), respectively, with the arrows indicating the directions of the crystal growth in each case. It is confirmed that the crystalline structures indeed grow from the moulding surfaces and extend through the whole thickness of the film to the Al substrate, because of the slow crystallisation. The single-layer crystalline structures in the PP films make the structural analysis of the molecular and crystallite

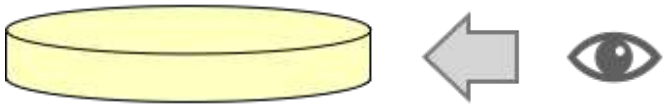

Figure 5.3: A schematic illustration of the direction for observing the crystalline structures in polypropylene films - The spherulites and the transcrystalline structures need to be viewed from the side of the PP films to observe the crystalline growth from one surface to the other.

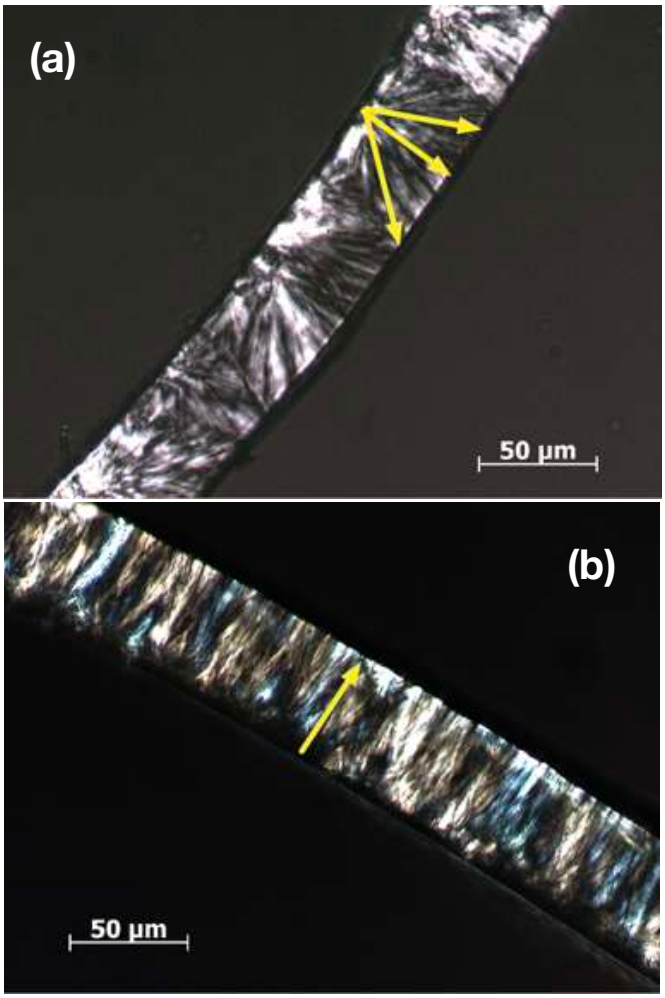

Figure 5.4: Polarised light microscopic (PLM) images of the spherulites and the transcrystalline structures in the polypropylene films - The images of the spherulitic (a) and transcrystalline (b) PP films are taken from the side view and the arrows indicate the directions of the crystal growth.

conformations less complex. Both FEP and PTFE have stronger surface heterogeneous nucleating effects than the Al substrate, hence crystalline growth from the Al side to the Teflon^{TM} side does not take place. The transcrystalline structure only propagates along the thickness direction, while the spherulite experiences the radial crystalline growth. The orientation of the spherulite and the transcrystalline structure in respect of the dimension of the PP films can be better illustrated with the three-dimensional reconstruction of the crystallised films shown in Figure 5.5 (a) and (b), respectively. The PLM images taken from different angles of the PP films are reconstructed together to reveal the crystalline structures. The size of both crystalline structures are restricted by the thickness of the PP films (50 μm), whereas on the plane of the film surface the spherulites can grow to the size of 100-200 μm in their diameter. However, the transcrystallisation in any lateral directions is forbidden by the densely populated neighbouring nucleating centres. Besides, the boundaries between the spherulites in Figure 5.4 and 5.5 are straight, indicating that they were nucleated simultaneously.

Figure 5.5: Three-dimensional reconstructions of the spherulitic and transcrystalline polypropylene films - The spherulitic (a) and transcrystalline (b) structures in the PP films are reconstructed with the PLM images taken from different angles of the samples.

The spherulitic and transcrystalline PP films differ not only in the crystalline and morphological structures, but also in the orientation of their molecular chains. Any crystalline structures in polymers consist of many lamellar crystallites packed in certain ordered structures. The covalent axis of the polymer chains, also known as the chain orientation, is perpendicular to the lateral dimensions of the lamellae [173], which is schematically illustrated as the parallel lines on the side of the cuboid crystallites in Figure 5.6. As the spherulite grows in the polymer, new lamellar crystallites (daughter

lamellae) branch from the existing ones (mother lamellae). In PP spherulites, there exists a characteristic "lath-like" branching pattern with a constant angle of 80° to 100° between the mother and daughter lamellae. Therefore, molecular chains in the crystalline phase are approximately packed in perpendicular or in parallel to the radial direction (the direction of crystalline growth) of a regular PP spherulite, seen in Figure 5.6 [174]. It has been introduced in section 3.3.3 that the transcrystalline structure is essentially a special spherulite which grows only towards one direction instead of exhibiting a radial growth [167]. As a result, in transcrystalline PP, the "radial" direction is the normal direction of the film surface, which means the molecular orientation in the crystalline phase of the transcrystalline structures is roughly perpendicular or parallel to the surface of the film. The rather strict organization of the morphological structure in the transcrystalline PP film is extended to the molecular structures in the crystalline phase.

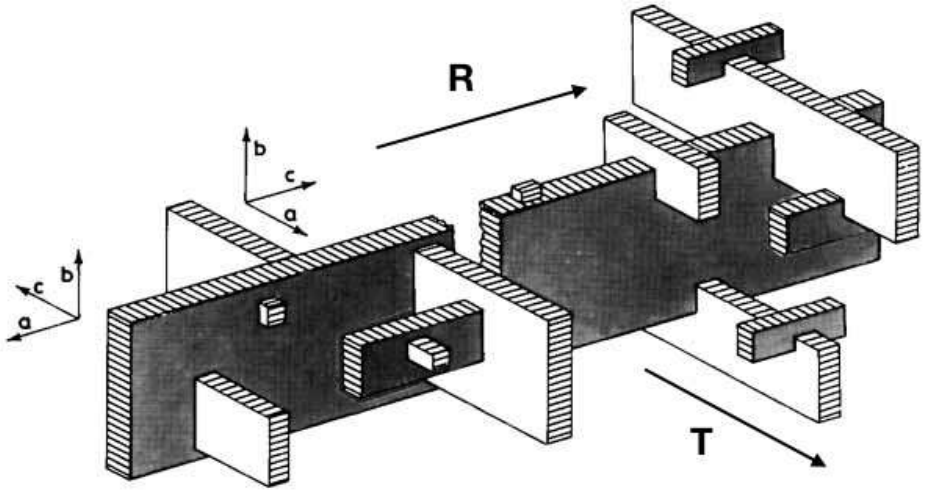

Figure 5.6: A schematic diagram of the crystallite branching in a regular polypropylene spherulite - The chain orientation is illustrated as the parallel lines on the cuboid lamellar crystallites, and the "R" and "T" arrows represent the radial and tangential directions of the PP spherulite, respectively [174].

5.1.3 Conformational and thermal chracteristics

The chemical composition and molecular conformation on the surface of the spherulitic and transcrystalline PP films were studied with the Bruker Alpha-P ATR-IR spectroscopy. The resulting absorption spectra of the two samples displayed in Figure 5.7

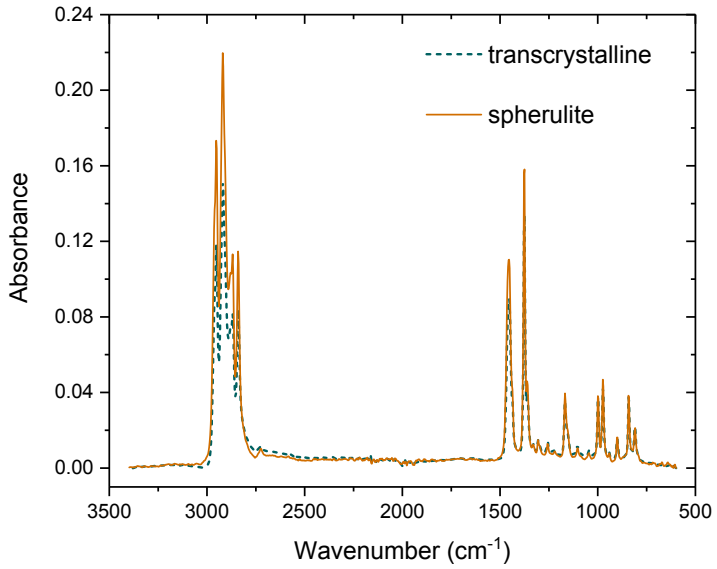

Figure 5.7: Attenuated-total-reflection infrared (ATR-IR) spectra of the spherulitic and transcrystalline polypropylene films - The two spectra overlap with each other, indicating no chemical compositional and molecular conformational differences between them.

Table 5.1: The melting temperatures (T_m) and degree of crystallinity (X_c) extracted from the DSC results of the spherulitic and transcrystalline PP samples

Crystalline type	T_m **range**	T_m **peak**	X_c
spherulite	158-168 °C	164 °C	46.5 %
transcrystalline	159-169 °C	165 °C	44.1 %

overlap with each other, which are also consistent with the spectrum of standard isotactic PP in the FTIR software database. It indicates that no detectable foreign chemicals have been introduced to the PP surfaces during the crystallisation of the spherulite and the transcrystalline structure. The difference between the two samples lies in their crystalline structures instead of their chemical compositions. In addition, the regularity bands of the spherulitic and transcrystalline PP between 700 and 1400 cm^{-1} that reflect the length of the molecular helices in the isotactic PP are also identical. The molecular conformation does not differ when the crystalline structure varies in the samples.

The curves in Figure 5.8 are obtained with the 214 Polyma DSC from NETZSCH. 5 mg of each spherulitic and transcrystalline PP films was tested in the DSC with a heating and cooling rate of 5 °C/min. The thermal transition peaks of the melting

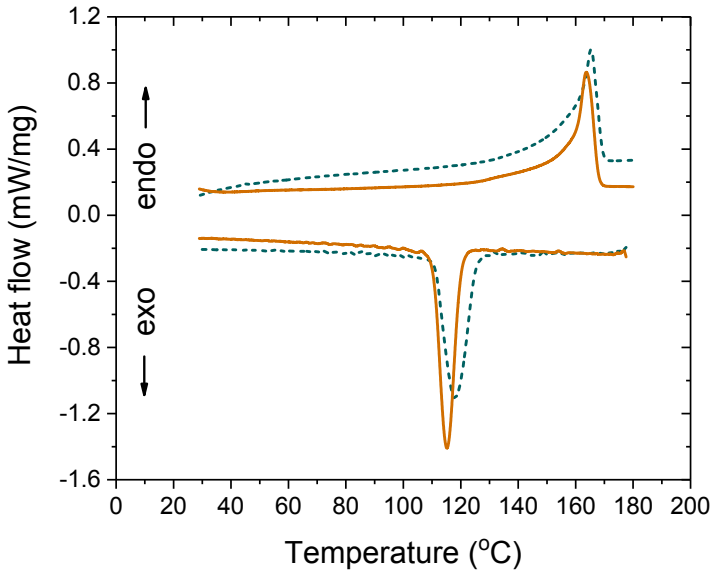

Figure 5.8: Differential scanning calorimetry (DSC) curves of spherulitic and transcrystalline polypropylene films - The DSC curves exhibit no dramatic variations on the thermal properties and crystallinity of the spherulitic (solid line) and transcrystalline (dashed line) PP films

and crystallisation of the two crystalline structures show some slight deviations. The crystallisation peak of the spherulitic PP film is narrower, but its melting peak is of the same width as that of the transcrystalline PP film. The melting temperatures (T_m) of the two samples are extracted from the curves and their values of crystallinity (X_c) are calculated based on (3.8), which are all listed in Table 5.1. The difference between their T_m is only 1 °C and the variation of their X_c is within the deviation of repeated measurements on identical PP samples. The thermal properties and crystallinity of PP are mostly controlled by the thermal history. During the crystallisation, the spherulitic and transcrystalline PP films experienced the same thermal history. Thus, they show very similar T_m and X_c but very different orientations of crystalline growth. The spherulitic and trascrystalline PP samples in this experiment are essentially built with the same "elementary structures", which, however, are assembled differently in each sample.

5.2 Characterisation of electret properties

5.2.1 Charging and discharging procedures

The crystalline structures of the spherulitic and transrcystalline PP films have been confirmed with the PLM. For the investigation of the electret behaviour of the different crystalline structures in PP, the sample films were charged with a corona triode in air for 15 seconds at room temperature. The charges were deposited on the nucleating surface of the PP films and the Al substrate was used as the electrode during charging and discharging. The corona point with a voltage of ±12 kV was positioned 20 mm away from the open surface of the PP samples, while the control grid was 7-8 mm above the sample surface. The voltage of the control grid was set at ±500 V, ±1 kV or ±2 kV to research the influence of the surface charge density on the electret properties of the PP films with the spherulites and transcrytalline structures.

Immediately after the corona charging, the transcrystalline and spherulitic PP electrets were transferred to the TSD set-up. The temperature of the PP electrets was increased linearly with a heating rate of 3 °C/min, and the surface potential decay was measured with a non-contact electrostatic voltmeter supplied by TREK (model 314B). The results are presented as surface-potential decay curves *versus* temperature. Each of the curves is the averaged result from three to six individual measurements on identical samples.

5.2.2 Charge storage and transport characteristics

The charge decay behaviours of the spherulitic (solid line) and transcrystalline (dashed line) PP electrets charged with various grid voltages (V_G) are exhibited in Figure 5.9 and 5.10 for the negative and positive surface charges, respectively. It is easily noticed that the initial surface potential of the spherulitic PP is still far below ±1 kV when the V_G increases above ±1 kV. To be more precise, the positively charged spherulitic PP films show potential saturation at approximately +700 V in Figure 5.10. The initial surface potential of the negatively charged samples still increase with the V_G, but the samples are severely undercharged when the V_G is set at −1 kV and −2 kV in Figure 5.9. On the other hand, the initial surface potential of the transcrystalline PP electrets can roughly meet the value of the set V_G up to at least ±2 kV. The potential-saturation phenomenon in PP electrets with large spherulites was reported

by Ikezaki and coworkers [155, 161]. However, it does not occur in the PP samples with the spherulites in smaller size and higher number density.

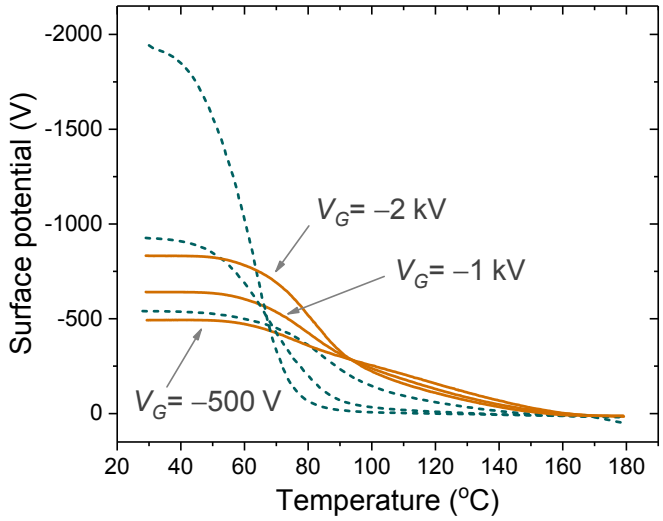

Figure 5.9: Thermally stimulated discharge (TSD) curves of the negatively corona charged spherulitic and transcrystalline PP electrets - The samples are charged with V_G= −500 V, −1 kV and −2 kV. The spherulitic PP (solid line) is undercharged when V_G is higher than −500 V, unlike the transcrystalline PP (dashed line).

In most of the experiments, the differently sized spherulites in PP are obtained by crystallising the melt at different cooling rates or isothermal conditions, hence the structural effect from the spherulite size is often intertwined with the molecular conformational effect from the different thermal history [169]. However, in this case, the spherulite and transcrsytalline PP samples are prepared with the same temperature profile as shown in Figure 5.2, and the similarity of their thermal properties and crystallinity is proven by the DSC method (as shown in Table 5.1). The charge saturation and undercharging in the large PP spherulites appear immediately after the corona charging, whereas the deposited charges on the surface only start to decay at *ca.* 50 °C. Therefore, it is highly likely that the saturation/undercharging phenomenon is a surface effect of the spherulitic PP films, which might be attributed to the lower density of surface nuclei and inter-spherulitic boundaries of the large spherulites compared to that of the transcrystalline PP.

The surface-potential saturation does not occur to the transcrytalline films, which can offer enough trapping sites to accommodate all the deposited corona charges. How-

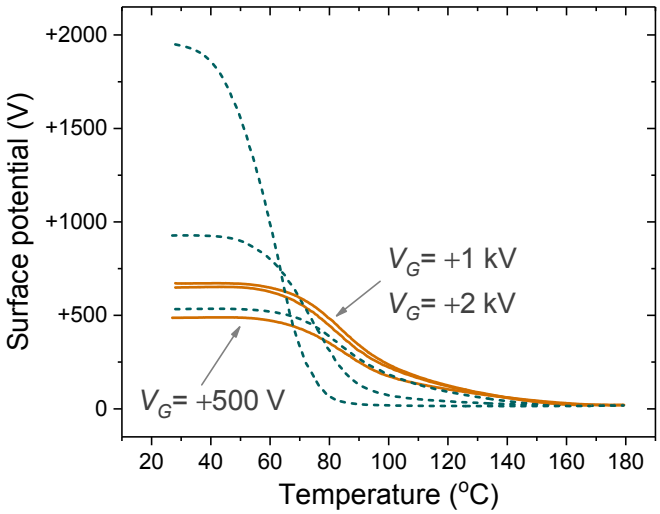

Figure 5.10: Thermally stimulated discharge (TSD) curves of the positively corona charged spherulitic and transcrystalline PP electrets - The samples are charged with V_G= +500 V, +1 kV and +2 kV. The spherulitic PP (solid line) shows charge saturation at *ca.* +700 V, but it does not occur in the transcrystalline PP (dashed line).

ever, among these traps, only a limited amount are sufficiently deep to withstand high temperatures. Many corona charges, especially when the charge density is high, are captured in the shallow traps. Therefore, in Figure 5.9 and 5.10, the "cross-over" phenomenon can be observed on the curves of the negatively and positively charged transcrystalline films: all three curves of the transcrystalline samples in each Figure intersect at approximately 70 °C. The deposited charges tend to populate the deep traps when the charge density is low, whereas more and more charges are pushed into the shallow traps with an increasing charge density. In the meantime, the stronger internal electric field of the deposited charges will give a higher driving force on the charges and lead to the charges drifting into the bulk of the transcrystalline PP films before being captured by the nearby deep traps. Similar as other electrets with the cross-over feature, the bulk traps of the transcrystalline PP may show much lower activation energy than the surface traps [170, 172, 175]. In addition, the highly ordered crystallite structures and molecular orientation in the crystalline phase of the transcrystallised PP films might serve as the charge-transport channels that are able to facilitate the charge drifting under high electric fields.

When the V_G is ±500 V, the charge saturation and undercharging phenomena have

not taken place in the spherulitic PP yet, and thus samples with either crystalline structure can be charged to $V_0 = \pm$ 500 V. But the transcrystalline and spherulitic PP still differ in their electret behaviour: the former exhibits a symmetrical charge stability for both polarities, whereas the latter has a $T_{1/2}$ of 97 °C for the negative surface charges and 90 °C for the positive. The difference is more obvious when taking the first-order derivative of the potential decay with respect to temperature (dV/dT). The resulting dV/dT curves of both negatively and positively charged spherulitic (solid line) and transcrystalline (dashed line) PP electrets are plotted with the temperature in Figure 5.11.

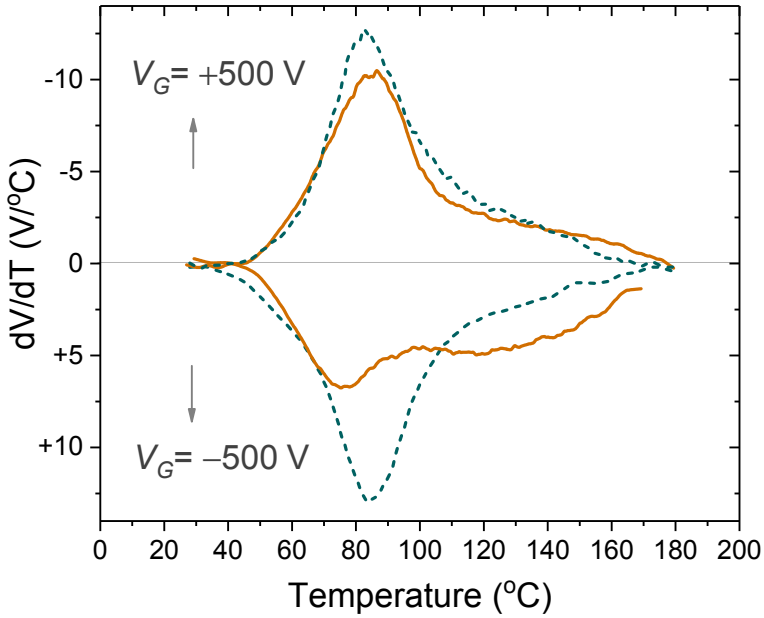

Figure 5.11: First-order derivative of the surface potential in respect of temperature (dV/dT) of the PP electrets with various crystalline structures. - The transcrystalline PP (dashed line) shows a symmetrical charge stability for different polarities, while the spherulitic PP (solid line) is slightly more stable when charged negatively.

The transcrystallised PP films show the single peak at 84 °C on their dV/dT curves with the surface charges of either polarity in Figure 5.11. The shape of the dV/dT curves from the spherulitic samples appear to be different for the positive and negative corona charges, indicating differences in their energetic distributions of electron and hole traps. The de-trapping behaviour of the negative charges in the spherulitic PP is more complex than that of the positive charges. It spreads over a broader energy

spectrum. The dV/dT curve of the spherulitic electret with a V_0 of +500 V displays one single peak at 85 °C, while there are two parts for the trap distribution in the spherulitic PP charged to −500 V. One part is a peak at 74 °C and the other is a shoulder-like distribution starting from *ca.* 110 °C.

The simple and complex trap distributions of the transcrystalline and spherulitic structures in the PP films, respectively, correspond to the orientation of their crystalline structures. The transcrystalline PP has a simpler structure with the crystalline growth only in the normal direction of the surface, as illustrated in Figures 5.4 and 5.5. The crystallites and molecules in the crystalline phase are oriented either perpendicular or parallel to the surface plane. The spherulitic PP samples, on the other hand, have a typical radial crystalline growth, where the crystalline structures propagate from the rather scarce surface nuclei in all directions into the film volume. The broad range of directions of the crystalline growth in the spherulitic PP electrets leads to the more diverse charge-transport pathways. The reason that only the negative corona charges are affected by the radial crystalline structure in the spherulitic PP is not well understood now. However, it implies that there might be some different mechanisms regarding the positive and negative charge transport in the spherulitic PP electrets. The electret properties of the transcrystalline and spherulitic PP vary significantly, which indicates that some polymeric electrets are highly sensitive to their microscopic crystalline structures and molecular orientations.

6

Charge distribution in transcrystalline PP

6.1 Single- and double-layer transcrystalline PP

6.1.1 Crystallisation of double-layer transcrystalline PP

The method for preparing the single-layer transcrystalline PP films was introduced in the last chapter 5.1.1. The single-layer structure was obtained by crystallising PP films from melt between a moulding surface of PTFE and a substrate of Al foil. For the double-layer transcrystalline structure, the Al foil was replaced with another PTFE moulding surface: A piece of commercial PP film from Pütz Folien with a nominal thickness of 50 μm and a diameter of 60 mm was placed in a FEP (Teflon^{TM}) thickness-control template from DuPont of the same thickness. The PP film and the FEP template were sandwiched between *two* identical PTFE films (Teflon^{TM}) with a thickness of 100 μm. The set-up is illustrated with the schematic diagram in Figure 6.1. All films were rinsed with isopropanol and dried with nitrogen before use.

As shown in Figure 6.1, the sandwich structure was heated under pressure to ensure a good contact between the melt PP and the moulding surfaces of PTFE. The temperature was kept at 210 °C for 10 min before being decreased slowly with the profile in Figure 5.2. The thermal history of the double-layer transcrystalline films was the same as that of the single-layer films. The transcrystallisation of the PP films proceeds from the heterogeneous nuclei on the PTFE moulding surfaces on both sides towards the middle of the film within *ca.* 30 min. A transcrystalline interface is created in

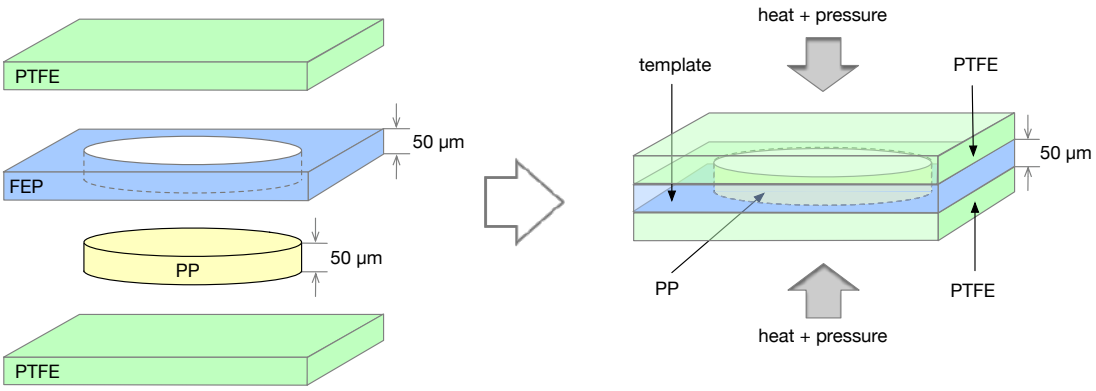

Figure 6.1: A schematic diagram for the crystallisation of the double-layer transcrystalline polypropylene - A piece of PP film with a thickness-control template around is placed between two PTFE moulding surfaces to form the double-layer transcrystalline structure.

parallel to the film surface planes. The moulding surfaces and the thickness template were carefully removed, after the PP films were completely solidified from the melt.

6.1.2 Structural and thermal characterisation

As demonstrated in the previous chapter 5.1.2, the crystalline structure needs to be visualised with the side view of the film as shown in Figure 5.3. The interface of the double-layer transcrystalline PP samples is only visible in this way, owing to the direction of the crystalline growth. Specimens of the single- and double-layer transcrystalline PP with a width of 40-50 µm were sliced off the film with the help of a template. To fix the specimen in the focal plane under the optical microscope, it is preserved between two glass slides. The thin (40-50 µm) specimens allow the transmittance of the polarised light in parallel to the film surfaces. The microscope images of the single- (a) and double-layer (b) transcrystalline PP films in Figure 6.2 were obtained with the Axio ImagerA1m PLM supplied by Zeiss.

The single-layer transcrystalline structure in Figure 6.2 (a) was nucleated from the PTFE moulding surface and extended through the entire film thickness to the Al foil side. This is because the PTFE surface has much stronger heterogeneous nucleating effect than the surface of the Al foil. The formation of the nuclei depends on the *relative* nucleating effect of the moulding surface. For instance, when the melted PP crystallises with one side in contact with an Al substrate and the other side open in the air, it will

result in a PP film with the surface spherulites nucleated from the Al substrate, for its stronger nucleating effect than the air [168]. If the melted PP film is cooled with both sides exposed to air, which is the case for most commercially produced PP films, there will be a thin layer of amorphous structure on both of the surfaces of the PP film [98].

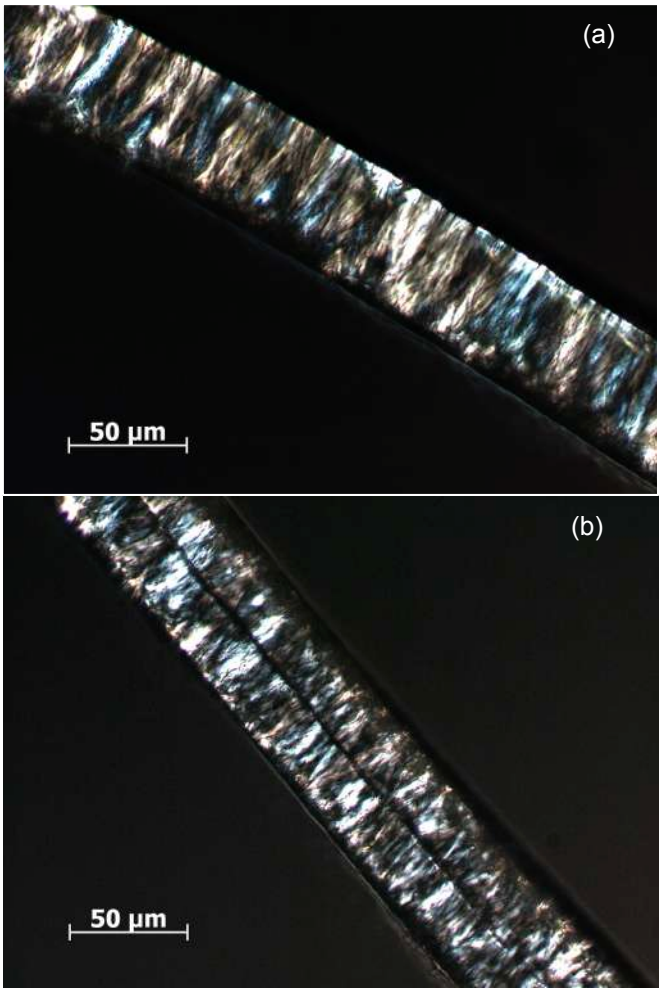

Figure 6.2: Polarised light microscopic (PLM) images of the (a) single- and (b) double-layer transcrystalline PP films - A clear interface is observed in the middle of the double-layer transcrystalline PP (b) from the side view, which is absent in the single-layer transcrystalline PP sample (a).

However, the melted PP film sandwiched between two PTFE films is under equal influence of the surface nucleation on both surfaces. Thus, the crystallisation starts from both sides simultaneously when it is cooled slowly. The high-concentration surface

nuclei on both surfaces lead to the transcrystallisation of the PP samples, instead of the spherulite formation. The crystalline structures originate from the surfaces and propagate in the normal direction to the surface into the bulk of the films, resulting in the double-layer transcrystalline PP in Figure 6.2 (b).

The interface between the two layers is located precisely in the middle of the film and appears to be straight in Figure 6.2 (b). It indicates that all the nucleation on the two surfaces of the double-layer transcrystalline PP films happened simultaneously. This is because the rate of crystalline growth, which relies on the temperature and cooling rate, is identical for all surface nuclei in this case. It was discussed in section 3.3.3 that the transcrystalline structure can be understood as a special one-dimensional surface spherulite with extremely dense nucleating centres. Hence, the interface in the double-layer transcrystalline PP has the same nature as the boundaries between two spherulites in Figure 5.4 and 5.5. The interface is essentially the point where two crystalline structures (transcrystalline or spherulite) originating from different nuclei meet from opposite sides. In addition, the characteristics within the crystalline phase, including correlation of the crystallite and molecular orientations to the film surfaces as illustrated in 5.6 [173, 174], are identical for the single- and double-layer transcrystalline PP films. The interactions and structures of the crystalline and amorphous phases remain the same within each layer of the transcrystalline structure in both samples.

The thermal properties of the single- and double-layer transcrystalline PP films were investigated with the 214 Polyma DSC from NETZSCH. The resulting thermal transition curves are plotted in Figure 6.3. For each measurement, 5 mg of a PP sample are heated and cooled with a rate of 5 °C/min. It is obvious from the DSC result that the number of the crystalline layers in the single- and double-layer transcrystalline films does not have measurable impact on their thermal properties. The parameters of the two thermal transitions, *i.e.* the melting temperatures (T_m), crystallisation temperatures (T_c), and degree of crystallinity (X_c) are extracted and listed in Table 6.1. There is no pronounced difference in the thermal properties and crystallinity of the two different PP samples. It proves that their crystallite structure and interaction at the crystalline-amorphous interface are the same, as mentioned earlier with the theoretical prediction [173, 174]. Different T_ms are normally observed in the PP films with different spherulite sizes. However, the films are often produced with different thermal histories, *e.g.* by means of isothermal crystallisation at different temperatures

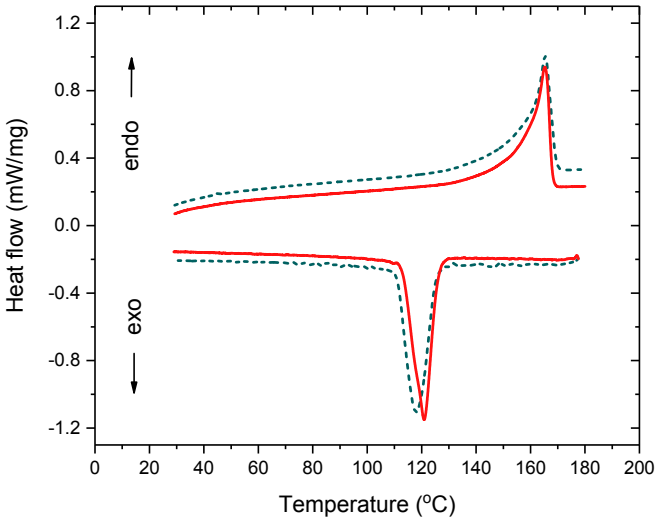

Figure 6.3: Differential scanning calorimetry (DSC) curves of the single- and double-layer transcrystalline polypropylene films - No discernible difference between the single- (dashed line) and double-layer (solid line) transcrystalline PP can be observed in terms of the thermal transitions and crystallinity.

Table 6.1: The melting temperatures (T_m), crystallisation temperature T_c and degree of crystallinity (X_c) extracted from the DSC results of the single- and double-layer transcrystalline PP samples

Transcrystalline type	T_m	T_c	X_c
single-layer	159-169 °C	111-125 °C	44.1 %
double-layer	158-168 °C	112-125 °C	45.6 %

or cooling rates. Their crystalline lamellar structures are influenced by the difference in the temperature profiles during crystallisation, which does not occur in this experiment. The characteristic difference between the single- and double-layer transcrystalline PP films is simply the absence and presence of the transcrystalline interface, respectively.

6.2 Interfacial charge distribution

6.2.1 Charge distribution after corona discharge

For the charging and electrical measurements, the PP samples were metallised on one side with a 120 nm sputtered Al electrode. The corona needle positioned 20 mm above the free sample surface was supplied with a voltage of ±12 kV to ionise the ambient air.

The control grid with a voltage (V_G) of ±2 kV was placed 7-8 mm above the sample surface to control the surface potential of the non-metallised surface at the same value as V_G. The corona discharge was carried out at room temperature for 15 seconds.

A partial thermal discharge technique (the same as that in chapter 4 section 4.2.2) was employed again for activating the charges in the transcrystalline PP electrets. The samples were partially discharged with the TSD set-up immediately after the corona charging under a linear heating rate of 3 °C/min. When the surface potential reduces to *ca.* 0.8 kV and the temperature reaches approximately 60 °C, the samples are quenched to room temperature to freeze the charge distribution at that moment. This method can mobilise some of the charges to escape from the shallow traps. The mobilised charges will be either captured in the deep traps or neutralised at the electrodes. In this way, one can pinpoint the location of the deep traps according to the spatial charge distribution. Furthermore, this process is equivalent to poling the PP electrets at elevated temperatures under the electric field of the deposited corona charges and quenching them to room temperature.

The reference group of the PP transcrystalline electrets were charged with the same arrangement of the corona set-up, except that the V_G was set to ±1 kV. So the reference samples will carry a similar potential *without* the follow-up partial discharge. The charges were deposited onto the surface of the single- and double-layer transcrystalline reference films and *not* activated/mobilised by any thermal stimulations. The charging was performed at room temperature, and the samples were not subjected to any thermal discharge. A comparison between the reference group and the partially thermal-discharged samples may distinguish the effect of thermal activation on the charges. It can illustrate the charge relocation (escaping from shallow traps and falling into deep traps) or dissipation (escaping from the shallow traps and being neutralised at the electrodes) during the thermal discharge.

The charge distributions of the single- and double-layer transcrystalline PP electrets were measured with the PPS method. For a crystalline structure that particularly grows along the thickness direction, the charge distribution regarding the thickness direction of the transcrystalline films is of great interest. It can offer more understanding about the morphology-related trap distribution in PP electrets. A piece of clean PP film with a thickness of 25 μm was placed between the corona charged surface of the PP samples and the rubber electrode of the PPS device in Figure 3.2 to protect the deposited surface

charges. Each charge distribution curve was the average of 4-10 results measured on individual samples. The vertical scale of the charge density was normalised to the absolute peak amplitude of the open-surface charges on the corresponding single-layer transcrystalline PP electret. It means that the surface charge density of each single-layer transcrystalline PP sample is presented as either +1.0 or −1.0, with the sign representing the polarity of the charges. The thickness of the sample films showed slight deviations from the nominal value, and thus it had to be normalised to 50 μm: 0 was the metallised surface and 50 μm was the charged open-surface of the PP sample.

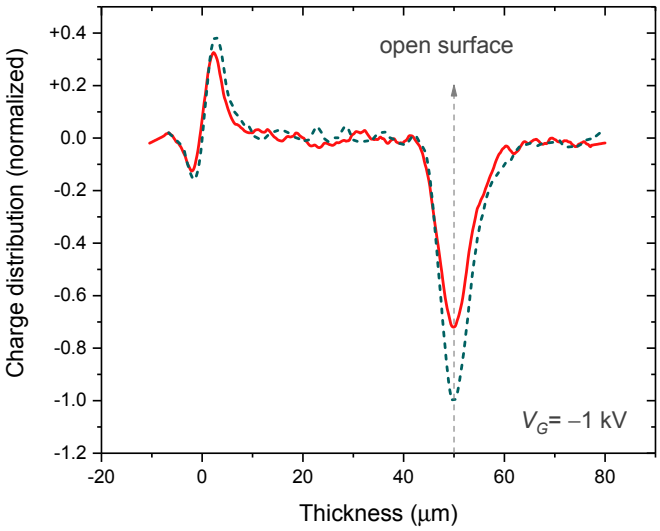

Figure 6.4: Charge distributions of the negatively charged single- and double-layer transcrystalline polypropylene without the partial thermal discharge - Both the single- (dashed line) and double-layer (solid line) transcrystallines only exhibit the deposited corona charges on the open surface and no charges in the bulk.

The charge distribution results in the single- (dashed line) and double-layer (solid line) transcrystalline PP electrets without the partial thermal discharge are shown in Figure 6.4 for the negative corona charges and in Figure 6.5 for the positive corona charges. In both figures, there are corona charges deposited only on the open surface of both transcrystalline samples and no charge injected into the bulk, which is typical for the *low energy* corona discharge at room temperature. The charge distributions on the rear electrode (at thickness 0) of the sample films suffer from the poor electrical contact of the electrode, similar as the cracked electrode on the PP films after heating in Figure 4.13 in section 4.2.2. But it does not influence the accuracy of the charge

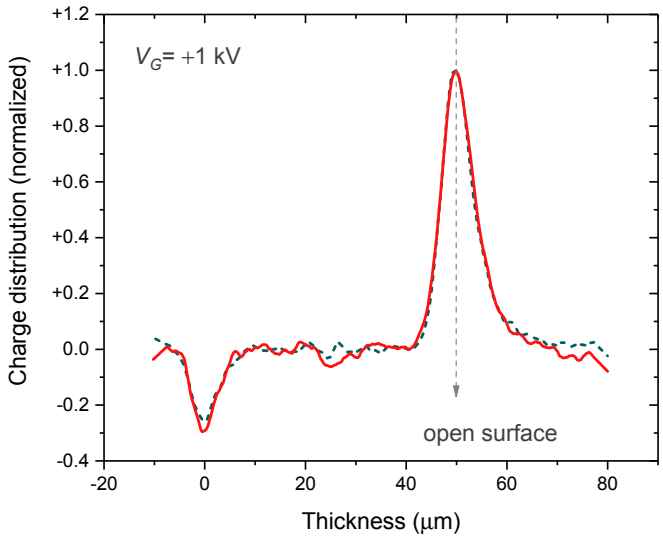

Figure 6.5: Charge distributions of the positively charged single- and double-layer transcrystalline polypropylene without the partial thermal discharge - Both the single- (dashed line) and double-layer (solid line) transcrystallines only exhibit the deposited corona charges on the open surface and no charges in the bulk.

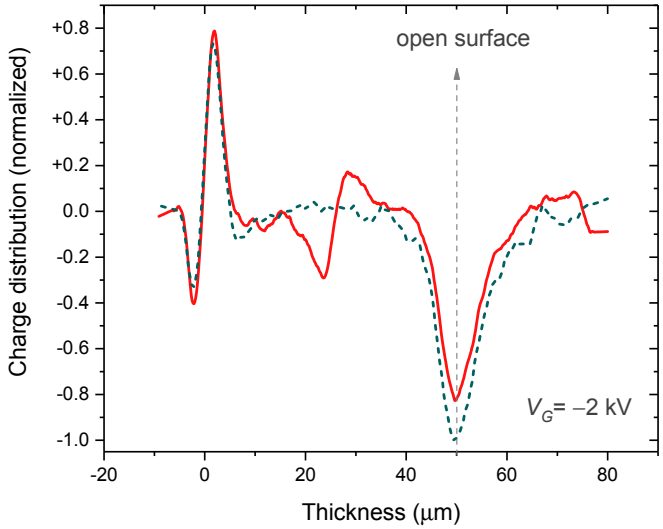

Figure 6.6: Charge distributions of the negatively charged single- and double-layer transcrystalline polypropylene after the partial thermal discharge - There are heterocharges present at both sides of the crystalline interface in the double-layer transcrystalline sample (solid line) but not in the single-layer one (dashed line).

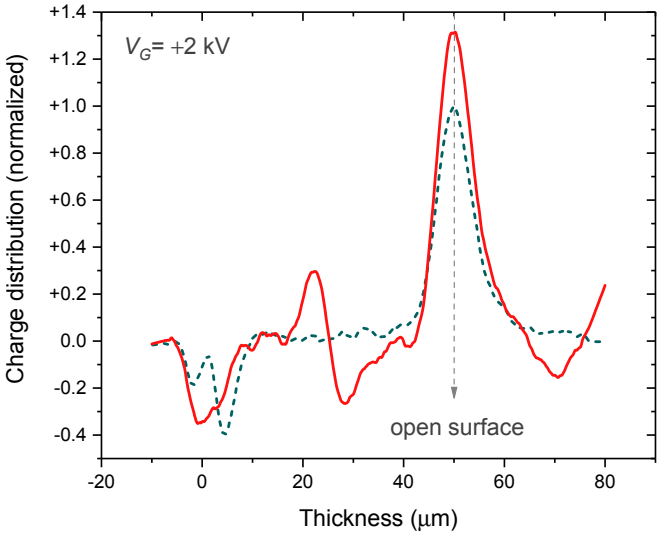

Figure 6.7: Charge distributions of the positively charged single- and double-layer transcrystalline polypropylene after the partial thermal discharge - There are heterocharges present at both sides of the crystalline interface in the double-layer transcrystalline sample (solid line) but not in the single-layer one (dashed line).

profiling on the surface and in the bulk of the samples, which are at the focus of this chapter. Without the thermal stimulation, the interface in the middle of the double-layer transcrystalline PP does not cause any visible difference on the charge distribution curves thereof in Figure 6.4 and 6.5.

However, when the deposited charges are activated/mobilised by the thermal stimulation during partial discharge, the charge distribution of the double-layer (solid line) transcrystalline PP starts to differ from that of the single-layer (dashed line) one. The results are shown in Figure 6.6 for the negative and in Figure 6.7 for the positive corona charges. Significant amounts of deposited charge are still captured in the surface traps of all the samples at this point. But one layer of charges can be observed on each side of the crystalline interface in the middle of the double-layer transcrystalline PP films. The interfacial charge layers appear to have the opposite sign of the adjacent electrode, *i.e.* heterocharges. The phenomenon does not occur to the single-layer transcrystalline samples. The charge distributions in Figure 6.7 are visualised with a schematic diagram of the positively corona charged single- (a) and double-layer (b) transcrystalline PP films in Figure 6.8.

Space charges in the bulk of the electrets mostly originate either internally from

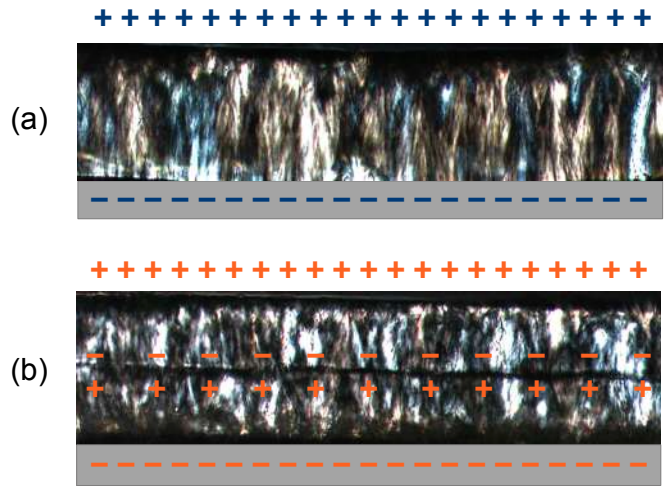

Figure 6.8: An example schematic diagram of the charge distributions after the partial discharge in the single- and double-layer transcrystalline polypropylene films - There are deposited corona charges on the open surface and compensation charges on the rear electrode of the single-layer transcrystalline PP (a), while there additionally are interfacial heterocharges in the double-layer transcrystalline sample (b).

the intrinsic charge carriers or externally from the charge injection from the adjacent electrode. The corona needle can be viewed as a distanced electrode that is a source with the unlimited charge supply. In this case of heterocharges at the interface of the double-layer transcrystalline PP, the external injection is very unlikely to be the reason. The interfacial charges with the same polarity of the electrode charges or the surface charges is located on the other side geometrically. Hence, these charges are most likely to be intrinsic charges at the interface that are thermally activated and poled by the deposited charges during the partial discharge, and eventually captured by the traps on each side of the interface. The origin of the interfacial charges will be investigated in the following section. Nevertheless, the charges are not completely neutralised by opposite charges on the surface and electrode or scattered within the transcrystalline layers. They are trapped at the interface at 60 °C instead, where the surface potential decays to less than half of the initial value. It indicates there are deep traps located near the crystalline interface that can withstand a temperature of 60 °C. Thus, the crystalline interfaces might be more significant than the transcrystalline structure *per se* in terms of charge storage at high temperatures. In addition, the ordered crystallite and molecules in the crystalline phase within the transcrystalline layers (illustrated in

Figure 5.6) may act as the quick transporting channels for charges. Once the charges escape the deep surface or interface traps, they might move swiftly along the internal electric field without the pronounced re-trapping within the transcrystalline layers.

6.2.2 Charge distribution after thermal poling

To examine the origin of the interfacial charges in the double-layer transcrystalline PP electrets, a special thermal poling technique was employed. The schematic diagram of the set-up is illustrated in Figure 6.9. Two PTFE films supplied by DuPont were used to block any possible charge injection from the electrodes. The films with a nominal thickness of 50 μm were inserted between the surface of the transcrystalline samples and the poling electrode. The excellent electret property and high electrical breakdown strength of the PTFE can prevent the charge injection from the upper copper electrode or the bottom grounded electrode that is also the heating plate. For recreating the poling condition in the last section, the thermal poling was carried out at 60 °C for 5 min under a poling electric field (E_p) of $\pm 4\times10^7$ V/m that is equivalent to a surface potential of ±2 kV on a 50 μm film. The positive sign of the electric field is defined as from the open surface to the rear electrode of the PP film. The as-received PP films without the transcrystallisation were also charged and examined in the same way as a reference.

Even the PTFE films can easily withstand a thermal poling of 60 °C for 5 min under $\pm 4\times10^7$ V/m without any charge penetrating. The blocking layers of PTFE films were still measured with the PPS method immediately after the poling for verification: no charge can be observed in the bulk of the PTFE. It indicates no sign of the charge injection. The single- and double-layer transcrystalline PP samples were carefully transferred from the charging set-up to the PPS measurements. Their charge distributions were examined with the same techniques described in the last section. The signal of charge density were also normalised by the absolute peak amplitude of the corresponding single-layer transcrystalline sample in each charging polarity. The thickness of the sample films had to be normalised to 50 μm for the final charge distribution results to eliminate the slight variation in the nominal value. The results are shown in Figure 6.10 and 6.11 for the transcrystalline samples charged with a negative and positive potential on the upper copper electrode, respectively.

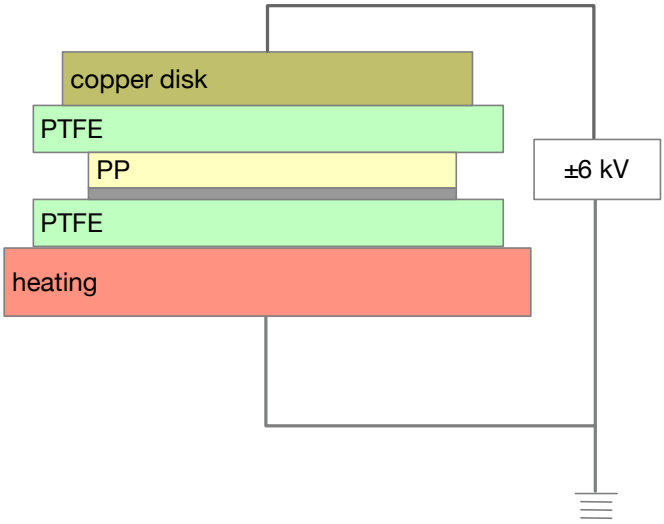

Figure 6.9: A schematic diagram of the special thermal poling method with the blocking layers for preventing charge injection - The thermal poling was carried out at 60 °C for 5 min with $E_p = \pm 4 \times 10^7$ V/m

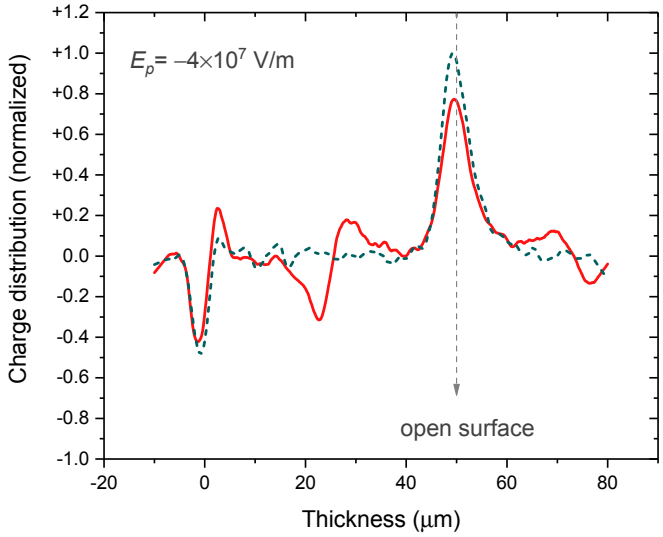

Figure 6.10: Charge distributions of the single- and double-layer transcrystalline polypropylene charged with a negative potential on the upper copper electrode - Heterocharges appear on the surface of the single-layer transcrystalline PP (dashed line) and on the surface and interface of the double-layer sample (solid line).

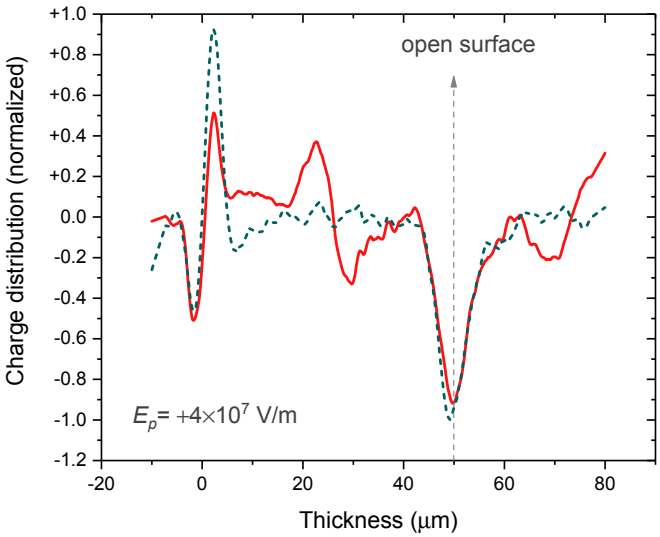

Figure 6.11: Charge distributions of the single- and double-layer transcrystalline polypropylene charged with a positive potential on the upper copper electrode - Heterocharges appear on the surface of the single-layer transcrystalline PP (dashed line) and on the surface and interface of the double-layer sample (solid line).

There are surface charges on all the PP electrets in Figure 6.10 and 6.11. The polarity of the surface charges is in the *opposite* correlation with the adjacent electrode as that of the surface charges on the samples in Figure 6.6 and 6.7, that is the surface charges in Figure 6.10 and 6.11 are heterocharges. However, the same heterocharge layers are present on both sides of the middle interface in the double-layer transcrystalline films in both cases of thermal poling (charging with the PTFE injection-blocking layers) and corona poling (thermally stimulated partial discharge). The charge distributions in Figure 6.11 are illustrated with the schematic diagrams in Figure 6.12 for both transcrytalline samples.

Solely heterocharges are observed in the single- and double-layer transcrystalline samples in Figure 6.10 and 6.11, and the blocking layers of PTFE can effectively eliminate the possibility of the external charge injection from the thermal poling. Therefore, it can be concluded that the surface and interfacial charges are most likely to be intrinsic charges. They were perhaps initially masked by the neighbouring charges of the opposite sign and later separated by applying electric field at elevated temperature. The process is similar to the charge carrier separation in the photoelectrets.

The phenomenon of the intrinsic charge carrier separation under thermal poling

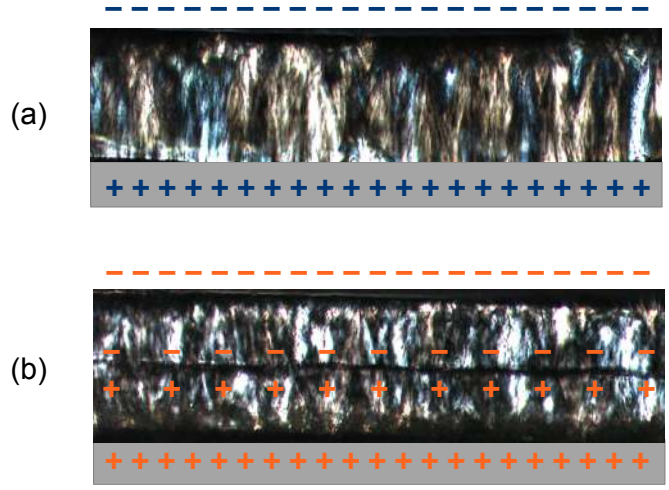

Figure 6.12: An example schematic diagram of the charge distributions in the thermally poled single- and double-layer transcrystalline polypropylene films with the positive voltage on the upper electrode - There are heterocharges on the surface of both single- (a) and double-layer (b) transcrystalline and at the interface of the latter.

was not observed in the reference as-received PP charged with the same injection-blocking technique. Thus, the heterocharges present in the single- and double-layer transcrystalline PP films might be introduced to the samples in the transcrystallisation process. They might be carried by the impurities or created by the triboelectrification between the PTFE moulding surface and the PP films. The charges later gain enough activation energy from the thermal stimulations to escape from the original shallow traps and to drift under the electric field. Eventually they are captured in the deep traps either at the interface or on the surface.

There are no charges detected within the transcrystalline layers regardless of the single- or double-layer composition and the charging methods. This evidently shows that the transcrystalline interfaces (surface included) can create traps of higher activation energy in comparison with the transcrystalline structure *per se*. The crystalline interface can provide a great disruption on the energy bands with its significant structural discontinuity. Additionally, when the polymers crystallise from the nucleating centres, the impurities are pushed further and accumulate at the interfaces, as the crystalline structure is expanding [138]. These impurities, including the chain ends, side groups and foreign chemicals of additives, may serve as deeper traps and bind

charges at higher temperatures.

It is interesting to notice that PP—a non-polar material—can be thermally poled to form two layers of opposite charges at a distance merely in the micrometer range. The two charge layers of opposite polarities separated by the crystalline interface in the middle of the double-layer transcrystalline PP films, to a certain extent, can be seen as the "micrometer-scale dipoles". By introducing voids into the PP films, the cellular PP ferroelectrets were invented as an alternative for the traditional ferroelectrics with intrinsic molecular dipoles. By manipulating the crystalline structures of the PP films, a layer of micrometer-scale "dipoles" can be built in the middle of the double-layer transcrystalline PP. The PP material, as one of the most common and simple polymer materials, still has much potential to offer to the modern world of the smart functional materials.

7

Conclusion and outlook

7.1 Conclusions

The influence of chemical surface modifications and crystalline reconstructions on the electret properties of PP films was investigated. The thermal charge stability and the charge distribution in the thickness direction were discussed. The molecular and structural changes from different chemical and crystallisation treatments were studied with infrared spectroscopy, microscopes, and thermal analysis. The results can provide an insight about the charge storage and transport processes, as well as the information of traps associated with various chemical and morphological properties.

The H_3PO_4-induced surface modification was able to increase the thermal stability of the PP electrets charged to −500 V and +500 V by 47 °C and 38 °C in their half-value temperature ($T_{1/2}$), respectively. However, the enhancement shows a dependence on the initial surface potential of the PP films and decreases dramatically as it reaches ±3 kV. This phenomenon was explained with the limited amount of newly-formed deep traps per unit modified open-surface area. The excess deposited charges might be forced to settle in the shallow intrinsic traps of the PP electrets when the surface charge density becomes significantly high ($\pm 1.2\times10^{-3}$ C·m^{-2}). At this point, more intrinsic traps may dominate the charge capture, leading to the early charge decay at low temperatures.

The foreign phosphorus- and oxygen-containing structures, responsible for the deep-trap formation on the chemically modified PP surfaces, exhibit a higher activation energy to the negative charges than to the positive charges. These negative-charge

preferential structures result in the asymmetrical surface-charge stability for different polarities in the H_3PO_4-modified PP electrets. Such asymmetry in the charge polarity does not appear in the non-treated PP. The modification with H_3PO_4 may be employed to optimise the performance of devices with the non-woven PP fabric filters and PP ferroelectrets.

The spherulite or transcrystalline structure can be formed in the PP film when it is crystallised from melt in contact with a smooth or rough moulding surface, respectively. The difference in the crystalline structure shows its influence on the electret behaviour of the PP films. The spherulitic PP charged to ±500 V shows asymmetrical charge stability: the negative surface charges are slightly more stable with a broader double-peak trap distribution extending to higher temperatures, while the positive charges decay faster with a less complex single-peak trap distribution. In addition, surface-potential saturation and undercharging phenomena can be observed on the PP electrets with the spherulites, which, however, do not take place on the transcrystalline PP films with virtually the same thermal properties and degree of crystallinity.

Although the transcrystalline PP electrets are able to obtain higher surface potentials of ±1 kV and ±2 kV, their surface charges decay faster with a higher initial potential, exhibiting the cross-over phenomenon. The charge distribution measurements reveal that the surface traps on the transcrystalline PP films are deeper than the bulk (volume) traps. Hence, when large amounts of charges are deposited on the surface, a great portion of the charges might be pushed to the shallow traps and decay at a lower temperature. Moreover, the one-dimensional transcrystalline structure may facilitate the charge transport under the high internal electric field.

A double-layer transcrystalline structure with a crystalline interface in the middle can be constructed by crystallising the PP film with rough moulding surfaces on both sides. A layer of heterocharges can be found on each side of the transcrystalline interface when the double-layer transcrystalline PP is subjected to a sufficiently high electric field at elevated temperatures (typically 60 °C). The heterocharges are most likely to be the internal charges introduced during the transcrytallisation. They are later separated by the thermal poling and captured in deep traps. The charge profiling shows that these heterocharges are trapped mainly at the interface and surfaces of the PP films. The experiment indicates the importance of the transcrystalline interface in terms of creating large energetic interruptions—deep traps.

Polymer materials are extremely versatile in terms of their molecular and morphological forms. This feature can lead to great advantages, or it may pose problems when it is overlooked. Polymers can be modified and reconstructed easily to fit the requirements of many applications. Electret properties of many polymer materials are highly sensitive to even minor changes of their chemical composition and crystalline structures. Therefore, it was emphasised in the present thesis that the slight variations during the polymer processing may lead to dramatic impact on the electret properties of the PP films. With proper chemical treatments on the surface, the charge stability of PP electrets can be improved. In the meantime, significant changes on the morphology of PP films can happen when the substrate for their crystallisation is different, resulting in a strong influence on their electret behaviour.

7.2 Outlook

The H_3PO_4 modification on the surface of the PP electrets can be applied to the non-woven PP fabric filters and the tubular-channel PP ferroelectrets for improving their performance, particularly the thermal stability. In addition, the island structures on the PP surface introduced by the H_3PO_4 treatment can be studied with the microscopic technique of Kelvin probe force microscope (KPFM). The nanoscale probe of the KPFM might be useful to investigate the charge trapping behaviour specifically on the islands. By comparing the electret properties of the foreign-chemical island and that of the PP matrix, the correlation between the trap depth and the chemical composition will be interpreted in a more direct way.

The same microscopic experiment can be implemented on the surface spherulites of the PP films to reveal the difference of traps at the spherulitic interface and the nucleating centres. Furthermore, the one-dimensional crystalline growth in the transcrystalline PP might exhibit certain anisotropic electret properties. PP electrets with large transcrystalline structures can be used for testing the charge transport in directions that are parallel or perpendicular to the transcrystalline growth, which can bring more understanding regarding the charge transport mechanism in the crystalline and amorphous phases of polymer electrets.

References

[1] D. B. Malpass and E. Band. *Introduction to Industrial Polypropylene: Properties, Catalysts, Processes*. Scrivener Publishing LLC, 2012. 1, 3, 4

[2] T. Taniike and M. Terano. *Polyolefins: 50 years after Ziegler and Natta I*, **257**, chapter The Use of Donors to Increase the Isotacticity of Polypropylene. Springer, Berlin, Heidelberg, 2013. 1

[3] J. A. Brydson. *Plastic Materials*. Butterworths, London, 5th edition, 1989. 2, 4, 5, 8

[4] D. Feldman. **Polymer History**. *Des. Monomers Polym.*, **11**(1):1–15, 2008. 2, 8

[5] R. B. Seymour and T. Cheng, editors. *History of Polyolefins: The World's Most Widely Used Polymers*. D. Reidel Publishing Company, Holland, 1986. 2

[6] J. Nicolas, S. Mura, D. Brambilla, N. Mackiewicz, and P. Couvreur. **Design, functionalization strategies and biomedical applications of targeted biodegradable/biocompatible polymer-based nanocarriers for drug delivery**. *Chem. Soc. Rev.*, **42**:1147–1235, 2013. 3

[7] F. Carpi and E. Smela, editors. *Biomedical Applications of Electroactive Polymer Actuators*. John Wiley & Sons, Inc., 2009. 3

[8] H. R. Sailors and J. P. Hogan. **History of Polyolefins**. *J. Macromol. Sci. A*, **15**(7):1377–1402, 1981. 3

[9] D. Tripathi. *Practical Guide to Polypropylene*. Rapra Technology LTD, UK, 2002. 4, 5

[10] J. R. Jambeck, R. Geyer, C. Wilcox, T. R. Siegler, M. Perryman, A. Andrady, R. Narayan, and K. L. Law. **Plastic waste inputs from land into the ocean**. *Science*, **347**(6223):768–771, 2015. 5

[11] K. Sudesh and T. Iwata. **Sustainability of Biobased and Biodegradable Plastics**. *Clean : soil, air, water*, **36**(5-6):433–442, 2008. 5

[12] Z. Li and B. Du. **Polymeric insulation for high-voltage dc extruded cables: challenges and development directions**. *IEEE Electr. Insul. Mag.*, **34**(6):30–43, 2018. 5, 41

[13] J. Zha, H. Yan, W. Li, and Z. Dang. **Morphology and crystalline-phase-dependent electrical insulating properties in tailored polypropylene for HVDC cables**. *Appl. Phys. Lett.*, **109**(22):222902, 2016. 5, 35, 41, 43

[14] X. Huang, Y. Fan, J. Zhang, and P. Jiang. **Polypropylene based thermoplastic polymers for potential recyclable HVDC cable insulation applications**. *IEEE Trans. Dielectr. Electr. Insul.*, **24**(3):1446–1456, 2017. 5, 41

[15] T. Andritsch, A. Vaughan, and G. C. Stevens. **Novel insulation materials for high voltage cable systems**. *IEEE Electr. Insul. Mag.*, **33**(4):27–33, 2017. 6

[16] M. Albertini, A. Bareggi, L. Caimi, L. de Rai, A. Dumont, S. F. Bononi, and G. Pozzati. **Development and high temperature qualification of innovative 320 kV DC cable with superiorly stable insulation system**. In *9th International Conference on Insulated Power Cables*, number A7.3, Versailles, France, 21-25 June 2015. 6

[17] J. van Turnhout, C. van Bochove, and G. van Veldhuizen. **Electret Fibres for High Efficiency Filtration of Polluted Gases**. *Staub-Reinhalt. Luft*, **36**(1):36–39, 1976. 6

[18] S. Bauer, R. Gerhard, and G. Sessler. **Ferroelectrets: Soft Electroactive Foams for Transducers**. *Phys. Today*, **57**(2):37–43, 2004. 6, 10, 11

[19] G. Sessler, editor. *Electrets*, **33** of *Topics in Applied Physics*. Springer Berlin Heidelberg, 2nd edition, 1987. 6, 7, 15, 16, 17, 18, 19, 20, 21, 23, 27, 28

[20] G. Odian. *Principles of Polymerization*. Wiley-Interscience, 2004. 6, 33

[21] G. Sessler and J. West. **Self Biased Condenser Microphone with High Capacitance**. *J. Acoust. Soc. Am*, **34**(11):1787–1788, 1962. 7

[22] R. Gerhard. **Dielectric materials for electro-active (electret) and/or electro-passive (insulation) applications**. In *International Conference on Electrical Materials and Power Equipment (ICEMPE)*, pages 91–96, Guangzhou, China, 7-10 April 2019. 7

[23] S. Gray. **A Letter from Mr. Stephen Gray to Dr. Mortimer, Secr. R. S. Containing a Farther Account of His Experiments concerning Electricity**. *Philos. Trans.*, **37**:285–291, 1732. 7

[24] M. Faraday. *Experimental researches in electricity*. R. and J. E. Taylor, London, 1839-1855. 7

[25] O. Heaviside. **Electromagnetic Induction and Its Propagation. Electrization and Electrification. Natural Electrets**. *The Electrician*, pages 230–231, 1885. 7

[26] M. Eguchi. **On Dielectric Polarisation**. *Proc. Phys. Math. Soc. Jpn.*, **3**(1):326–331, 1919. 7, 21

[27] M. Eguchi. **Further Researches on Permanently Polarised Dielectric**. In *Proceedings of the Physico-Mathematical Society of Japan. 3rd Series*, **2**, pages 169–176, 1920. 7

[28] M. Eguchi. **XX. On the permanent electret**. *Philos. Mag.*, **49**(289):178–192, 1925. 7

[29] P. Selenyi. **Uber die durch Kathodenstrahlung bewirkte electrische Aufladung des Glases**. *Z. Tech. Phys.*, **9**:451–454, 1928. 7, 20

[30] P. Selenyi. **On the Electrographic Recording of Fast Electrical Phenomena**. *J. Appl. Phys.*, **9**(10):637–641, 1938. 7, 20

[31] C. F. Carlson. **Electron photography**. *US Patent*, page 2221776A, 1940. 7

[32] L. B. Schein. *Electrophotography and Development Physics*. Springer-Verlag Berlin Heidelberg, 2nd edition, 1992. 7

[33] J. Van Turnhout. **The use of polymers for electrets**. *J Electrostat.*, **1**(2):147–163, 1975. 7, 13, 26

[34] P. C. A. Hammes and P. P. L. Regtien. **An integrated infrared sensor using the pyroelectric polymer PVDF**. *Sensor. Actuat. A-Phys.*, **32**(1):396–402, 1992. 9

[35] I. Grabec and M. Platte. **A comparison of high-performance acoustic emission transducers**. *Sensor. Actuat.*, **5**(4):275–284, 1984. 9

[36] Y. Wada and R. Hayakawa. **Piezoelectricity and Pyroelectricity of Polymers**. *Jpn. J. Appl. Phys.*, **15**(11):2041–2057, 1976. 9

[37] R. Gerhard. **From electrode charges on dielectric elastomers to trapped charges and electric dipoles in electrets and ferroelectrets: fundamental and applications-relevant aspects of diversity in electroactive polymers**. In *Proceedings of SPIE, Electroactive Polymer Actuators and Devices (EAPAD)*, **9798**, page 97980T, Las Vegas, USA, 20-24 March 2016. 9

[38] J. N. Wilson, J. M. Frost, S. K. Wallace, and A. Walsh. **Dielectric and ferroic properties of metal halide perovskites**. *APL Mater.*, **7**(1):010901, 2019. 10

[39] M. Nakamura and K. Yamashita. **Polarization effect on wettability of bioceramic electrets**. *IEEE Trans. Dielectr. Electr. Insul.*, **19**(4):1247–1252, 2012. 10

[40] A. Savolainen and K. Kirjavainen. **Electrothermomechanical Film. Part I. Design and Characteristics**. *J Macromol. Sci. A*, **26**(2-3):583–591, 1989. 10

[41] X. Qiu, A. Mellinger, M. Wegener, W. Wirges, and R. Gerhard. **Barrier Discharges in Cellular Polypropylene Ferroelectrets: How Do They Influence the Electromechanical Properties?** *J. Appl. Phys.*, **101**(10):104112, 2007. 10, 11, 20

[42] R. Gerhard. **A matter of attraction: Electric charges localised on dielectric polymers enable electromechanical transduction**. In *IEEE Conference on Electrical Insulation and Dielectric Phenomena (CEIDP)*, pages 1–10, Des Moines, USA, 19-22 October 2014. 12

[43] R. Gerhard, S. Bauer, and X. Qiu. **Charge-spring model for predicting the piezoelectric response of dielectric materials: Considering tetragonality extends validity to ferroelectric crystals**. In *IEEE Conference on Electrical Insulation and Dielectric Phenomena (CEIDP)*, pages 81–84, Toronto, Canada, 16-19 October 2016. 12

[44] G. S. Neugschwandtner, R. Schwödiauer, S. Bauer-Gogonea, S. Bauer, M. Paajanen, and J. Lekkala. **Piezo- and pyroelectricity of a polymer-foam space-charge electret**. *J. Appl. Phys.*, **89**(8):4503–4511, 2001. 12

[45] S. Bauer. **Polymer electrets in flexible electronics**. In *IEEE 14th International Symposium on Electrets (ISE)*, pages 25–26, Montpellier, France, 28-31 August 2011. 12

[46] O. Voronina, M. Wegener, W. Wirges, R. Gerhard, L. Zirkel, and H. Münstedt. **Physical foaming of fluorinated ethylene-propylene (FEP) copolymers in supercritical carbon dioxide: single-film fluoropolymer piezoelectrets**. *Appl. Phys. A*, **90**(4):615–618, 2008. 12

[47] R. A. P. Altafim, X. Qiu, W. Wirges, R. Gerhard, R. A. C. Altafim, H. Basso, W. Jenninger, and J. Wagener. **Template-based Fluoroethylenepropylene Piezoelectrets with Tubular Channels for Transducer Applications**. *J. Appl. Phys.*, **106**(1):014106, 2009. 12

[48] R. A. P. Altafim, R. A. C. Altafim, X. Qiu, S. Raabe, W. Wirges, H. Basso, and R. Gerhard. **Fluoropolymer Piezoelectrets with Tubular Channels: Resonance Behavior Controlled by Channel Geometryith Tubular Channels: Resonance Behavior Controlled By Channel Geometry**. *Appl. Phys. A*, **107**:965–970, 2012. 12

[49] J. Van Turnhout, W. J. Hoeneveld, J. C. Adamse, and L. M. Van Rossen. **Electret Filters for High-Efficiency and High-Flow Air Cleaning**. *IEEE Trans. Ind. Appl.*, **IA-17**(2):240–248, 1981. 13

[50] R. Thakur, D. Das, and A. Das. **Electret Air Filters**. *Sep. Purif. Rev.*, **42**(2):87–129, 2013. 13, 20

[51] B. Gross. **Experiments on Electrets**. *Phys. Rev.*, **66**:26–28, 1944. 15

[52] B. Gross. **On Permanent Charges in Solid Dielectrics. II. Surface Charges and Transient Currents in Carnauba Wax**. *J. Chem. Phys.*, **17**(10):866–872, 1949. 15

[53] R. Gerson and J. H. Rohrbaugh. **Experiments on the Carnauba Wax Electret**. *J. Chem. Phys.*, **23**(12):2381–2388, 1955. 16

[54] B. Gross and R. J. de Moraes. **Polarization of the Electret**. *J. Chem. Phys.*, **37**(4):710–713, 1962. 16, 26, 30

[55] M. M. Perlman. **Thermal Currents and the Internal Polarization in Carnauba Wax Electrets**. *J. Appl. Phys.*, **42**(7):2645–2652, 1971. 16, 26

[56] J. F. Fowler and H. Fröhlich. **X-ray induced conductivity in insulating materials**. *Proc. Royal Soc. Lond. A*, **236**(1207):464–480, 1956. 16

[57] A. Miller and E. Abrahams. **Impurity Conduction at Low Concentrations**. *Phys. Rev.*, **120**:745–755, 1960. 16

[58] N. F. Mott. **On The Transition To Metallic Conduction In Semiconductors**. *Can. J. Phys.*, **34**(12A):1356–1368, 1956. 16, 18

[59] N.F. Mott. **Conduction in glasses containing transition metal ions**. *J. Non-Cryst. Solids*, **1**(1):1 – 17, 1968. 16

[60] E. M. Conwell. **Impurity Band Conduction in Germanium and Silicon**. *Phys. Rev.*, **103**:51–61, 1956. 16, 18

[61] H. Scher and E. W. Montroll. **Anomalous transit-time dispersion in amorphous solids**. *Phys. Rev. B*, **12**:2455–2477, 1975. 16, 28

[62] W.A. Schneider and J.H. Wendorff. *Electronic Properties of Polymers and Related Compounds*, **63**, chapter Polymeric Electrets. Springer, Berlin, Heidelberg, 1985. 16, 18, 19

[63] H. Bauser. **Ladungsspeicherung in Elektronenhaftstellen in Organischen Isolatoren**. *Kunststoffe*, **62**:192–196, 1972. 16, 17, 18, 28, 35, 63

[64] J. van Turnhout. **Thermally Stimulated Discharge of Polymer Electrets**. *Polym. J.*, **2**(2):173–191, 1971. 17, 26, 28, 30

[65] P. Würfel. *Physics of Solar Cells: From Principles to New Concepts*. Wiley-VCH, 2005. 17, 21

[66] H. von Seggern. **Detection of Surface and Bulk Traps**. *J. Appl. Phys.*, **52**(6):4086–4089, 1981. 19, 26, 56

[67] J. Giacometti, S. Fedosov, and M. Costa. **Corona Charging of Polymers: Recent Advances on Constant Current Charging**. *Braz. J. Phys.*, **29**(2):269–279, 1999. 20, 22, 23

[68] P. Murphy, S. Ribeira, F. Milanez, and R. Moraes. **Effect of Penetrating Radiation on the Production of Persistent Internal Polarization in Electret-Forming Materials**. *J. Chem. Phys.*, **38**(10):2400–2404, 1963. 20, 21

[69] R. Gerhard-Multhaupt, G. M. Sessler, J. E. West, K. Holdik, M. Haardt, and W. Eisenmenger. **Investigation of piezoelectricity distributions in poly(vinylidene fluoride) by means of quartz- or laser-generated pressure pulses**. *J. Appl. Phys.*, **55**(7):2769–2775, 1984. 21, 23, 31, 33

[70] T. Yovcheva, I. Avramova, G. Mekishev, and T. Marinova. **Corona-Charged Polypropylene Electrets Analyzed by XPS**. *J. Electrostat.*, **65**:667–671, 2007. 23, 37, 59

[71] R. Ono, M. Naakazawa, and T. Oda. **Charge Storage in Corona-Charged Polypropylene Films Analyzed by LIPP and TSC Methods**. *IEEE Trans. Ind. Appl.*, **40**(6):1482–1488, 2004. 23, 62

[72] R. Gerhard-Multhaupt, G. Eberle, Z. Xia, G. Yang, and W. Eisenmenger. **Electric-field profiles in corona- or electron-beam-charged and thermally treated Teflon PTFE, FEP, and PFA films**. In *IEEE Conference on Electrical Insulation and Dielectric Phenomena (CEIDP)*, pages 61–66, Victoria, Canada, 18-21 October 1992. 23

[73] P. Southgate. **Room-temperature Poling and Morphology Changes in Pyroelectric Polyvinylidene Fluoride**. *Appl. Phys. Lett.*, **28**(5):250–252, 1976. 23

[74] R. Moreno and B. Gross. **Measurement of Potential Buildup and Decay, Surface Charge Density, and Charging Currents of Corona-charged Polymer Foil Electrets**. *J. Appl. Phys.*, **47**(8):3397–3402, 1976. 23

[75] E. Motyl. **Charging of polypropylene foils in corona triode system**. *J. Electrostat.*, **30**:57–64, 1993. 23

[76] J. D. Brodribb, D. M. Hughes, and T. J. Lewis. *Electrets: Charge Storage and Transport in Dielectrics*, chapter The Energy Spectrum of Traps in Insulators by Photon-induced Current Spectroscopy, pages 177–187. The Electrochemical Society, 1973. 25

[77] A. Mellinger, F. C. Gonzalez, R. Gerhard-Multhaupt, L. F. Santos, and R. M. Faria. **Photostimulated discharge of corona and electron-beam charged electret polymers**. In *IEEE 11th International Symposium on Electrets (ISE)*, pages 7–10, Melbourne, Australia, 1-3 October 2002. 25

[78] A. Mellinger. **Dielectric resonance spectroscopy: a versatile tool in the quest for better piezoelectric polymers**. *IEEE Trans. Dielectr. Electr. Insul.*, **10**(5):842–861, 2003. 25

[79] A Mellinger, F. C. González, and R. Gerhard-Multhaupt. **Ultraviolet-induced discharge currents and reduction of the piezoelectric coefficient in cellular polypropylene films**. *Appl. Phys. Lett.*, **82**(2):254–256, 2003. 25

[80] A. Mellinger, F. C. Gonzalez, and R. Gerhard-Multhaupt. **Photostimulated discharge in electret polymers: an alternative approach for investigating deep traps**. *IEEE Trans. Dielectr. Electr. Insul.*, **11**(2):218–226, 2004. 25

[81] A. Mellinger, R. Singh, and R. Gerhard-Multhaupt. **Fast thermal-pulse measurements of space-charge distributions in electret polymers**. *Rev. Sci. Instrum.*, **76**(1):013903, 2005. 25

[82] J. D. Brodribb, D. O'Colmain, and D. M. Hughes. **The theory of photon-stimulated current spectroscopy**. *J. Appl. Phys. D*, **8**(7):856–862, 1975. 26

[83] P. Ma, Y. Zhang, S. Holé, F. Zheng, Min Gu, and Z. An. **Effect of photoemission from electrode on photo-stimulated discharge spectra**. In *2016 IEEE International Conference on Dielectrics (ICD)*, **1**, pages 187–190, Montpellier, France, 3-7 July 2016. 26

[84] R. W. Tyler, J. H. Webb, and W. C. York. **Measurements of Electrical Polarization in Thin Dielectric Materials**. *J. Appl. Phys.*, **26**(1):61–68, 1955. 26, 27

[85] R. A. Creswell and M. M. Perlman. **Thermal Currents from Corona Charged Mylar**. *J. Appl. Phys.*, **41**(6):2365–2375, 1970. 26

[86] H. von Seggern. **Identification of TSC Peaks and Surface-voltage Stability in Teflon FEP**. *J. Appl. Phys.*, **50**(4):2817–2821, 1979. 26

[87] L. Kelvin. **V. Contact electricity of metals**. *Philos. Mag.*, **46**(278):82–120, 1898. 26

[88] M. A. Noras. **Non-contact surface charge/voltage measurements: capacitive probe-principle of operation**. Technical report, Trek Inc., 190 Walnut Street, Lockport, New York 14094, USA, 2002. 27, 28

[89] M. A. Noras. **Non-contact surface charge/voltage measurements: Fieldmeter and voltmeter methods**. Technical report, Trek Inc., 190 Walnut Street, Lockport, New York 14094, USA, 2002. 27

[90] P. Molinié. **A Review of Mechanisms and Models Accounting for Surface Potential Decay**. *IEEE Trans. Plasma Sci.*, **40**(2):167–176, 2012. 29

[91] J. Simmons, G. Taylor, and M. Tam. **Thermally Stimulated Currents in Semiconductors and Insulators Having Arbitrary Trap Distributions**. *Phys. Rev. B*, **7**(8):3714–3719, 1973. 29, 56

[92] P. Watson. **Transport and trapping of electrons in polymers**. *IEEE Trans. Dielectr. Electr. Insul.*, **2**(5):21–27, 1995. 29

[93] J. Li, F. Zhou, D. Min, S. Li, and R. Xia. **The energy distribution of trapped charges in polymers based on isothermal surface potential decay model**. *IEEE Trans. Dielectr. Electr. Insul.*, **22**(3):1723–1732, 2015. 29

[94] W. Shen, H. Mu, G. Zhang, J. Deng, and D. Tu. **Identification of electron and hole trap based on isothermal surface potential decay model**. *J. Appl. Phys.*, **113**(8):083706, 2013. 29

[95] J. Wang, D. Rychkov, and R. Gerhard. **Chemical modification with orthophosphoric acid enhances surface-charge stability on polypropylene electrets**. *Appl. Phys. Lett.*, **110**(19):192901, 2017. 29, 49, 50

[96] F. Johann and E. Soergel. **Quantitative measurement of the surface charge density**. *Appl. Phys. Lett.*, **95**(23):232906, 2009. 30

[97] R. A. Fletcher. **Electrostatic microprobe for determining charge domains on surfaces**. *Rev. Sci. Instrum.*, **86**(11):113702, 2015. 30

[98] D. van Krevelen, editor. *Properties of Polymers*. Elsevier, 3rd edition, 1997. 30, 43, 83

[99] R. E. Collins. **Analysis of spatial distribution of charges and dipoles in electrets by a transient heating technique**. *J. Appl. Phys.*, **47**(11):4804–4808, 1976. 31

[100] R. E. Collins. **Practical application of the thermal pulsing technique to the study of electrets**. *J. Appl. Phys.*, **51**(6):2973–2986, 1980. 31

[101] S. B. Lang and D. K. Das-Gupta. **A technique for determining the polarization distribution in thin polymer electrets using periodic heating**. *Ferroelectrics*, **39**(1):1249–1252, 1981. 31

[102] P. Bloss and H. Schaefer. **Investigations of polarization profiles in multilayer systems by using the laser intensity modulation method**. *Rev. Sci. Instrum.*, **65**(5):1541–1550, 1994. 31

[103] G. M. Sessler, J. E. West, D. A. Berkley, and G. Morgenstern. **Determination of Spatial Distribution of Charges in Thin Dielectrics**. *Phys. Rev. Lett.*, **38**:368–371, 1977. 31

[104] P. Laurenceau, G. Dreyfus, and J. Lewiner. **New Principle for the Determination of Potential Distributions in Dielectrics**. *Phys. Rev. Lett.*, **38**:46–49, 1977. 31

[105] G. Sessler, J. West, and G. Gerhard. **High-Resolution Laser-Pulse Method for Measuring Charge Distribution in Dielectrics**. *Phys. Rev. Lett*, **48**(8):563–566, 1982. 31

[106] A. Migliori and J. D. Thompson. **A nondestructive acoustic electric field probe**. *J. Appl. Phys.*, **51**(1):479–485, 1980. 31

[107] W. Eisenmenger and M. Haardt. **Observation of charge compensated polarization zones in polyvinylindenfluoride (PVDF) films by piezoelectric acoustic step-wave response**. *Solid State Commun.*, **41**(12):917 – 920, 1982. 31

[108] R Gerhard-Multhaupt, M Haardt, W Eisenmenger, and G M Sessler. **Electric-field profiles in electron-beam-charged polymer electrets**. *J. Phys. D: Appl. Phys.*, **16**(11):2247–2256, 1983. 31, 33

[109] R. Gerhard-Multhaupt. **Analysis of pressure-wave methods for the nondestructive determination of spatial charge or field distributions in dielectrics**. *Phys. Rev. B*, **27**:2494–2503, 1983. 32, 33

[110] P. Bloss, M. Steffen, H. Schafer, G. Eberle, and W. Eisenmenger. **Polarization and electric field distribution in thermally poled PVDF and FEP**. *IEEE Trans. Dielectr. Electr. Insul.*, **3**(3):417–424, 1996. 32, 33

[111] C. Alquie, G. Dreyfus, and J. Lewiner. **Stress-Wave Probing of Electric Field Distribution in Dielectrics**. *Phys. Rev. Lett*, **47**(20):1483–1487, 1981. 33

[112] R. Creswell, M. Perlman, and M. Kabayama. *Dielectric Properties of Polymers*, chapter The Electret Properties of a Series of Corona-Charged Substituted Polyolefins, pages 295–312. Plenum Press, Boston, 1972. 34

[113] H. J. Wintle. **Introduction to electrets**. *J. Acoust. Soc. Am*, **53**(6):1578–1588, 1973. 34

[114] M. Sato, A. Kumada, and K. Hidaka. **First-principles determination of electronic charge transport properties in polymer dielectrics using a crystalline-based model system**. *IEEE Trans. Dielectr. Electr. Insul.*, **26**(4):1204–1210, 2019. 34

[115] Seonwoo Kim, Kuniko Suzuki, Ai Sugie, Hiroyuki Yoshida, Masafumi Yoshida, and Yuji Suzuki. **Effect of end group of amorphous perfluoro-polymer electrets on electron trapping**. *Science and Technology of Advanced Materials*, **19**(1):486–494, 2018. 34

[116] M. Sato, A. Kumada, K. Hidaka, T. Hirano, and F. Sato. **Quantum chemical calculation of hole transport properties in crystalline polyethylene**. *IEEE Trans. Dielectr. Electr. Insul.*, **23**(5):3045–3052, 2016. 34

[117] P. de Gennes. *Scaling Concepts in Polymer Physics*. Cornell Univerisity, New York, 1979. 35

[118] A. Yagishita, H. Yamanouchi, and K. Ikezaki. **Charge Trapping Sites in Spherulitic Polypropylene**. *Jpn. J. Appl. Phys.*, **38**(4R):2053–2058, 1999. 35, 41, 43

[119] R. Nath and M. Perlman. **Effect of Crystallinity on Charge Storage in Polypropylene and Polyethylene**. *IEEE Trans. Dielectr. Electr. Insul.*, **24**(3):409–412, 1989. 35, 43

[120] M. Meunier, N. Quirke, and A. Aslanides. **Molecular modeling of electron traps in polymer insulators: Chemical defects and impurities**. *J. Chem. Phys.*, **115**(6):2876–2881, 2001. 35, 63

[121] D. Rychkov and R. Gerhard. **Stabilization of Positive Charge On Polytetrafluoroethylene Electret Films Treated with Titanium-Tetrachloride Vapor**. *Appl. Phys. Lett.*, **98**(12):122901, 2011. 35, 42

[122] D. Rychkov, R. Altafim, X. Qiu, and R. Gerhard. **Treatment with orthophosphoric acid enhances the thermal stability of the piezoelectricity in low-density polyethylene ferroelectrets**. *J. Appl. Phys.*, **111**(12):124105, 2012. 35, 37, 42, 48, 50

[123] S. Haridoss and M. M. Perlman. **Chemical modification of near-surface charge trapping in polymers**. *J. Appl. Phys.*, **55**(5):1332–1338, 1984. 35, 42

[124] M. A. Ramazanov and A. S. Guseinova. **Effect of the electrothermopolarization on the electret properties and the charge state of polyethylene nanocomposites with Cr and PbCrO4 additives**. *Surf. Engin. Appl.Electrochem.*, **49**(2):97–100, 2013. 35

[125] B. Chen, W. Tang, C. Zhang, L. Xu, L. Zhu, L. Yang, C. He, J. Chen, L. Liu, T. Zhou, and Z. Wang. **Au nanocomposite enhanced electret film for triboelectric nanogenerator**. *Nano Res.*, **11**(6):3096–3105, 2018. 35

[126] H. von Seggern and J. West. **Stabilization of Positive Charge in Fluorinated Ethylene Propylene Copolymer**. *J. Appl. Phys.*, **55**(7):2754–2757, 1984. 36

[127] G. Yang. **Thermally Stimulated Discharge of Electron-beam- and Corona-charged Polypropylene Films**. *J. Phys. D: Appl. Phys.*, **26**(4):690–693, 1993. 36, 43

[128] L. Reimer. *Scanning Electron Microscopy: Physics of Image Formation and Microanalysis*. Springer-Verlag Berlin Heidelberg, 2nd edition, 1998. 37

[129] D. Rychkov, A. Kuznetsov, and A. Rychkov. **Electret Properties of Polyethylene and Polytetrafluoroethylene Films with Chemically Modified Surface**. *IEEE Trans. Dielectr. Electr. Insul.*, **18**(1):8–14, 2011. 37

[130] B. Stuart. *Infrared Spectroscopy: Fundamentals and Applications*. Analytical Techniques in the Science. Wiley, Sydney, 1st edition, 2004. 38, 49

[131] J. D. Menczel and R. B. Prime, editors. *Thermal Analysis of Polymers: Fundamentals and Applications*. John Wiley & Sons, Inc., 2009. 39

[132] A. J. Müller and R. M. Michell. *Polymer Morphology*, chapter Differential Scanning Calorimetry of Polymers, pages 72–99. John Wiley & Sons, Inc., 2016. 39

[133] B. Wunderlich. *Thermal Analysis*, pages 417–431. Academic Press, 1st edition, 1990. 39

[134] L. Sawyer, D. T. Grubb, and G. F. Meyers. *Polymer Microscopy*. Springer, 3rd edition, 2008. 39, 40

[135] H. Awaya. **Morphology of different types of isotactic polypropylene spherulites crystallized from melt**. *Polymer*, **29**(4):591 – 596, 1988. 40

[136] H. D. Keith and Jr. F. J. Padden. **A discussion of spherulitic crystallization and spherulitic morphology in high polymers**. *Polymer*, **27**(9):1463–1471, 1986. 40

[137] D.C. Bassett and R.H. Olley. **On the lamellar morphology of isotactic polypropylene spherulites**. *Polymer*, **25**(7):935 – 943, 1984. 40

[138] C. Vasile, editor. *Handbook of Polyolefins*. CRC Press, 2nd edition, 2000. 40, 41, 94

[139] N. Behrendt, N. Mohmeyer, J. Hillenbrand, M. Klaiber, X. Zhang, G. Sessler, H. Schmidt, and V. Altstädt. **Charge Storage Behavior of Isotropic and Biaxially-Oriented Polypropylene Films Containing alpha- and beta-Nucleating Agents**. *J. Appl. Polym. Sci.*, **99**:650–658, 2006. 41, 43

[140] G. Krause, D. Meurer, and D. Klee. **Space Charge Formation Related to the Morphology of Polymers**. *IEEE Trans. Dielectr. Electr. Insul.*, **24**(3):419–424, 1989. 41

[141] X. Li, Q. Du, J. Kang, and D. Tu. **Influence of microstructure on space charges of polypropylene**. *J. Polym. Sci. B*, **40**(4):365–374, 2002. 41

[142] J. Ho and T. R. Jow. **High field conduction in biaxially oriented polypropylene at elevated temperature**. *IEEE Trans. Dielectr. Electr. Insul.*, **19**(3):990–995, 2012. 41

[143] T. Mizutani, E. Nakane, K. Kaneko, M. Ishioka, and H. Takino. **Space charge and charge transport in polypropylene**. In *IEEE 12th International Symposium on Electrets (ISE)*, pages 475–478, Salvador, Brazil, 11-14 September 2005. 41

[144] K. Ikezaki and D. Fujii. **Space Charge Limited Currents in Spherulitic Polypropylene**. In *IEEE 7th International Symposium on Electrets (ISE)*, pages 183–188, Berlin, Germany, 25-27 September 1991. 41, 43

[145] H. Fujii, T. Sakamoto, H. Matsuura, and A. Kishi. **Electrical Conduction and Charge Storage of Thin Polypropylene Films Due to Electron Beam Irradiation**. In *IEEE Conference on Electrical Insulation and Dielectric Phenomena (CEIDP)*, pages 624–628, Montreal, Canada, 14-17 October 2012. 41

[146] D. Rychkov, M. Yablokov, and A. Rychkov. **Chemical and physical surface modification of PTFE films—an approach to produce stable electrets**. *Appl. Phys. A*, **107**(3):589–596, 2012. 42

[147] D. Rychkov, A. Rychkov, N. Efimov, A. Malygin, and R. Gerhard. **Higher Stabilities of Positive and Negative Charge on Tetrafluoroethylene-hexafluoropropylene Copolymer (FEP) Electrets Treated with Titanium-tetrachloride Vapor**. *Appl. Phys. A*, **112**(2):283–287, 2013. 42

[148] D. Rychkov, R. Gerhard, V. Ivanov, and A. Rychkov. **Enhanced Electret Charge Stability on Polyethylene Films Treated with Titanium-Tetrachloride Vapor**. *IEEE Trans. Dielectr. Electr. Insul.*, **19**(4):1305–1311, 2012. 42

[149] Z. An, M. Zhao, J. Yao, Y. Zhang, and Z. Xia. **Improved piezoelectric properties of cellular polypropylene ferroelectrets by chemical modification**. *Appl. Phys. A*, **95**(3):801–806, 2009. 42

[150] Z. An, M. Zhao, J. Yao, Y. Zhang, and Z. Xia. **Influence of fluorination on piezoelectric properties of cellular polypropylene ferroelectrets**. *J. Phys. D: Appl. Phys.*, **42**(1):015418, 2009. 42

[151] Z. An, J. Yao, M. Mao, Y. Zhang, and Z. Xia. **Significantly Improved Charge Stability of Cellular Polypropylene Films by Fluorination and Subsequent Annealing**. *J. Electrostat.*, **68**:523–527, 2010. 42

[152] Z. An, M. Mao, J. Cang, Y. Zhang, and F. Zheng. **Significantly improved piezoelectric thermal stability of cellular polypropylene films by high pressure fluorination and post-treatments**. *J. Appl. Phys.*, **111**(2):024111, 2012. 42

[153] M. Tang, Z. An, Z. Xia, and X. Zhang. **Electret properties and chemical modification of cellular polypropylene films**. *J. Electrostat.*, **65**:203–208, 2007. 42

[154] R. Joshi, R. Schulze, A. Meyer-Plath, M. Wagner, and J. Friedrich. **Selective Surface Modification of Polypropylene using Underwater Plasma Technique or Underwater Capillary Discharge**. *Plasma. Process. Polym,*, **6**:S218–S222, 2009. 42

[155] K. Oka and K. Ikezaki. **Effect of Etching Treatment on Thermally Stimulated Current in Spherulitic Polypropylene**. *Jpn. J. Appl. Phys.*, **31**(4):1097–1101, 1992. 42, 76

[156] J. S. Mijovic and J. A. Koutsky. **Etching of polymeric surfaces: a review**. *Polym.-Plast. Technol. Eng.*, **9**(2):139–179, 1977. 43

[157] E. Sheng, I. Sutherland, D.M. Brewis, and R.J. Heath. **Effects of the chromic acid etching on propylene polymer surfaces**. *J. Adhesion Sci. Technol.*, **9**(1):47–60, 1995. 43

[158] A. Voss, R. W. Stark, and C. Dietz. **Surface versus Volume Properties on the Nanoscale: Elastomeric Polypropylene**. *Macromolecules*, **47**(15):5236–5245, 2014. 43

[159] A. Thyssen, K. Almdal, and E. V. Thomsen. **Electret stability related to spherulites in polypropylene**. *IEEE Trans. Dielectr. Electr. Insul.*, **22**(5):2858–2863, 2015. 43

[160] A. Baba and K. Ikezaki. **Drawing and annealing effects on thermally stimulated currents in polypropylene films**. *J. Appl. Phys.*, **72**(5):2057–2059, 1992. 43

[161] N. Saito and K. Ikezaki. **Electrical Charging Characteristics of Spherulitic Polypropylene**. *Jpn. J. Appl. Phys.*, **28**(3R):418–422, 1989. 43, 76

[162] Z. Xia. **Improved Charge Stability in Polymer Electrets Quenched before Charging**. *IEEE Trans. Dielectr. Electr. Insul.*, **25**(3):611–615, 1990. 43

[163] T. Hata, K. Ohsaka, T. Yamada, K. Nakamae, N. Shibata, and T. Matsumoto. **Transcrystalline Region of Polypropylene: Its Formation, Structure and Mechanical Properties**. *J. Adhesion*, **45**(1-4):125–135, 1994. 44

[164] C. W. Lin, S. Y. Ding, and Y. W. Hwang. **Interfacial crystallization of isotactic polypropylene molded against the copper surface with various surface roughnesses prepared by an electrochemical process**. *J. Mater. Sci.*, **36**(20):4943–4948, 2001. 43

[165] C. Wang and C.-R. Liu. **Transcrystallization of polypropylene composites: nucleating ability of fibres**. *Polymer*, **40**(2):289 – 298, 1999. 43

[166] E. Jenckel, E. Teege, and W. Hinrichs. **Transkristallisation in hochmolekularen Stoffen**. *Kolloid-Z.*, **129**(1):19–24, 1952. 43

[167] H. Schonhorn. **Transcrystalline growth at a polymer-metal interface**. *J. Polym. Sci. B Polym. Lett.*, **2**(4):465–467, 1964. 44, 72

[168] D. R. Fitchmun and S. Newman. **Surface crystallization of polypropylene**. *J. Polym. Sci. A-2*, **8**(9):1545–1564, 1970. 44, 83

[169] X. Zhu, D. Yan, and Y. Fang. **In Situ FTIR Spectroscopic Study of the Conformational Change of Isotactic Polypropylene during the Crystallization Process**. *J. Phys. Chem. B*, **105**(50):12461–12463, 2001. 48, 76

[170] M. Ieda, G. Sawa, and U. Shinohara. **A Decay Process of Surface Electric Charges across Poyethylene Film**. *Jpn. J. Appl. Phys.*, **6**(6):793–794, 1967. 55, 77

[171] E. A. Baum, T. J. Lewis, and R. Toomer. **Decay of electrical charge on polyethylene films**. *J. Phys. D: Appl. Phys.*, **10**(4):487–497, 1977. 55

[172] T. J. Sonnonstine and M. M. Perlman. **Surface-potential decay in insulators with field-dependent mobility and injection efficiency**. *J. Appl. Phys.*, **46**(9):3975–3981, 1975. 55, 57, 64, 77

[173] F. Rodriguez, C. Cohen, C. K. Ober, and L. A. Archer, editors. *Principles of Polymer Systems*. Taylor & Francis Books, Inc., 5th edition, 2003. 71, 84

[174] B. Lotz and J. C. Wittmann. **The molecular origin of lamellar branching in the α (monoclinic) form of isotactic polypropylene**. *J. Polym. Sci. B Polym. Phys.*, **24**(7):1541–1558, 1986. 72, 84

[175] B. Tabti, M. R. Mekideche, M. C. Plopeanu, L. M. Dumitran, A. Antoniu, and L. Dascalescu. **Factors That Influence the Decay Rate of the Potential at the Surface of Nonwoven Fabrics After Negative Corona Discharge Deposition**. *IEEE Trans. Ind. Appl.*, **46**(4):1586–1592, 2010. 77

Glossary

ε_0	electric constant or vacuum permittivity that equals to 8.85×10^{-12} F·m^{-1}.
e	the elementary charge, the absolute value of the electric charge carried by an electron, which is 1.60×10^{-19} C.
k	the Boltzmann constant, a constant that relates the average relative kinetic energy of particles in a gas with its temperature. $k = 1.38 \times 10^{-23}$ kg·m^{2}s^{-2}K^{-1}.
ATR-IR	attenuated-total-reflection infrared spectroscopy, a method for detecting the chemical composition of a material surface.
DSC	differential scanning calorimetry, a widely used measurement for the thermal properties of polymers.
FEP	tetrafluoroethylene hexafluoropolypropylene copolymer, a fluoropolymer, often with trademark—Teflon^{TM} FEP, with glass transition temperature of 60 °C and melting point of 290 °C.
PLM	polarised light microscope, a microscopy method often used for observing the crystalline structure in polymers.
PP	polypropylene, a plastic material with density of 0.905 g/cm^3, melting point of 165 °C and glass transition temperature of −18 °C. The polypropylene used in this thesis is isotactic, which can crystallise into different degrees of crystallinity.
PPS	piezoelectrically generated pressure step, a method for profiling the charge distributions in the electrets.
PTFE	polytetrafluoroethylene, commonly known with the trademark—Teflon^{TM} TFE, with a melting point of 327 °C, dielectric strength o f 60 MV/m and dielectric constant of 2.1 (at 1 MHz).
SEM	scanning electron microscope, a method for examining the surface properties of samples with high resolutions.
TSD	thermally stimulated discharge, a measurement for studying electret charge decay behaviour induced by linear heating.

$\mathbf{V}_0$	initial surface potential of the charged electrets
$\mathbf{V}_C$	the voltage supplied to the needle of the corona triode apparatus for ionising the molecules in the vicinity
$\mathbf{V}_G$	the voltage supplied to the control grid of the corona triode apparatus, which is also the desired value of the initial surface potential on the electrets

List of Figures

List of Tables